Department of Human Biology

Division of Biomedical Engineering

Thesis for MSc (Med) in Biomedical Engineering

# Optimization of the Hydrogel Injectate Therapy used in the Treatment of Myocardial Infarction

*Author*: Peter Wise (Student No: WSXPET004)

*Supervisor*: A/Prof. Thomas Franz

*Co-Supervisor*: Dr. Neil Davies

Cardiovascular Research Unit, University of Cape Town

10 October 2013

# Declaration

I, *Peter Craig Wilson Wise*, hereby declare that the work on which this dissertation/thesis is based is my original work (except where acknowledgements indicate otherwise) and that neither the whole work nor any part of it has been, is being, or is to be submitted for another degree in this or any other university.

I empower the university to reproduce for the purpose of research either the whole or any portion of the contents in any manner whatsoever.


Signature: …………………………………


Date: …………………………………….

# Acknowledgements

# Abstract

A substantial proportion of deaths worldwide are caused by cardiovascular diseases of which about one third result from myocardial infarction (MI). Therefore there is a worldwide concern to develop therapies for MI. Recent studies have shown potential for an upcoming therapy which involves the injection of a biomaterial into the MI. Although promising results are recorded, a clearer understanding is still needed to determine the full achievable benefit from biomaterial injectate. Additionally, computational modelling has proved to be a useful and reliable technique in analysing the effects of the biomaterial injectate.

Rat cardiac magnetic resonance images were used to create a computational geometry of a healthy heart to be modelled using the finite element software package *Continuity 6.4*. This geometry was used to create additional geometries of a series of ischemic infarct sizes and infarcts with the biomaterial/hydrogel treatment incorporated. Infarcts that were modelled included a 10 % infarct of the left ventricle wall volume without hydrogel injectate, as well as 25 %, 50 % and 75 % hydrogel volume of the infarct volume. Other models analysed included a 20 % infarct without the hydrogel treatment and with 50 % hydrogel; and 38 % infarct without hydrogel and with 25 % hydrogel. The biomaterial injectate displayed beneficial functional and mechanical improvement from the impaired infarct cases. The 50 % hydrogel exhibited improvement in ejection fraction (EF) from the 10 % infarct from 44.9 % to 47.4 % and in the 20 % infarct from 29.2 % to 40.6 % (Healthy EF: 49.7 %). Similarly improvement in cardiac performance was recorded with the 25 % hydrogel volume in the 10 % and 38 % infarcts (10 % infarct EF: 44.9 % to 46.4 %, i.e. 3.2 % improvement; 38 % infarct EF: 25.8 % to 26.7 %, i.e. 3.4 % improvement). Furthermore, myocardial stress and strain decreased in most models.

Although a beneficial decrease in average in-fibre end-systolic (ES) stress was recorded in the 10 % infarct with 75 % hydrogel, results indicated a slight decrease in performance from the 50 % hydrogel model. Furthermore, an increase in ES strain was observed (50 % hydrogel EF: 47.4 %; 75 % hydrogel EF: 47.3 %).

This thesis marked the start of determining the optimal hydrogel volume for various infarct sizes. This information would have a valuable clinical application in the treatment of patient specific infarct sizes. For the purpose of determining the optimal hydrogel volume, an attempt was made to define the relationship between hydrogel volume and infarct size. Although, this study was unable to conclusively determine this relationship, it marks the start for proceeding research to continue the development of this crucial, clinical data. It is

hoped that this thesis will form the foundation for following studies to determine this critical relationship for all healing phases as well as infarcts in different regions of the heart.

# Table of Contents

# List of Figures

# List of Tables

# List of Symbols

| | |
|---|---|
| $\alpha$ | Healthy ratio term |
| $\beta$ | Infarct ratio term |
| $\bar{\sigma}$ | Average stress |
| $\sigma_j$ | Stress per Gauss point |
| $\gamma$ | Gel ratio term |
| $b$ | Time-intercept of the linear relaxation duration – sarcomere length relation |
| $B$ | Parameter giving the shape of the peak isometric tension to sarcomere length relation |
| $C_{10}$ | Neo-Hookean material parameter |
| $(Ca_0)_{max}$ | Maximum peak in concentration of intracellular calcium |
| $b_{ff}$ | Fibre strain coefficient |
| $b_{cc}$ | Cross-fibre strain coefficient |
| $b_{fc}$ | Shear strain coefficient |
| $C$ | Stress scaling factor |
| $Ca_0$ | Maximum calcium concentration within the tissue |
| $C_{comp}$ | Bulk modulus |
| $E_{cc}$ | Cross fibre in-plane strain |
| $E_{cs}$ | Transverse plane shear strain |
| $E_{es}$ | End-systolic elastance |
| $E_{fc}$ | Fibre – cross-fibre shear strain |
| $E_{ff}$ | Fibre strain |
| $E_{fs}$ | Fibre – radial plane shear strain |
| $E_{max}$ | End-systolic elastance |
| $E_{ss}$ | Transverse to the fibre and is the radial strain |
| $I_3$ | Volume ratio of the stretch tensor |
| $i$ | Element number |
| $j$ | Gauss point |
| $k$ | Number of Gauss points within the element |
| $l_0$ | Sarcomere length for zero active tension |
| $l_R$ | Sarcomere length for zero stress present |
| $m$ | Gradient |
| $n$ | Number of elements in the region of interest |
| $Q$ | Exponent of strain energy $W$ for passive myocardium |
| $T_{max}$ | Peak isometric tension for the longest sarcomere length |

| | |
|---|---|
| $T_0$ | Active fibre directional component |
| **U** | Stretch tensor |
| $\overline{V}$ | Average volume for all the elements |
| $V_0$ | Dead volume |
| $V_i$ | Volume per element |
| $W$ | Strain energy function for passive myocardium |

# Abbreviations

| | |
|---|---|
| AA | Anterior apical |
| BZ | Border zone |
| CT | Computer tomography |
| CVD | Cardiovascular disease |
| DTMRI | Diffusion tensor magnetic resonance imaging |
| ED | End diastole |
| EDP | End-diastolic pressure |
| EDPVR | End-diastolic pressure volume relationship |
| EDV | End-diastolic volume |
| EF | Ejection fraction |
| Epi | Epicardium |
| ES | End systole |
| ESP | End-systolic pressure |
| ESPVR | End-systolic pressure volume relationship |
| EPV | End-systolic volume |
| FE | Finite element |
| FEM | Finite element modelling |
| HF | Heart failure |
| LV | Left ventricle |
| MI | Myocardial infarct |
| MRI | Magnetic resonance imaging/image |
| ODE | Ordinary differential equation |
| PDE | Partial differential equation |
| PEG | Polyethylene glycol |
| PET | Positron emission tomography |
| RMS | Root mean squared |
| ROI | Region of interest |
| RV | Right ventricle |
| RVSEPTUM | Right ventricle septum |
| RVFW | Right ventricle free wall |
| SV | Stroke volume |

# 1   Introduction

In 2007, the overall death rate due to cardiovascular disease (CVD) was 251.2 per 100,000 people (Roger et al., 2011). The World Health Organization (WHO, 2008) stated that about 17 million people die from CVDs each year worldwide. From Figure 1-1 it is shown that coronary heart disease is responsible for the majority of CVD death, and second is stroke (WHO, 2008). Myocardial infarction is typically a result of coronary heart disease and is therefore responsible for many CVD deaths.
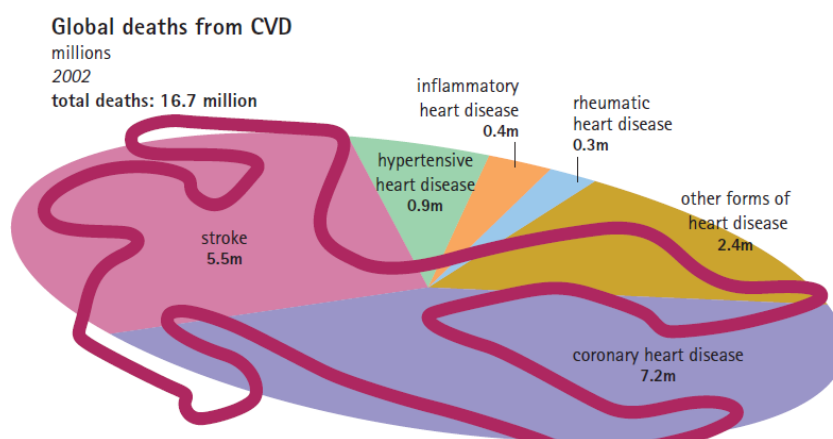


*Figure 1-1: Statistic for CVD's (WHO, 2008)*

It is clear from Figure 1-1 that CVD is a worldwide concern and more specifically coronary heart disease should be focused on. High risk areas include the lower income countries including southern Africa; this is due to a lack of medical care for CVD's. Deaths in these low income countries are expected to increase over the next decade as a result of obesity, diabetes and hypertension. According to Lloyd-Jones et al. (2010) CVD's are expected to be the number one cause of deaths by the year 2020, becoming responsible for more deaths than the infectious diseases such as TB and HIV among others. CVD's are accountable for roughly 33 % of deaths worldwide at present, with a third of these as a result of coronary heart disease including myocardial infarction (MI) (AHA, 2008).

During the cardiac cycle oxygenated blood fills the left ventricle (LV) and the cavities are passively enlarged. This stage is known as diastole. This blood is then pumped to the systemic system of the body by the active contraction of the LV during systole. The blood includes the necessary oxygen and nutrients for the tissues within the body to survive and maintain a healthy homeostasis. The heart muscle tissue obtains its blood supply via the coronary arteries. During MI, a blockage or occlusion occurs within one of the coronary arteries starving the cardiomyocytes (cardiac muscle cells) of the oxygen. This leads to cardiomyocyte necrosis and this tissue loses the active ability to contract. During acute

ischemia, or in the early stages after MI, there is very little if any negative effect on diastole, but since contractile ability is lost, the systolic function is significantly impaired. Healthy tissue continues to contract causing an increase in the internal cavity pressure resulting in bulging of the ischemic wall. Consequently, there is a large amount of energy loss leading to lack of performance in the heart function. According to (Whelan et al., 2007), the increased volume represented gives rise to increased tissue wall stresses as a mechanism to maintain the essential stroke volume. Healthy tissue therefore needs to compensate for the loss in stroke volume (SV) and uses more energy than prior to the MI. Eventually heart failure (HF) could occur as a result of the elevated stress and LV volume (Opie et al., 2006). It has even been indicated by (Konstam, 2005) that minor increases in the LV volume can lead to HF. It is therefore imperative that both forms of prevention as well as therapies for the treatment of CVD's are focused on.

## 1.1  Problem Identification

Despite the 27.8 % reduction in CVD deaths during the period from 1997 to 2007, CVD is still a major worldwide problem demanding urgent attention (Roger et al., 2011). In Africa it is expected that there will be a drastic increase in cardiovascular diseases as a result of increasing economic wealth as well as an increase in obesity, diabetes and hypertension (Wang et al., 2009). CVD's have been a leading cause for deaths worldwide where myocardial infarction is responsible for many of these deaths. Most CVD deaths are caused by myocardial infarction and strokes (WHO, 2008). It is estimated that there will be about 785,000 people who will suffer a new coronary heart attack, and about 470,000 people will suffer a repeated myocardial infarction in the US, every year.

As indicated above, MI is the death of heart tissue due to occlusion in one of the coronary arteries. Once cell death has occurred, the tissue loses its ability to actively contract and becomes purely passive. The heart undergoes a healing process whereby adverse remodelling takes place (this is discussed in detail in section 2.2). This leads to a reduction in cardiac functionality, as well as increased wall stresses. As a result in severe cases heart failure may occur (Tsur-Gang et al., 2009, Holmes et al., 2005).

Many therapies for the treatment of myocardial infarction have emerged, among which is a therapy whereby a hydrogel is injected into the infarcted region or its border zone (BZ). The injection of biomaterial has shown promising benefits in the restoration of cardiac functionality and reduction of wall stress (Nelson et al., 2011, Kofidis et al., 2005) in animal models. Although much research has been performed in this field, the full benefit and potential from the therapy is yet to be achieved. Specific parameters of the treatment

display potential to increase the functional improvement of the heart (Nelson et al., 2011). These parameters include the volume of hydrogel to be injected into the myocardium, the position and depth of injection, the mechanical properties of the hydrogel itself, among others.

Computational cardiac modelling has been shown to be accurate by the validation and close correlation of results to myocardial strains measured by implanted markers or tagged magnetic resonance imaging (Bovendeerd et al., 1996, Omens et al., 1993). Therefore the use of finite elements has proved to be a useful non-invasive technique in the study of the effect of hydrogels on the functionality of an infarcted heart (Kortsmit et al., 2012).

## 1.2 Aim and Objectives

After a myocardial infarction the heart undergoes a healing process whereby adverse remodelling takes place. This adverse remodelling can eventually lead to cardiac failure. A therapy which has been developed for the treatment of myocardial infarction is the injection of hydrogel into the infarcted region of the myocardium.

The aim of this study is to obtain a clearer understanding of the parameters of the hydrogel injectate affecting the cardiac functionality in an infarcted heart, such that this understanding could be used to optimise the effects of the injectate.

The aim of this study includes determining the relationship between the infarct size and the corresponding cardiac impairment, as well as determining a relationship of the optimal hydrogel volume as a treatment per infarct size. In this case the optimal volume of hydrogel would be the most effective volume to be used to improve the positive effect of biomaterial injection into the infarcted myocardium. This optimization is based on cardiac function; contractility, SV, ejection fraction (EF), and biomechanics; myocardial stresses and strains, for an acute infarct. The cardiac function is optimized by increasing the contractility, SV or EF of the LV, while biomechanics are improved by decreasing stresses and strains in the myocardial wall.

In this study, the research will first be focused on the relationship of cardiac impairment to the corresponding infarct size, followed by the relationship of the optimal hydrogel volume to the size of infarct.

The project objectives included within the aim are as follows:

1. Determine the cardiac function of a healthy rat heart geometry based on MRIs

2. Analyse the effect of an ischemic infarct sizes on the cardiac function and myocardial stress and strain

3. Analyse the effect of immediate biomaterial injections post infarction on ventricular function and wall mechanics with particular focus on different injectate volumes

# 2 Literature Review

## 2.1 The Heart

### 2.1.1 Background

#### 2.1.1.1 Heart Anatomy and Physiology

The heart is an efficient pump that is responsible for supplying the body with blood. The heart can be viewed as two pumps; one pump represented by the right atrium and right ventricle (RV) and the other pump by the left atrium and LV. The right atrium and RV section of the heart pumps the deoxygenated blood from the systemic circulation into the pulmonary circulation where the blood becomes oxygenated. The second pump, the left atrium and LV, receives blood from the pulmonary circulation and pumps the oxygenated blood to the systemic circulation (Little and Little, 1981). Figure 2-1 shows the blood flow through the heart and through the systemic and pulmonary systems.
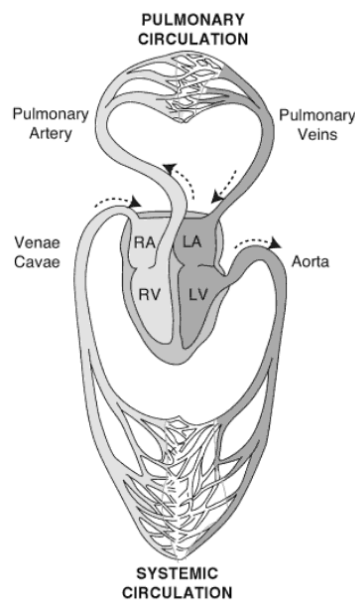


*Figure 2-1: Blood circulation through the heart (Little and Little, 1981)*

Four valves are located in the heart; two atrioventricular valves and two semi-lunar valves. One of the atrioventricular valves is located between the right atrium and the RV and the other between the left atrium and the LV. Atrioventricular valves prevent the blood from flowing back from the ventricles into the atria. For the semi-lunar valves, one valve is located between the RV and the pulmonary artery and the other valve between the LV and the aorta. The semi-lunar valves prevent blood from flowing from the arteries back into the respective ventricles (Little and Little, 1981).

The cardiac cycle of the heart involves the filling of the ventricles and the ejection of blood from the heart. This cycle consists of four different phases which are divided into two main phases, which are systole and diastole. At the start of systole and in the case of a human heart, the LV cavity volume is about 115 ml, with a pressure of about 5 mmHg. Systole is started by isovolumic contraction; during this phase the cardiac muscle contracts causing an increase in the pressure while the volume is constant. This contraction results from ventricular depolarisation. During isovolumic contraction, the pressure increases until the pressure inside the LV is larger than the aortic pressure of about 80 mmHg. This pressure difference causes the aortic valve to open; blood is then ejected at approximately constant pressure, giving a volume change from about 115 ml to about 45 ml. The ejection of blood into the aorta is defined as the ejection phase.

The active contraction responsible for ejection is caused by an electrical impulse through the myocardium. This electrical impulse is initiated at the sinus node (also known as the sinoatrial node) for a normal rhythmical impulse. This impulse is then conducted over the internodal pathways to the atrioventricular node (A-V node) where the impulse is delayed before propagating to the ventricles. The A-V bunble conducts the impulse from the A-V node to the left and right ventricles. This impulse propagates to the apex of the heart and causes active contraction to begin at the apex of both ventricles. Contraction traverses along the Purkinje fibres, causing contraction to start from the apex moving to the base of the ventricles. Therefore blood from the ventricles is ejected from the heart. Figure 2-2 shows the Purkinje fibres and the electrical propagation pathways.
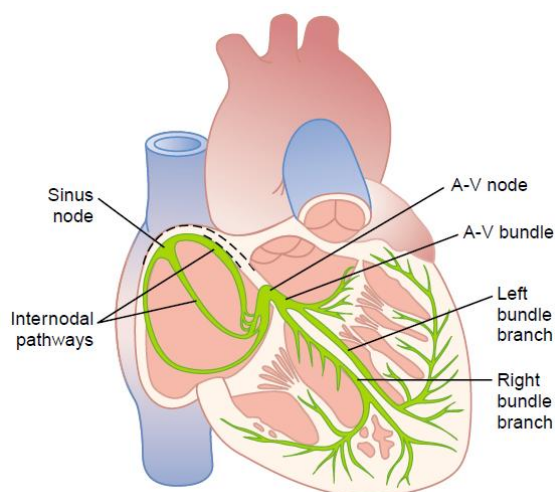


*Figure 2-2: Electrical propagation pathways along the Purkinje fibres (Guyton and Hall, 2006)*

Diastole involves the filling of the LV with oxygenated blood from the lungs. The start of diastole is marked by isovolumic relaxation, where the volume remains constant while the

pressure decreases. The pressure decreases until the pressure inside the LV falls below the pressure within the left atrium. At this point the cavity volume and pressure are about 45 ml and 0 mmHg. Thereafter, blood flows from the left atrium into the LV which is called the filling phase. Once filling has been completed, the cardiac cycle starts again (Burkhoff et al., 2005, Suga and Sagawa, 1974, Guyton and Hall, 2006). Figure 2-3 shows LV pressure-volume relationship in the four phases of the cardiac cycle and Figure 2-4 shows the pressure curves as well as volume curves depicting the phases of the cardiac cycle.
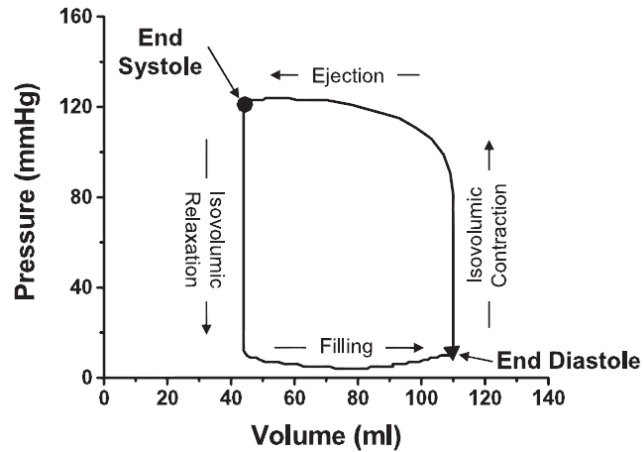


*Figure 2-3: Left ventricle pressure-volume loop (Burkhoff et al., 2005)*
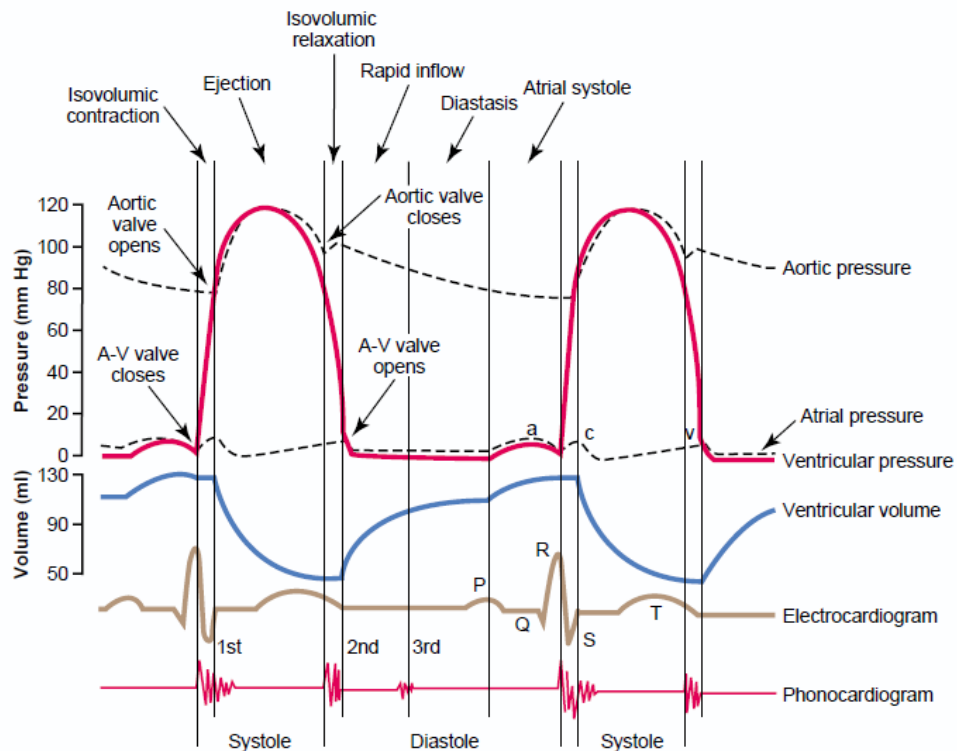


*Figure 2-4: Pressure and volume curves over time (Guyton and Hall, 2006)*

## 2.1.1.2   Functional Parameters

An analysis of the pressure-volume relationship is used to analyse the ventricular performance and the overall cardiac function. It is found that the point marking end diastole is a point at the lower right corner of the pressure-volume loop. Likewise, the point marking end systole is a point found at the top left of the pressure-volume loop. These two points remain constant for a given heart under constant loading conditions and give a fixed pressure-volume loop under steady state conditions with a fixed time interval. In the case where the loading conditions are changed without affecting the contractility of the myocardium, a series of pressure-volume loops are obtained. These loops appear to show two distinct boundaries formed by the end diastole points and the other formed by the end systole points. The boundaries EDPVR (End Diastolic Pressure Volume Relationship) and ESPVR (End Systolic Pressure Volume Relationship) are two important characteristic curves used in the analysis of cardiac functionality. Figure 2-5 shows the EDPVR and ESPVR (Burkhoff et al., 2005).
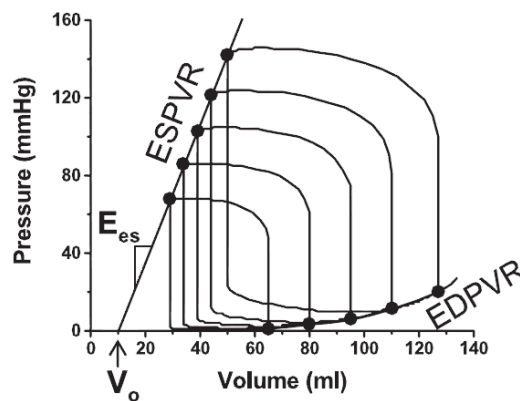


Figure 2-5: EDPVR and ESPVR (Burkhoff et al., 2005)

Cardiac functionality is indicated by different functional parameters obtained from the EDPVR and ESPVR curves in the pressure-volume relationship of the LV. End-systolic elastance and dead space volume ($V_0$) are obtained from the ESPVR curve, while the SV and EF are derived from a combination of the EDPVR and ESPVR curves, finally the end-diastolic compliance is obtained from the EDPVR curve.

Although experimentally ESPVR is non-linear, it is approximated to be linear in cardiac modelling. It represents the active physical properties of the myocardium in state of full muscular contraction. The slope of the ESPVR is given by $E_{es}$, which represents the end-systolic elastance. The volume $V_0$ shows the volume intercept of ESPVR. $E_{es}$ is shown to increase with an increase in the myocardial contractility and likewise decreases with a decrease in the myocardial contractility. Therefore the $E_{es}$ value gives a measure of the contractility of the myocardium. EDPVR represents the passive physical properties of the

myocardium at a state of full muscular relaxation. Literature shows experimentally that a large tissue stiffness corresponds to a high ED pressure or volume value and similarly when the tissue stiffness is low, this corresponds to a low ED pressure or volume value (Burkhoff et al., 2005).

The EF is an important parameter that is used to gauge the functionality of the heart (Nagy, 2001). The EF is found by definition:

$$\text{EF} = {}^{\text{SV}}\!/_{\text{EDV}} \qquad\qquad (\ 2\text{-}1\ )$$

where

$$\text{SV} = \text{EDV} - \text{ESV}. \qquad\qquad (\ 2\text{-}2\ )$$

Here SV is the stroke volume and EDV is the end diastolic volume. The EF is a useful parameter when using non-invasive techniques to gauge the functionality of the heart (Frangi, 2001).

## 2.1.2   Structure and Mechanics

The cardiac wall consists of three layers; the epicardium, myocardium and the endocardium. The epicardium forms the outermost layer and is defined as a serous membrane with blood capillaries, lymph capillaries and nerve fibres (Cingolani et al., 2003). The middle layer, the myocardium, forms most of the heart mass and consists of cardiac muscle tissue. This tissue is mostly made up of muscle fibres, which are responsible for the active contraction during the systole phase of the cardiac cycle. The inner surface of the heart wall is defined as the endocardium. This layer provides a protective layer on the inner surface of the heart (Cingolani et al., 2003). Since the myocardium forms most of the heart tissue and is responsible for the pumping function of the heart it is the most important cardiac layer. The myocardium consists of striated muscle fibres which are connected to each other both in parallel and in series. This interconnected nature marks the main difference between skeletal and cardiac muscle tissue (Wu et al., 2008). Fibre orientation is an area of great interest in the study of cardiac mechanics since the orientation of the fibres has a direct influence on the mechanics of the heart. It determines the method by which stress is distributed throughout the heart tissue, and, therefore has an influence on the contraction of the heart during systole. It has been shown that the fibre directions rotate through the transmural direction. An article by Holzapfel and Ogden (Holzapfel and Ogden, 2009) shows that the orientation of the fibres within the wall of the human LV changes from about 50 to 70° at the epicardium to about -50 to -70° at the endocardium with respect to the circumferential direction. (Omens et al., 1993) show that the fibre

orientation of a rat heart rotates from -52° to 53° through the transmural direction from the epicardium layer to the endocardial layer. The transition in the rotation of fibre orientation from the epicardium to the endocardium is said to be smooth through the thickness of the ventricle wall (Holzapfel and Ogden, 2009). Apart from the transmural rotation, in fibre orientation, it has been noted by Rohmer et al. (2007) that the fibre orientations also change through the longitudinal direction of the ventricle following a helical pattern (Geerts et al., 2002).

In the case of a geometry describing the biventricular heart, the fibre orientation of the right ventricle free wall (RVFW) also needs to be determined. In the study by Göktepe et al. (2010) the myofibres within the LV wall was shown to rotate from 55° on the endocardial surface to -55° on the epicardial surface, a similar arrangement was also seen from the endocardial to the epicardial surface of the RVFW. This can be seen in Figure 2-6.
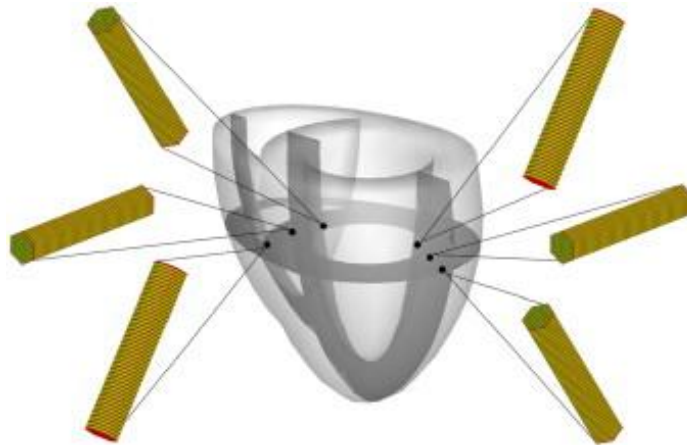


*Figure 2-6: Fibre orientation for the left ventricle in a biventricular model (Göktepe et al., 2010)*

In 1991, a paper by Nielsen et al. (1991) stated that there is no realistic case of a three dimensional biventricular model that accurately describes the fibre orientation. The objective of Nielsen's study was therefore to address this issue and develop a realistic finite element model of a canine biventricular heart with the fibres fully incorporated. It was shown that the fibre orientation rotates from -60° on the epicardial surface of the RVFW to +90° on the endocardial surface of the RVFW. Following this data, it was shown that the septal wall fibre orientation varied from -90° on the RV endocardium to +80° at the surface of the LV endocardium (Nielsen et al., 1991). This data indicated a discontinuity in the fibre orientation at the junction between the septal wall and the right ventricular free wall.

A study by Hautemann et al. (2007), indicated that there was still a need for an accurate region specific fibre orientation model. In this study a rat heart was used and analysed. The results presented agreed with fibre orientation trends presented by Geerts et al. (goat

heart) (2002) and Chen et al. (rat heart) (2003), through the transmural direction of the myocardium. Moreover it was observed that, from the LV endocardium the helix angle rotates from about 80° to about -60° on the epicardium. It was shown that within the RV cavity, the septal wall had a helix angle of about -80° and the free wall helix fibre orientation was observed to be about 60° on the endocardial surface. Figure 2-7 shows the fibre angles defined by Chen et al. (2003) in a rat heart in a short axis slice.
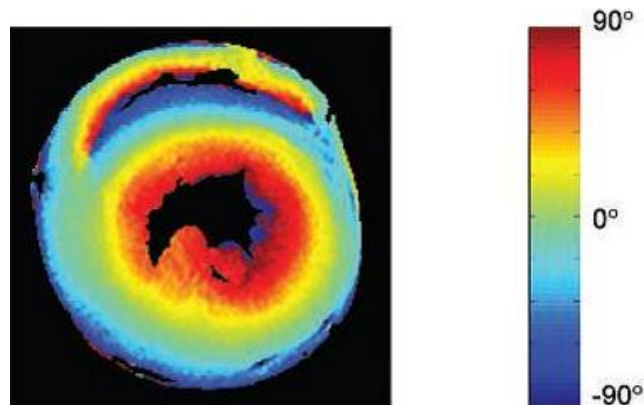


*Figure 2-7: Contour map showing the helix angle of the myofibres (Chen et al., 2003)*

In literature, the material properties are discussed with respect to specific loading conditions. In general it is noted that the myocardium exhibits nonlinear elastic properties. It is considered to be nonlinear since the tissue response to loading conditions is highly nonlinear. Furthermore it is considered elastic since the tissue follows the same loading and unloading paths, it exhibits a time-dependent behaviour as well as responds instantaneously to an applied load, and finally, the tissue regains its original dimensions after relaxation (Herrmann et al., 2003).

An important characteristic of the myocardium which should be noted is that it is anisotropic. That is the response displayed by the myocardium to various loading conditions is dependent on the direction of the applied load. This anisotropic behaviour is largely due to the fibre orientation present within the myocardium. It is due to this anisotropic behaviour that some studies refer to the myocardial tissue as being orthotropic. Orthotropy is a unique case of anisotropy, in this case, there are three orthogonally preferred directions (Holzapfel and Ogden, 2009). Other studies such as Guccione et al. (1995) refer to the myocardium as being transversely isotropic, which is also a special case of anisotropy. In this case, the material behaviour is constant in all directions except in a specific predefined direction. Although both of these methods represent an approximation of the nonlinear anisotropic material properties, orthotropic behaviour more accurately describes the true material behaviour. Although the heart tissue shows orthotropic

behaviour in reality, transversely isotropic behaviour is most commonly used (Guccione et al., 1995, Kortsmit et al., 2012, Lafortune et al., 2011).

Compressibility is another area which should be discussed. Incompressible materials do not alter their volume under applied loads (Herrmann et al., 2003). It has been shown by Yin et al. (1996) that the myocardium exhibits a small amount of compressibility under physiological loading conditions. The compressibility exhibited is understood to be due to the relocation of the myocardial fluids present within the tissue during physiological loading.

The stress and strain characteristics of the myocardium are important since they are used for the inputs of the strain energy functions used in cardiac modelling and need to be determined in order to be able to successfully model a heart using finite element modelling techniques. The stress experienced by the tissue gives an indication of whether there would be a risk of cardiac failure. After myocardial infarction, the LV wall stress increases as a result of dysfunctional myocardium. Increased stress leads to greater strain and as a result dilation of the ventricle occurs. There are a few different experimental tests that can be performed to obtain the stress and strain characteristics of the myocardium. These tests include uniaxial testing as well as biaxial testing. Although uniaxial testing methods have most commonly been used and are easily performed, the tests unfortunately are unable to give an indication of the three dimensional material characteristics of the material. Similarly in biaxial tests, the third dimension is neglected (Gibbons et al., 2004). Another method of determining the stress and strain characteristics is by the use of magnetic resonance tagging. This method measures the deformations experienced by the myocardium under certain loading conditions and the strain energy function parameters are fitted to obtain the same deformations (Guccione et al., 2001). The advantage of this form of testing is that it is non-invasive.

## 2.2 Myocardial Infarction

### 2.2.1 Description

Myocardial infarction (MI) is commonly known as a heart attack with the most common symptom being chest pain. MI is defined as myocardial necrosis caused by prolonged ischemia. This occurs when the coronary artery supplying the myocardium with nutrients and oxygen becomes occluded (Antman et al., 2000). It is shown in literature that with an increase in the infarct size there in a decrease in the cardiac functionality (Janz and Grimm, 1972).

Coronary arteries supply the heart tissue with necessary nutrients and oxygen to survive. Therefore an occlusion of the coronary artery would prevent the myocardium from receiving a blood supply. This leads to ischemia and therefore cellular death (necrosis) of the myocardium. Irreversible damage is caused if the blood supply is not returned within 20 to 40 min of the initial occlusion (Marks, 2012).

### 2.2.2 Causes

Myocardial infarction occurs as a result of a complete blockage of one or more coronary arteries supplying the myocardium. The blockage could also be due to the formation of arterial plaque causing clots to form in various parts of the heart tissue (Maier, 2011).

Atherosclerosis is the collection of cholesterol within the arteries which takes place over a long period of time. The heart attack occurs during the rupture of the surface plaque within the coronary artery. A blood clot forms and causes complete occlusion. Factors which increase the possibility of rupture and clot formation are nicotine intake, increased levels of low-density lipoprotein cholesterol, increased amount of blood catecholamines or adrenaline, high blood pressure, among others (Marks, 2012).

### 2.2.3 Effect on Cardiac Function

After the onset of a myocardial infarction, the infarcted tissue undergoes changes during the healing process (Janz and Grimm, 1972). The healing process of an infarcted heart can have a detrimental effect on cardiac function. The degree to which the LV performance is affected is dependent on the severity of the infarct itself (Holmes et al., 2005).

### 2.2.4 Mechanics of the Infarcted Region

Holmes et al. (2005) divided the healing process after a myocardial infarction into four phases. These phases are the acute ischemic phase, the necrotic phase, the fibrotic phase and the remodelling phase. It is shown that each phase is characterised by changes in the cardiac tissue. These changes are discussed later (Janz and Grimm, 1972, Holmes et al., 2005).

Bogen et al. (1980) approximated the effects of large infarcts on the end-systolic and end-diastolic pressure-volume relations. These estimations are represented in Figure 2-8. Three of the four phases are shown in the figure, where C represents the control or healthy heart, I represents the acute ischemic phase, N represents the necrotic phase and F represents the fibrotic phase.
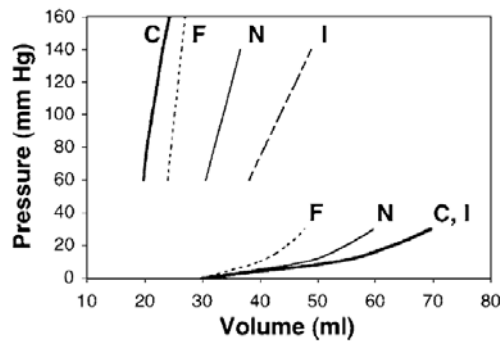
*Figure 2-8: EDPVR and ESPVR of the acute ischemic phase, necrotic phase, fibrotic phase and a healthy control, showing the effects of large infarcts on the end-systolic and end-diastolic pressure-volume relations. In the figure, C indicates the healthy heart or the control; F is the heart under the fibrotic phase; N corresponds to the heart in the necrotic phase; and I corresponds to the heart during the ischemic phase (Holmes et al., 2005).*

For various species, the four phases of healing are observed to occur over different periods of time. It is shown by Holmes et al. (2005) that the healing phases in a rat heart are much quicker than those seen in a human or even canine heart. The image in Figure 2-9 represents the time points at which the phases take place in a rat, dog and a human heart. The four phases of healing are described in greater detail below.
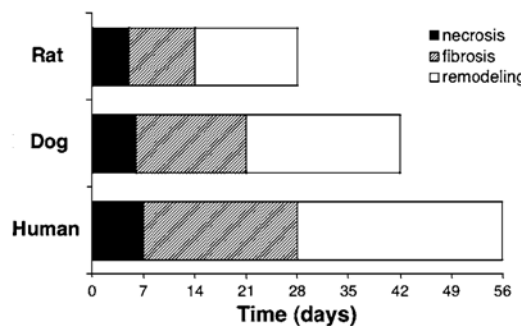


*Figure 2-9: Healing phases in rat, dog and human hearts (Holmes et al., 2005)*

### 2.2.4.1   Acute Ischemia

Acute ischemia starts when the coronary artery supplying the heart becomes occluded. This phase ends when the infarcted tissue starts stiffening. The infarcted tissue during this period acts as passive myocardium and therefore has no contractility and only affects the systolic function of the ventricle (Holmes et al., 2005). It is shown that two of the mechanisms which reduce the ventricular performance are present during this phase. The first mechanism is the waste in the energy of the healthy myocardium due to stretching of the affected area. It has been shown that if 40 % of the LV myocardium has been lost due to an infarct, the LV could fail (Page et al., 1971, Alonso et al., 1973). The second mechanism is

the wall stress is increased as a result of dilation of the LV and expansion due to the infarct (Weisman and Healy, 1987, Bogaert et al., 2000).

### 2.2.4.2 Necrosis

Necrosis starts when the stiffening of the infarcted tissue begins. During this phase, oedema, cell death and degradation take place. The necrotic phase ends when collagen starts to form. There is also an increase in the stiffness and strength of the tissue. As a result, the systolic function is detrimentally affected. An extreme consequence during this phase is that rupture could occur: This is the most extreme case and results in heart failure and death (Wehrens and Doevendans, 2004, Birnbaum et al., 2003). It is stated by Holmes et al. (2005), that most infarct ruptures occur during this phase of healing. Other than this consequence, the same mechanisms seen in acute ischemia are also observed; although the wastage of energy due to stretching is limited since there is moderate stiffening of the infarcted tissue. Additionally infarct expansion and ventricular dilation could cause an increase in the wall stress (Holmes et al., 2005).

### 2.2.4.3 Fibrosis

The formation of collagen marks the start of fibrosis and once the collagen formation starts to decrease this phase ends. The collagen or scar tissue causes a large increase in the stiffness of the infarcted tissue (Holmes et al., 2005). Two mechanisms that cause a depression in the LV functionality are typically observed during this phase. The first is the increased stiffness of the scar tissue could limit the required diastolic function of the rest of the LV (Smith et al., 1974). The second is the impaired systolic function of the non-infarcted tissue adjacent to the infarcted myocardium (Holmes et al., 2005).

### 2.2.4.4 Remodelling

Remodelling is the final stage of the healing infarct; the start is marked by the decrease in collagen formation. During this phase, the scar tissue is seen to shrink and collagen cross-linking is observed. This causes a decrease in the stiffness and the LV starts to regain functionality. It has been observed in many cases that the functionality is partially restored during this final phase of the healing process. All the mechanisms seen in the previous phases that cause impaired cardiac performance except the mechanism relating to rupture are present during this phase. An extra mechanism that is observed is in the long term an infarct could cause detrimental remodelling of the ventricle which causes increased stresses within the wall myocardium. The remodelling in this case is known as a volume-overload hypertrophy of the healthy remaining tissue. This tissue thins and lengthens causing cavity dilation (Pfeffer and Braunwald, 1990).

### 2.2.5 Infarct Sizes

Infarct sizes vary from patient to patient. The infarct is classified according to the size or percentage of cardiac tissue that is dysfunctional. An infarct less than 10 % of the LV mass is classified as a small infarct, a medium infarct is considered to be between 10 and 30 % of the LV wall volume and a large infarct is considered to be any infarct that affects more than 30 % of the cardiac tissue in the LV (Antman et al., 2000). At the point where more than 20 % of the LV is infarcted, mortality and morbidity is increased (Miura and Miki, 2008). Therefore this is considered the critical point. The relationship between infarct size and the cardiac dysfunction is unknown. It is clear that with increasing infarct sizes there is a decrease in the cardiac performance as well as increased mortality.

Literature shows a large range of studies performed with a variety of different infarct sizes. The range in infarct sizes used for experimental studies is infarcts mostly from 20 to 30 % of the LV wall. Studies by Okada et al. (2010) show infarct sizes as large as about 70 % in porcine hearts, whereas most other studies show maximum infarct sizes less than 40 % (Christman et al., 2004, Hochman and Bulkley, 1982). A standard size of 20 % was taken to be the minimum on most studies performed (Jiang et al., 2009, Dobner et al., 2009, Hao et al., 2007, Ifkovits et al., 2010). A study performed by Dia et al. (2005) used Fischer rats and obtained infarct sizes between 40 and 50 %.

## 2.3 Infarction Therapies

Myocardial infarction as explained can cause impaired cardiac performance and in severe cases can lead to cardiac failure. Therefore it is pertinent that an effective therapy is found for the treatment of myocardial infarction. The aim of the treatment would be to prevent heart failure and if possible to restore cardiac functionality. Many different types of therapies have been developed including pharmaceutical based and surgical based therapies.

### 2.3.1 Pharmaceutical Therapies

Pharmaceutical treatment is often the initial type of treatment used since there are no surgical processes needed. This form of treatment aims to prevent and treat any complications that may arise as a result of the infarction healing process, as well as aims to restore the balance between the oxygen supply and demand, preventing further ischemia (Flather et al., 2000). Although pharmaceutical treatment does not require invasive techniques to treat myocardial infarction, it is not always an effective form of treatment. Pharmaceutical treatment cannot rectify the mechanical and physical changes that occur during the healing phases (Hannan et al., 1999, Hannan et al., 2005). These changes have a

detrimental effect on the cardiac functionality often leading to cardiac failure. In this case other forms of treatment are needed and such treatments often involve surgery.

### 2.3.2 Surgical Therapies

An alternative to the pharmaceutical treatment of myocardial infarction are the surgical methods. Surgical treatments, although often effective, are clearly more invasive. Some surgical therapies that have been used in the treatment of myocardial infarction focus on the return of the blood flow to the infarcted region of the heart. For example the use of coronary bypass grafting or stent placement (Hannan et al., 1999, Hannan et al., 2005). For the most severe cases of CVD there is the possibility of a heart transplant, although there is the issue of availability of a donor heart (John et al., 2001).

Dilation of the LV is one of the greatest adverse effects that take place and must be avoided. There are mechanical devices that have been developed to prevent this from happening. These mechanical approaches attempt to reduce the myocardial wall thinning and stress as well as restore the cardiac geometry. Such mechanical devices include the CorCap (Acorn Cardiovascular Inc.) and the HeartNet (Paracor Medical Inc.) (Starling et al., 2007). Other mechanical devices that have been tested include for example the Myosplint (Myocor Inc.) and the CardioClasp (CardioClasp Inc.) which directly reduce the wall stress of the myocardium (Fukamachi and McCarthy, 2005). Apart from these mechanical devices and treatment techniques there are also procedures and techniques such as the Dor procedure and the Batista procedure that physically restructure a dilated ventricle into a more natural form (Sartipy et al., 2005). It has been indicated by Nelson et al. (2011) that although some of these procedures are very effective in the treatment of even severe cases of myocardial infarction, they involve highly invasive methods.

### 2.3.3 Biomaterial Intramyocardial Injectate Therapy

Over the past ten years a new area of treatment has been developed. It involves the injection of biomaterials into the cardiac tissue to prevent adverse remodelling after myocardial infarction (Christman and Lee, 2006). The injectate is inserted directly into the infarcted tissue or its periphery, forming a bulk within the cardiac wall. There are several potential benefits which can be obtained by using this form of treatment. For example not only can the injection of biomaterials provide support of the mechanical structure and geometry of the heart, but due to hydrogels being coupled to biomaterials and nutrients which possess biological functions, the repair and healing process of the heart could also be promoted (Nelson et al., 2011). Biological functions such as cardiomyocyte protection, angiogenesis and stem cell recruitment have been found to show beneficial outcomes

(Laflamme and Murry, 2005, Menasché, 2007, Segers and Lee, 2008, Wollert and Drexler, 2005).

Many types of hydrogel injectates have been developed, which can be divided into two main types, biodegradable and non-degradable. An article by Dobner et al. (2009) shows that a non-degradable polyethylene glycol hydrogel can prevent to some extent the adverse remodelling similar to support devices. The tests in this study were performed on rats. The results showed that the hydrogel was effective in the early stages post-infarction, but did not show any effect preventing dilation from occurring in the long-term (Dobner et al., 2009). Jiang et al. (2009) proposed that the functionality of the LV can be conserved by preventing the bulging that occurs during the systolic phase after an infarct. The study was performed on a rabbit with the use of 200 µl of α-cyclodextrin hydrogel. After a 28 day period post the injection of the hydrogel, it was observed that the scar growth as well as the thinning of the myocardial wall had been prevented when compared to the control. Tests were undertaken using echocardiography to determine the EF of the LV. These tests showed that the EF was substantially increased in the hydrogel group, showing an EF of approximately 56.09 % as compared to the control group with an EF of approximately 37.26 %. Furthermore, the end systolic and end diastolic diameters were shown to have reduced in the hydrogel treated hearts, indicating that the characteristic dilation had been prevented (Jiang et al., 2009).

There have been various studies performed on hydrogels to attempt to determine the parameters, (of both the treatment and the hydrogel) that have the greatest beneficial effect in the treatment of a myocardial infarct. A study by Ifkovits et al. (2010) shows a comparison between two hydrogels differing only in elastic modulus. The moduli were approximately 8 kPa and 43 kPa. These hydrogels are hyaluronic acid hydrogels, which display similar degradation properties and tissue distribution after injection. It was found that after injection of the hydrogels into an ovine heart, the ventricle wall thickness was substantially increased. Furthermore, it was found that in the case of the hydrogel with modulus of 43 kPa a smaller infarct area was present when compared to the control. Additionally, the end-systolic and end-diastolic volumes were observed to be lower. The study showed that the hydrogel with a higher modulus displayed better functional cardiac performance than the control group as well as the group with the modulus of 8 kPa (Ifkovits et al., 2010).

Another article regarding the effects of an injectate on the cardiac remodelling and function of infarcted rat hearts stated that after a myocardial infarction, adverse remodelling occurred, which increased the risk of heart failure (Landa et al., 2008). It was proposed that

the injection of in situ-forming alginate hydrogel in both older and newer infarcts would provide a support to the cardiac wall tissue, prevent the adverse remodelling and decrease the chance of heart failure. The study used a low viscous solution, which after being injected became more viscous and formed the hydrogel scaffold. It was observed that the hydrogel had occupied 50 % of the scar region. Additionally the study showed that due to the injection of the alginate biomaterial seven days after the infarct, the scar thickness had increased preventing dilation and dysfunction of the LV. Results of the experiments were comparable and were in some cases better than the results obtained by neonatal cardiomyocyte transplantation. Furthermore it was found that the injection of the biomaterial into an old infarct, that is 60 days, was also beneficial, showing improvement in the cardiac function, although less. Although the research showed positive results, it did have some limitations. Firstly the follow-up period was only two months, and it is therefore unclear whether the beneficial effects on the remodelling and cardiac function are maintained for longer periods (Landa et al., 2008).

Many studies have been performed on the use of hydrogel in the treatment of myocardial infarction showing that this form of treatment has promising potential and could become a powerful form of therapy. It has also been noted that there is a maximum follow up period of 13 weeks, indicating that there is a lack of results showing what the long term effects are (Nelson et al., 2011). Therefore it is unclear what the long term effects of the hydrogel treatment are on the cardiac performance. Consequently, there is still a need for research to be performed in this field in order to determine the most optimal and most effective capabilities of this treatment.

## 2.4   Cardiac Analysis and Imaging Techniques

For a comprehensive and accurate study of MI and various therapies, the heart needs to be analysed. In the case of computational methods, the geometry is constructed based on medical images to ensure computational accuracy. Various techniques are used for imaging the heart, and include magnetic resonance imaging (MRI), echocardiography, as well as computer tomography (CT). The imaging of the heart is both useful as a diagnostic tool as well as analysis use for studies when comparing a computational geometrical structure to a realistic heart. It has been stated by Frangi et al. (2001) that spatio-temporal imaging is useful in the understanding and study of the cardiac cycle. Additionally, imaging techniques allow for three dimensional images, giving rise to increasing accuracy in computational studies due to increased accuracy in geometries used.

MRI, as a form of imaging, is non-invasive and is therefore very useful in viewing the condition of the heart. Images are usually taken as a series of either the long or short axis. Either of these could be used to reconstruct the heart geometry. The imaging of murine hearts are challenging since the heart volume is very small in comparison to larger animals such as ovine and canine hearts. Very high resolution images are therefore required to be able to accurately differentiate the various regions of a rat heart. High resolution images are also important to ensure accuracy in the reconstruction of a computer generated geometry of a rat heart.

Typically echocardiaographic is a common form of cardiac imaging, which uses ultrasound techniques. A typical echocardiogram is performed on the chest surface, but more recent techniques use a transesophageal echocardiogram. Transesophageal echocardiogram removes the interference from the ribs and lungs, providing an image of improved detail. Echocardiography can be used for real time analysis of the heart to determine EDV and ESV as well as allow for other quantitative analyses such as motion investigation (Frangi, 2001). It has been shown that transesophageal echocardiogrphy is useful in identifying cardiac diseases such as hypertrophic cardiomyopathy, mitral stenosis and endocarditis (Pothineni et al., 2007).

Although CT has its place in medicine even in the diagnosis and analysis of CVD's (Ohnesorge et al., 2000), it has been shown that with increased heart rate there is a decrease in image quality (Hong et al., 2001). The heart rate of a rat is about 250 bpm (Dai et al., 2005), therefore CT would not be practical for cardiac imaging of rats.

## 2.5   Finite Element Modelling

Finite element modelling (FEM) is a non-invasive process where computational methods are used to simulate real life situations in order to predict the outcome. Computational methods use numerical methods to solve algorithms describing a physical process. Algorithms used in FEM are known as step-wise functions which give output approximations based on inputs given in the system.

Since FEM is a computational approximation of real life situations there are many simplifications that are implemented. These simplifications are considered to be necessary to reduce the computational cost without reducing the accuracy of the results to a point that the results are meaningless. Some simplifications made in cardiac modelling are the geometry used; earlier geometries used were mostly of ellipsoidal shape (Guccione et al., 1995, Janz and Grimm, 1972). More recent models use methods to reconstruct the cardiac geometry from imaging techniques in order to remove the inaccuracies of the simplified

geometry (Guccione et al., 2001, Kortsmit et al., 2012, Lafortune et al., 2011). Other simplifications used include material properties and boundary conditions. These are continuously under adjustment to improve their approximation.

Computational modelling uses a few different approaches in order to discretize model. Discretization is necessary since algorithms use approximate values at each discretized point in the geometry. Methods used include finite element, finite volume, boundary element and finite difference methods. FE is the method that is used for this study.

## 2.6 Computational Modelling of the Heart

Other studies have been performed to determine the effect of the hydrogel treatment, some of which are computer simulations (Macadangdang, 2010). These computational models are used to determine the cardiac functionality of the heart at various phases of the myocardial infarction. Computational methods in this field have great potential and have proved to be effective.

Computational mechanics is the use of computational methods to simulate real life applications. The benefit of computational mechanics is that it provides a form of non-destructive testing, and allows for testing of real life situations where either the studies would be too expensive or require a large amount of time and space. Applications of computational modelling range widely, and in the case of this study, include cardiac modelling (unknown, 2012).

Complex geometries with different material properties and many variables each affecting the outcome of the model under various situations need to be simplified. These geometries are estimated using partial differential equations that govern the model in a computational simulation. One of the methods used to simplify the model is to discretize the structure into finite calculation points. Although in reality physical situations can only be described exactly by continuous calculation points, in computational mechanics, this is not possible and a finite number of calculation points are used whereby the region in between these points is found by interpolation. There are many methods used in the discretization process, namely, finite element method, finite difference method, finite volume method, boundary element method among others. The most common of these methods appears to be the finite element method (FEM). The reason for this is due to the high degree of geometrical flexibility when compared to other methods.

There are two approaches in the solution process using the FEM, the first of which involves approximating the situation as steady state by eliminating the partial differential equations

(PDE), and the second approach is to approximate the PDEs as ordinary differential equations (ODE). The ODEs can then be integrated trivially and a solution is then found.

In the FEM, a structure is divided into a finite number of functions which represent subdomains known as elements. For simple 1D problems, rod elements are used, whereas for 2D structures either quadrilaterals or triangles are used and 3D structures are discretised by the use of tetrahedral or hexahedral elements among others. In these cases, the element has vertices which define the element; these vertices are the nodes or nodal points.

The governing equations in the FEM are given in integral form as opposed to differential form. The integral of the entire domain is then given by the sum of all the subdomains. Generally, a group of PDEs are defined as follows:

$$A(u) = \begin{Bmatrix} A_1(u) \\ A_2(u) \\ \vdots \end{Bmatrix} = 0$$

( 2-3 )

where $u$ is an unknown function. The boundary conditions are represented by:

$$B(u) = \begin{Bmatrix} B_1(u) \\ B_2(u) \\ \vdots \end{Bmatrix} = 0$$

( 2-4 )

The aim of the FEM is to estimate the solution to $\hat{u}$ given by:

$$u \cong \hat{u} = \sum_1^r \psi_i a_i$$

( 2-5 )

where $\psi_i$ form the basis functions and some or all of the parameters $a_i$ are unknown.

A study by Taras P. Usyk and Andrew D. McCulloch was undertaken to develop an integrative computational technique for describing soft tissues based on FEM (Usyk, 2002). Steps followed in finite element methods outlined in the study are as follows:

1. Weighted residual is formulated.
2. Either the use of the Green-Gauss theorem to determine the vector or tensor variables, or integration by parts takes place.
3. Problem is discretized into subdomains.
4. Bubnov-Galerkin finite element equations are derived.
5. Element stiffness matrix is computed as well as the load vector.
6. Element stiffness matrices are then combined to form the global stiffness matrix, and the individual load vectors are combined to form the global load vector.
7. Important boundary conditions are applied.

8. Global equations are solved for the unknown nodal variables.

9. Element solutions are computed by the interpolation the dependant variables and finding their derivatives.

10. Solution is plotted and displayed on a graphical interface.

11. Finally a solution is successfully obtained and the mesh is refined and the solution process is repeated.

Generally a more accurate solution to the exact continuous solution can be obtained with higher order basis functions. To ensure the continuity of each subdomain, the individual solution is enforced across the elemental boundaries. In the case of this study, both tri-linear Lagrange and tri-cubic Hermite basis functions were used. The high order tri-cubic Hermite functions are defined using 8 derivatives at each nodal point; this ensures the continuity of the solution between neighbouring elements.

Another technique used to increase the accuracy of the solution is to increase the mesh density. In the case of highly complex structures, a finer mesh where more elements and more nodes are used is necessary. This allows the element boundaries to accurately form the entire structure. In particular, in regions where the variation in the solution is expected to be large, a greater mesh density in that region would increase the accuracy of the solution. Increasing the number of nodes and elements to an infinite number would then represent a real continuous model, but the greater the number of nodes and elemental points, the greater the number of PDEs and therefore the greater the time for calculation of the solution. This proves to have high computational cost. Another point that should be made is that the increase in accuracy of the solution approaches the exact continuous solution logarithmically. The Figure 2-10 represents this:
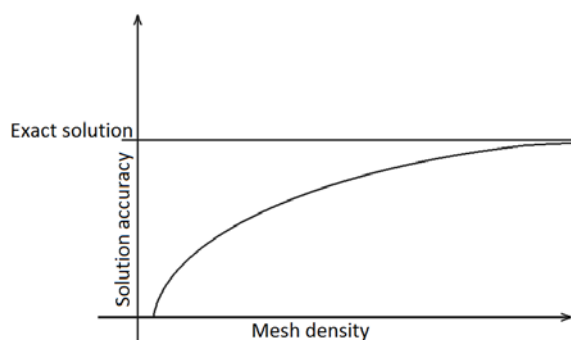


*Figure 2-10: Increasing mesh density to accuracy*

It is therefore seen that the computational time and cost starts to outweigh the increase in accuracy as the number of nodes and elements increase. Therefore it is necessary to

determine the degree of accuracy which would be deemed acceptable for a particular situation.

### 2.6.1 Biomechanical Model: Finite Element Method

Computational studies have been used to analyse cardiac functionality under various conditions. This has proved to be beneficial since it does not require invasive laboratory testing and it is also easier to define the exact conditions of the heart. In the case of laboratory testing, it is necessary to have many test subjects in order to obtain reliable results. In contrast, only one parameterized computational model can be used to model different responses. The results of the computational studies are only validated by experimental studies once the required predictions are achieved and verified.

#### 2.6.1.1 Geometry

The LV is responsible for pumping blood to the extreme parts of the body and therefore experiences greater pressures than the other cavities of the heart. Due to these high pressures, there are higher stresses and therefore the LV has often been modelled in previous studies. In cardiac modelling, many different heart geometries have been used. Some of these geometries have been simplified as an ellipsoid representing only the left ventricle. The ellipsoid approach tends to neglect the effect of the RV and the atria on the geometry. Although this is the case, the LV models are able to give an accurate prediction of the functionality and wall stresses since the internal loading on the LV is much greater than the external loading.

More recent studies have used biventricular geometries (Vetter and McCulloch, 2000, Kortsmit et al., 2012, Nash and Hunter, 2000, Aguado-Sierra et al., 2011) to include the effect of the RV on the function of the LV. Many of these models are simplifications of the realistic structure, such as modelling the LV as an ellipsoid with a pocket to represent the RV. Studies are moving toward using an accurate geometry of patient specific hearts (Miller, 2012, Aguado-Sierra et al., 2011), providing more realistic structures. Although these models still obtain many simplifications depending on the study, they give a good prediction of the heart functionality with taking into account with the LV and the RV.

Many different heart species have been used in literature for example ovine LV geometries have been used by Guccione et al. (2001) and Walker et al. (2005). Canine LVs have been modelled by Guccione et al. (1995) and Aguado-Sierra et al. (2011). In the study by Aguado-Sierra et al. (2011) a cardiac geometry containing both the left and RV was used. This is more accurate than simulating only the LV, but requires greater computational cost in terms of simulation time.

There are two main imaging methods which have been used in the reconstruction of the cardiac geometry; these are the MRI and CT. Due to the relatively high resolution in these images, they prove to be useful in the reconstruction stage of cardiac modelling. It is common that the geometry is created from a series of images built up by using slices of the short-axis images and assigning a mesh to the observed cardiac structure. Automated as well as semi-automated software have been developed to assign data points to the contours or the various regions of the heart structure. Many automated methods of assigning contour data from images are based on a threshold input by a user (Paragios, 2003). Conversely to the efficiency and accuracy of the automated methods, there have been some areas and sources of inaccuracies, namely; signal loss due to blood flow and partial volume effects (González Ballester et al., 2002).These inaccuracies make it difficult to attain a high level of accuracy in automated techniques. Deductions based on previous studies and reconstruction techniques were made by Kaus et al. (2004) in an attempt to fully automate the segmentation process.

Although MR and CT images are useful in the reconstruction of the cardiac geometry, due to the high resolution, in the case of very small geometries such as a rat or mouse heart, the resolution accuracy to structure size decreases significantly. Furthermore, there are challenges faced in the segmentation process, for instance, many geometries created from MRI's don't include the papillary muscles, the left and right atria, trabeculae or different cell types or tissue types. Burton et al. (2006) attempted using histological images to improve the tissue accuracy of MRI and DTMRI, this also involved incorporating fibre angles. In most computational studies though, the papillary muscles and atria are ignored as this is seen to increase the computation time without a great increase in the accuracy.

Lund University and Medico AB in Sweden have developed an open-source software package called *Segment (Sirry et al., 2013)* specifically for image analysis and segmentation of cardiovascular images. A semi-automated segmentation process is available within the software package, which allows for MRI, CT, positron emission tomography (PET) as well as single photon emission computed tomography. Another software package available for this purpose is the *ITK-SNAP* (Yoo et al., 2002), this software takes advantage of its semi-automated segmentation processes to segment and analyse various structures within the anatomy. It was noted by Yushkevich et al. (2005) that although *ITK-SNAP* has a wider range of application, the software requires the user to input a greater number of parameters. This creates room for input errors by inexperienced users, affecting the overall outcome of the segmentation.

After the segmentation process has been performed, the contour points or data set are imported into an FEM software where an elemental mesh is created to represent the cardiac structure. The FEM software Continuity uses a method known as the least squares method to fit a simple mesh to the more complex contours defined by the segmentation process. Previous studies show many simplifications that have been used in computational cardiac modelling. For instance, spheroidal (Beyar and Sideman, 1984), ellipsoidal (Wenk et al., 2009) are amongst other variations.

For the purpose of this study, the segmentation process was performed using the *Segment* package with the use of short-axis cardiac MR imagess and the meshing and modelling process used the FEM software *Continuity*.

### 2.6.1.2   Boundary Conditions

Boundary conditions of a cardiac computational modelling have the purpose of representing the external conditions to the model. External conditions which are described in cardiac modelling for example are the forces of the lungs and diaphragm on the epicardium as well as the connection of the ventricles to the arteries and vena carva. Accurately and carefully implemented boundary conditions can improve the accuracy of the simulation. These boundary conditions constrain the cardiac geometry which is used, to ensure greater stability.

In the case of the cardiac computational mechanics in this study, the base of the myocardium needs to be assigned a boundary condition to represent the connection to the systemic and pulmonic systems as well as the venous system. Furthermore, depending on the type of element method and cardiac modelling program used, more boundary conditions may be needed. The boundary conditions used in this study will be described in the methodology section.

### 2.6.1.3   Passive Material Properties

During diastole, the LV is passively filled with blood. In this phase, the myocardium tissue is not stimulated to contract. Consequently, the stress experienced by the myocardial tissue during diastole should be modelled using a function that describes only the passive mechanical properties of the tissue. This function is known as the strain energy function.

There are a few variations of strain energy functions used in cardiac modelling. Each variation has different parameters depending on the make-up of the function as well as the type of tissue being modelled. The material characteristics that affect these parameters include the stress-strain characteristics of the tissue. The parameters are also affected by how the tissue is modelled, for example, as compressible or incompressible; elastic,

viscoelastic or inelastic; and transversely isotropic or orthotropic. Other properties such as the stiffness of the material also change the value of the parameters of these strain energy functions.

Guccione et al. (2001) proposed a strain energy function which has been used often in the literature (Wenk et al., 2009, Dai et al., 2005, Wall et al., 2006, Sun et al., 2009, Christman et al., 2004). In one study where this function was used, passive myocardium tissue during diastolic filling is approximated using a nearly incompressible, transversely isotropic strain energy function (Kortsmit et al., 2012):

$$W = \frac{1}{2}C(e^Q - 1) + C_{comp}(I_3 ln I_3 - I_3 + 1) \qquad (2\text{-}6)$$

where

$$Q = b_{ff}E_{ff}^2 + b_{cc}(E_{cc}^2 + E_{ss}^2 + E_{cs}^2 + E_{sc}^2) + b_{fc}(E_{fs}^2 + E_{sf}^2 + E_{fc}^2 + E_{cf}^2). \qquad (2\text{-}7)$$

In Eq. (2-7), $E_{ff}$ is the fibre strain, $E_{cc}$ is the cross fibre in-plane strain, $E_{ss}$ is transverse to the fibre and is the radial strain. The shear strains are $E_{cs}$ in the transverse plane, $E_{fc}$ in the fibre-cross-fibre and $E_{fs}$ in the fibre − radial plane. The $b$ values are the fibre strain coefficient, transverse strain coefficient and transverse fibre shear coefficient respectively. $C_{comp}$ is the bulk modulus of the tissue and was set to 100 kPa and $I_3$ represents the volume ratio of the stretch tensor **U** (Kortsmit et al., 2012).

A strain energy function proposed by Holzapfel and Ogden is based on physiological considerations and is given by (Holzapfel and Ogden, 2009):

$$\Psi = \frac{a}{2b}e^{b(I_1-3)} + \sum_{i=f,s}\frac{a_i}{2b_i}(e^{b_i(I_{4i}-1)^2} - 1) + \frac{a_{fs}}{2b_{fs}}(e^{b_{fs}I_{8fs}^2} - 1), \qquad (2\text{-}8)$$

where $a, b, a_f, a_s, b_f, b_s, a_{fs},$ and $b_{fs}$ are parameters that are material dependant (Holzapfel and Ogden, 2009).

In a study performed by Lafortune et al. (2011), the cardiac model of a rabbit heart was modelled. The heart was modelled as compressible, transversely isotropic and viscoelastic tissue properties due to the presence of water within the myocardium. The strain energy function used is (Lafortune et al., 2011):

$$W = \frac{a}{2b}e^{b(I_1-3)} - \frac{a}{2}(I_1 - 3) + \frac{a_f}{2b_f}\{e^{b_f(I_4-1)^2} - 1\} + \frac{K}{2}(J - 1)^2. \qquad (2\text{-}9)$$

For a rabbit, healthy heart tissue the following parameters were used: $a$ = 4.3 kPa, $b$ = 9.7, $a_f$ = 1.69 kPa, $b_f$ = 15.78. Parameters describing the infarcted tissue were not found (Lafortune et al., 2011).

*I* is a strain invariant in terms of *b*, the first invariants are:

$$I_1 = tr\boldsymbol{b}, \qquad I_2 = ((tr\boldsymbol{b})^2 - tr\boldsymbol{b}^2), \qquad I_3 = det(\boldsymbol{b}), \qquad I_4 = f_0\boldsymbol{b}f_0 \qquad (\ 2\text{-}10\ )$$

*b* is the right Cauchy-Green deformation and is given by:

$$\boldsymbol{b} = \boldsymbol{F}\boldsymbol{F}^T \qquad\qquad (\ 2\text{-}11\ )$$

where *F*, is the deformation gradient.

The strain energy function used in a study by Lafortune et al. (2011) is similar to the Holzapfel and Ogden (2009) strain energy function. The first difference is the term J has been added. This term represents volumetric energy which allows for the material to be modelled as compressible. The second difference is the term $a/2(I_1 - 3)$, used to represent the initial conditions.

The strain energy functions described have been used often in cardiac modelling. Other strain energy functions have been used, but all seem to have a similar form and have similar parameters. The strain energy functions proposed by Holzapfel and Ogden (2009); and Lafortune et al. (2011) describes compressible material behaviour whereas the strain energy function proposed by Guccione et al. (2001) describes material properties that are incompressible. Since myocardium does display compressible behaviour and orthotropic behaviour, it would appear that the strain energy functions proposed by Holzapfel and Ogden (2009); and Lafortune et al. (2011) is a better approximation, but due to the greater complexity of the function it has not often been used.

### 2.6.1.4   Active Material Properties

Systole describes the phase of the cardiac cycle where contraction of the myocardial tissue occurs (Suga and Sagawa, 1974, Burkhoff et al., 2005). In the modelling of the systolic phase a function is required that can describe the stress and strain of the tissue caused by the active contraction of the myocardium (Guccione and McCulloch, 1993).

The electrical and mechanical properties are analysed separately by the use of different tests. The excitation contraction coupling is determined by the calcium ion concentration within the myocardium, and therefore there are many models made that are based on this property.

An active stress function proposed by Guccione and McCulloch (1993), where systolic contraction of the canine heart was defined by finding the sum of the passive stress and the active fibre directional stress. The active contraction model used in the study by Guccione

and McCulloch (1993) is the active contraction model chosen for use in *Continuity*. The active part is given by (Walker et al., 2005):

$$T_0 = T_{max} \frac{Ca_0{}^2}{Ca_0{}^2 + ECa_{50}{}^2} C_t \qquad (2\text{-}12)$$

where:

$$ECa_{50} = \frac{(Ca_0)_{max}}{\sqrt{exp[B(l - l_0)] - 1}} \qquad (2\text{-}13)$$

*and*

$$C_t = \frac{1}{2}\left[1 - cos\left(\pi \frac{0.25 + m \cdot l + b}{m \cdot l + b}\right)\right]. \qquad (2\text{-}14)$$

The model used by Lafortune et al. (2011) is simplified by the assumption that the active stress runs along the direction of the fibre only. The Cauchy stress is given by:

$$\sigma = \sigma_{pas} + \sigma_{act}(\lambda, [Ca^{2+}])\mathbf{f} \otimes \mathbf{f}. \qquad (2\text{-}15)$$

Here $\mathbf{f}$ in the stress equation is a unit vector which is aligned with the fibre. In order to calculate the active stress a model is proposed (Hunter et al., 1997, Lafortune et al., 2011):

$$\sigma_{act} = \frac{[Ca^{2+}]^n}{[Ca^{2+}]^n + C_{50}^n} \sigma_{max}\left[1 + \beta(\lambda_f - 1)\right]. \qquad (2\text{-}16)$$

Where $C_{50}$ is the intracellular calcium concentration associated with 50 % of the maximum stress, *n* controls the shape of the output curve. $\sigma_{max}$ Represents the maximum isometric active tensile stress created at the point where $\lambda_f = 1$ (Lafortune et al., 2011).

The active stress models used in cardiac modelling have similar forms dependent on the concentration of calcium ions within the myocardium. Both models described here have been based on experimental results and can be verified in comparing computational results to the experimental results.

### 2.6.1.5  Infarcted Myocardium

Infarcted myocardium becomes impaired and some physical characteristics present in the healthy myocardium are adversely affected. These characteristics are necessary for the heart to function effectively and therefore when compromised, causes a decrease in the overall performance of the heart. The affected characteristics include the ability of the myocardium to contract as well as the stiffness of the wall tissue. Firstly, the dead tissue
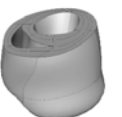
loses the ability to contract and therefore acts as passive myocardium. Secondly the stiffness is affected depending on the phase of healing after myocardial infarction. This has been explained in section 2.2. It should be noted that the infarcted heart geometry used in many studies contained an anterior apical (AA) infarct (Guccione et al., 2001, Walker et al., 2005, Sabbah et al., 2008, Kortsmit et al., 2012).

In cardiac modelling the tissue stiffness in the infarcted myocardium has been modelled as stiffness reduced to 50 % and 25 % of the healthy tissue (necrotic phase). Other parameters are kept the same as the healthy tissue. In the case where scar tissue is present, a drastic increase in the tissue stiffness as well as loss of all contractility within the affected tissue is modelled (Kortsmit et al., 2012). Guccione et al. (2001) used a stiffness increased by a factor of ten on a scar infarcted canine computer modelled heart. The study by Guccione et al. (2001), modelled the stress in the active myocardium as the sum of the passive stress from the strain energy equation and an active fibre directional stress component. In this study, the active contraction was turned off for the infarcted region. This was achieved by setting $Ca_0 = 0$ (Kortsmit et al., 2012). It was shown by Walker et al. (2005) that a 22 week old scar infarct had properties corresponding to a stiffness of 15 times the healthy tissue and displayed less anisotropic behaviour. The non-scarred tissue still displays some active properties which have a peak force 27 % less than that observed in the healthy tissue and the relaxation time was 17 % longer (Fishbein et al., 1978, Sabbah et al., 2008).

The region of tissue representing the transition from the infarcted region and the remaining healthy tissue is referred to as the BZ. In literature the BZ of the infarcted region has been defined differently from study to study. Some studies modelled the BZ by decreasing the maximum isotropic tension to 50 % of the healthy myocardium (Walker et al., 2005, Guccione et al., 2001). Another study modelled the BZ by varying the maximum isotropic tension from 0 % to 100 % of the healthy myocardium (Okada et al., 2010).

From the studies discussed, the infarcted tissue as well as the BZ tissue presents different characteristics and properties to that seen in the healthy myocardium. For this reason, the BZ needs to be defined separately from the healthy and infarcted myocardium to obtain accurate predictions of the cardiac performance. The properties and characteristics displayed by the infarcted tissue change depending on the phase of healing, for example the stiffness increases during the fibrotic phase. Therefore the time after the infarct should be noted when performing cardiac computational simulations. The research performed in this study deals with early infarcts. An early infarct is defined in this study as the stage before mechanical changes take place other than the loss of contractility within the infarcted region.

### 2.6.1.6 *Intramyocardial Biomaterial Injectates*

The hydrogel therapy of myocardial infarction is a process whereby a biomaterial is injected into the myocardium, either in or around the area of the infarction. Studies have been performed to determine the effect of hydrogel injection on cardiac performance and biomechanics.

There has been previous research done on hydrogel injection using finite element modelling and computer simulations to determine the effects of the hydrogel in the treatment of myocardial infarction. Wall et al. (2006) determined the effect of a non-contractile injectate on the wall stress in the LV. Due to the increased wall thickness from the injected biomaterial, the wall stress is lowered. The results show that with a volume of injectate 4.5 % of the LV wall, with stiffness 20 % that of the healthy myocardium, a reduction in the wall stress of an infarcted heart of approximately 20 % can be obtained when compared to a simulated control. It was also found that the stress could be further lowered with an increased amount of injectate volume as well as an increase in the stiffness of biomaterial (Wall et al., 2006).

Wenk et al. (2009) described the development of a technique to automatically optimise the injection distribution pattern of the hydrogel, using a computer package called FE pre-processor TRUEGRID and FE software LS-DYNA. For the purpose of optimization the package LS-OPT was used. A canine heart model was used in this study. The target aim was to minimize the mean end-diastolic and end-systolic myofibre stresses within the LV wall tissue. In addition, the SV of the LV should be maximised in order to successfully identify the optimized injection pattern. The hydrogel injection deposits were simulated as spherical deposits within the cardiac wall. A set pattern distribution form was used, in other words, there were a total number of 30 differing distributions of the biomaterial that were analysed. The goal of this study was achieved in the sense that the study claims that a method for automatically optimizing vital design characteristics had been developed. There are some limitations though, for instance the hydrogel deposits were estimated to be spherical inclusions, and this is unlikely in reality. These inclusions would logically be more of an ellipsoidal shape due to filling of the hydrogel between layers of cardiac tissue. There were a few aspects that were not investigated such as the optimization of the amount of biomaterial injected each time. In addition, a simplified model of the LV was used without including the RV and the atria (Wenk et al., 2009).

Previous studies on numerical simulations based on this technique have been simplified models. A recent study uses a more realistic computational simulation of a distribution of injected biomaterial within the myocardium (Kortsmit et al., 2012). In this study the effects

on cardiac function as well as the effects on biomechanics of the heart tissue are studied. Four different chronological stages of the heart remodelling were studied and simulated using *Continuity®6.3b* (University of California in San Diego, CA, USA). This was achieved by using a validated finite element heart geometry with an anterior apical infarct present. It was found that the hydrogel had a positive effect on the infarcted heart in the early stages of remodelling, whereas in the latter stages, where scarring was present, no effect was observed (Kortsmit et al., 2012).

Furthermore histological studies show that the distribution of hydrogel is most accurately represented by thin layers for early infarcts, but thicker layers in older infarcts (Kadner et al., 2012). These findings can be seen in Figure 2-11 below. Thin layers were found to be difficult to achieve when higher order finite elements are used in computational methods. Methods used to model the hydrogel use bulk layers of a mixture of hydrogel and infarcted tissue.
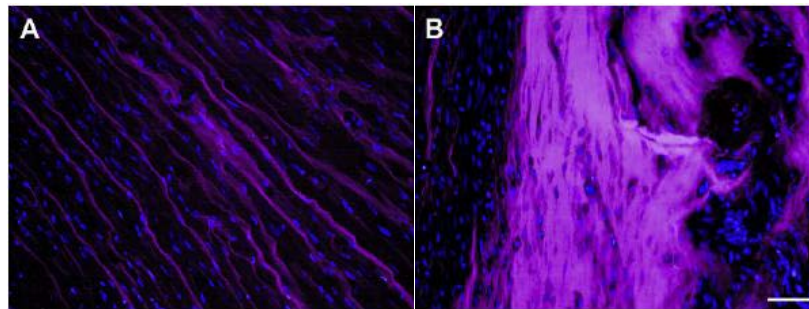


*Figure 2-11: A: Hydrogel injection into and early infarct. B: Hydrogel injection into an old infarct. (Kadner et al., 2012)*

Some studies performed previously, implemented the hydrogel layers as purely hydrogel element layers (Miller, 2012). These element layers are not as thin as the realistic case observed in the figure above and therefore are an estimation of the real case. In these cases the stiffness of the hydrogel used was half that of the healthy tissue and the other material properties were all taken to be constant to represent homogeneous material properties (Kortsmit et al., 2012).

Wall et al. (2006) used a method where injection regions were defined along the BZ of the infarct. The material properties in this region represented a material that consisted of both BZ and hydrogel. A volume mixing rule was used to determine these combined hydrogel and tissue material properties.

The delivery of hydrogels into the myocardium has proved to have potential benefits in the treatment of myocardial infarction (Nelson et al., 2011). Many different hydrogels have been used, each containing their own mechanical properties and characteristics. When hydrogels are modelled it is clear that the material properties need to be defined separately from both the healthy and the infarcted tissue. The hydrogel may for instance display different stiffness characteristics and will not be able to contract. Therefore the hydrogel used in any study should be clearly defined and must be based on experimental tests.

### 2.6.2  Optimisation

In spite of significant research performed on biomaterial injectates as a form of treatment for myocardial infarction, there is uncertainty as to which parameters and mechanical properties (e.g. the stiffness) of the hydrogel cause the greatest improvement to the cardiac performance. The parameters of the hydrogel include the volume of the injectate, the number of injection sites, and the position of the injections (e.g. either directly into the infarcted region or around the edge of the affected tissue) (Wall et al., 2006). It is expected that these parameters will have an effect on the healing process and therefore the cardiac performance, but the precise effects are unknown. A separate issue brought up in an article from Nelson et al. (2011) states that studies in this field tend to perform tests or analyses on dissimilar scenarios. For example the time at which the biomaterial was injected varies from minutes to days after the infarction. It would seem that the sooner the injectate is injected after an infarct, the better in order to prevent adverse remodelling effects. Although this is the case, Kadner et al. (2012) suggested that greater benefit can be achieved from later injections. Additionally, there are other variables that differ from study to study; these include the type and extent of the infarct itself. For example, the more severe the infarct, the longer it will take to recover as well as the smaller the chance of recovery and the greater the adverse effect on the ventricular performance. Furthermore, there is also the issue of differing types of biomaterials used in literature.

It is recognised that more design parameters are necessary for optimizing the volume of injectate effectively. Greater consideration will need to be taken with regard to the shape of the deposits or inclusions. The effects on contractility of the cardiac tissue would also need to be analysed (Wenk et al., 2009). The optimization process in this study mainly looks at the most effective volume of hydrogel for set infarct sizes. This aims at finding a relationship of hydrogel volume to infarct size which could be a useful tool in a clinical application. The study does not address the issue of how deep the inclusion should be. It also does not address the issue of determining whether it would be more effective for the

inclusion to be directly within the affected myocardium or along the border of the affected myocardium.

# 3   Methodology

## 3.1   Process of Creating the Rat Cardiac Model

### 3.1.1   Geometry

To begin, it was necessary to create a validated cardiac geometry. This involves firstly obtaining a set of MRI's of a healthy rat heart (Saleh et al., 2012). The healthy case was then modified to implement an infarcted region for each case simulated and analysed. The healthy case acted as the control to which all other simulations were compared. The final step was then to implement various volumes of hydrogel into the infarcted regions and determine the effect.

Once the healthy case was simulated, the infarcted models with and without hydrogel injectate was simulated. Three infarct sizes were modelled namely 10 %, 20 % and 38 %. The hydrogel injectate models included 25 % gel, 50 % gel and 75 % in the 10 % infarct, with additional models of the 20 % infarct with 50 % gel and the 38 % infarct with the 25 % hydrogel treatment.

It is important to clearly define the time point at which the study is performed since the material properties of the infarcted myocardium do not remain constant after ischemia occurs. Table 3-1 shows a closer look at some of the important properties to be considered at the early and late time point after an infarct. It was decided to model the early stage infarcts since treatment for a heart attack is performed as early as possible. In the table, the $W_T$ represents the wall thickness; the subscripts H, I and G represent healthy, infarcted and hydrogel models respectively.

*Table 3-1: Comparison of early and late stages post infarction*

|  | Early (Ischemic phase) | Late infarct (Remodelling phase) |
|---|---|---|
| Tissue stiffness | Decrease | Increase |
| Cavity volume | Constant to small increase | Large increase |
| **Wall thickness** |  |  |
| Without hydrogel | $W_{TH} = W_{TI}$ | $W_{TI} < W_{TH}$ |
| With hydrogel | $W_{TIG} > W_{TH}$ | $W_{TIG} \approx W_{TH}$ |

The rat heart geometry which was created is a 4 week 290 g sham rat heart at the stage of end systole. The sham rat hearts in the (Saleh et al., 2012) study experienced all procedures of the test samples except ligation of the left anterior descending coronary artery. The end-systolic point was used as a simplification to the unloaded heart. The unloaded state is the state in which the heart experiences zero external forces or pressures. This unloaded state is not experienced during the cardiac cycle and therefore it is not feasible to obtain MRI's of the unloaded state. The geometry was created based on MRI's to obtain an accurate geometry of the rat heart. In previous studies (Guccione et al., 1995, Janz and Grimm, 1972) simplified models were used, and therefore it was seen to be necessary to attempt to create a model of greater geometric accuracy without increasing the complexity of the geometrical structure to such an extent that the simulation time would increase significantly.

The software package *Segment* (Heiberg et al., 2010) was used to define the main regions of the heart within the MRI's. These regions were the LV cavity, RV cavity and the epicardium. The segmentation process used an automated algorithm to determine the required borders of each region (Heiberg et al., 2005). Manual adjustments were performed to remove the undesired effect of papillary muscles and valves. This procedure involved the creation of data points/contour points which are used to represent the edge of the various regions within the cardiac geometry. Data points of the LV, the RV and the epicardium were obtained from a set of 11 slices of MRI's. The data set comprised short-axis cine images which were obtained using an ECG with respiratory gated cine FLASH procedure. The parameters used were: Ratio of repetition time (TR) to echo time (TE): 7.7/3.5 ms, resolution: $0.234 \times 0.234 \times 1 \text{mm}^3$ and a flip angle of 25-40° with the number of signal averages of 3 (Saleh et al., 2012). Figure 3-1 is a sample image from the set of MRI's used.
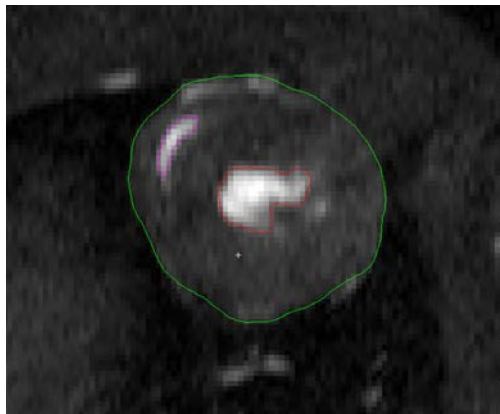


*Figure 3-1: Sample MRI showing the segmented regions of the rat heart. Red, purple and green represents the LV, RV and epicardium respectively*

The LV data points were observed from the basal most slice to the 10<sup>th</sup> MRI slice and the RV had data points present from the basal most slice to the 7<sup>th</sup> MRI slice. Each data set for each image slice contained a total of 80 data points. The dimension of the data points that were exported from Segment used pixels with mm/pixel scale of 1.875. Before importing the data points into Continuity, the z-dimensions needed to be included into the data set. Each Image has a thickness and gap between slices, therefore the z-dimension was adjusted appropriately. The data points for the geometry were then imported into Continuity with these dimensions in mm. Figure 3-2 shows the data set that was defined from the software package *Segment* and viewed using the software package *Continuity 6.4*.



*Figure 3-2: Data points of an end-systolic 4 week sham rat heart*

### 3.1.2  Finite Element Model

The contour points were then imported into *Continuity 6.4* onto which a mesh was fitted. The coordinate system was set to prolate spheroidal with a focal of 9.0. Basis functions that were set for the starting point were bi-cubic Hermite 3*3 and bi-linear Lagrange 3*3.

The mesh that was used for the fitting was a standard ellipsoidal mesh. With only one cavity, this standard mesh needed to be modified by adding extra nodes and elements to incorporate the second cavity, the RV. Modifications to both the nodal coordinates as well as the derivatives of these nodal values were adjusted to obtain a suitable and acceptable fit for the data set. The derivative values define the gradient of the element boundary leaving each node.

The fitting of the mesh in *Continuity* is an automated process where only constraints and weighting is needed to ensure a successful fit. This automated process uses a least-squares mesh fitting method to match the mesh as close as possible to the data set. The constraints or boundary conditions to be added were used to constrain the apical nodes such that they remained constant relative to each other. Due to the meshing method used within *Continuity 6.4*, the mesh contains a "hole" at the apex of the LV; therefore the constraints

remove the effect of the "hole", preventing this from enlarging. Other boundary conditions were also needed for the running of the simulations and are explained in greater detail in section 3.1.4. Weights were added for the fitting calculation to successfully calculate the derivatives between the nodes. These weights were as follows:

*Table 3-2: Weighting for mesh fitting*

|  | Coordinate 1 | Coordinate 2 | Coordinate 3 |
|---|---|---|---|
| Wrt s(1) | 0.5 | 0.5 | 0.5 |
| Wrt s(1)s(1) | 0.5 | 0.5 | 0.5 |
| Wrt s(2) | 0.01 | 0.01 | 0.01 |
| Wrt s(1)s(2) | 0.02 | 0.02 | 0.02 |
| Wrt s(2)s(2) | 0.01 | 0.01 | 0.01 |

All other weights were set to zero. Once these steps were completed, the fitting of the mesh to the data points was complete. A series of fitting procedures needed to be performed to ensure increased accuracy. The epicardium, LV endocardium and RV endocardium are all fitted separately, and therefore the respective data points to elements need to be indicated. Manual adjustments were made to improve the accuracy and remove possible regions of error within the mesh.

At this point, each surface was represented by a surface mesh, that is the LV and epicardium meshes were not yet connected. This surface mesh was joined to other surfaces to create a 3D mesh composed of Hermite elements. The elements were defined using Microsoft excel and imported into Continuity. Basis functions are used in Continuity to compute stresses, strains and deformations. The basis functions were redefined to: Cubic-Cubic-Linear 3D Hermite function, Cubic-Cubic-Cubic 3D Hermite function and Linear-Linear-Linear 3D Lagrange function. For coordinate 1 in the nodes form the basis function was set to Cubic-Cubic-Linear, whereas for coordinates 2 and 3 the function was set to Linear-Linear-Linear. For the field variable 1 of the field vector the function was set to Cubic-Cubic-Linear.

Once the derivatives had been recalculated for these higher order elements, the basis functions for the coordinates as well as for the field variable 1 were set to tri-cubic coordinates. Figure 3-3 shows the fitted mesh and the final 3D rat heart geometry. This

mesh is composed of 40 tri-cubic Hermite elements and 77 nodes. The mesh was later refined through the transmural direction, rendering 80 elements and 127 nodes.
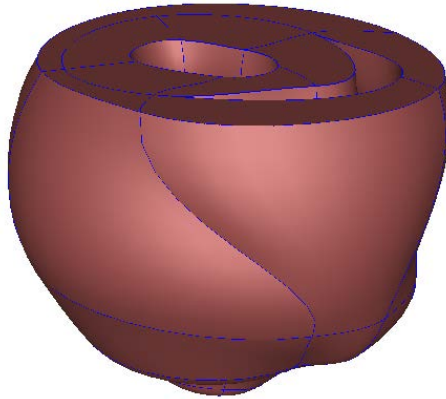


*Figure 3-3: 4 week sham rat heart geometry*

The next step was to create the fibre field for the rat heart geometry. It has been shown that there are no significant changes in the fibre orientation from diastole to systole (Zienkiewicz, 1967) and therefore the simplification that fibre orientation remains constant has been used. Although there is very little information on the orientation of the myofibres of myocardium specifically for the rat heart, fibre orientation which have been used are 90° at the epicardial surface following the dominant fibre direction to an angle of 90° at the endocardial surface (Janz and Grimm, 1972, Klein, 1970). A more recent study by Omens et al. (1993) shows that the fibre angle rotates from 52° on the epicardial surface to 53° on the endocardial surface. Since the geometry in this study is a biventricular geometry, both the fibre orientations in the left and RV walls needed to be defined. It has been shown in other animal species, for instance the canine model developed by Nielsen et al. (1991) that a discontinuity is observed in the junction between the septal wall and the RVFW. For the sake of this study, a simplification was made such that FEM errors would be avoided due to the observed discontinuity. The fibre orientations for the endocardial and epicardial surfaces were set while no constraints were defined for the fibre orientation on the endocardial surfaces of the RV, ensuring continuity of fibre angles throughout. The fibre orientation constraints were set by assigning transmural fibre angles to the nodes on the LV endocardial surface and on the epicardial surface. The derivatives were then recalculated to obtain the smooth transition of fibre angles from the epicardial surface to the endocardial surface. The geometry was then complete and ready for the biomechanical simulations. The fibre angle, transverse angle and the sheet angle were set to have tri-linear basis functions.
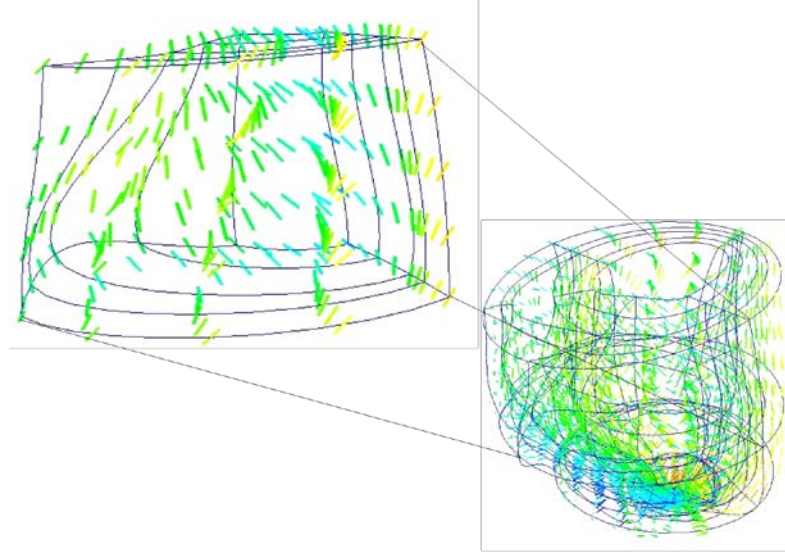
*Figure 3-4: Fibre orientation through the transverse plane*

Although studies performed in Aukland (LeGrice et al., 2001) indicate that changes in the fibre architecture are recorded in the infarcted region post-infarction, the infarcts modelled in this study are taken to be early infarcts which have not yet undergone any of these changes. Therefore, the fibre orientation used for the infarcted regions was taken to be the same as for the healthy case.

The geometry was then converted to Cartesian coordinates and the nodal and element information was saved. A new model was then created using the nodal and elemental coordinates.

### 3.1.3   Constitutive Modelling

#### *3.1.3.1   Modelling of a Healthy and an Infarcted Rat Heart*

In cardiac modelling, a constitutive model is used to describe the material behaviour to determine the pressure volume relationships during the cardiac cycle. The myocardium during the diastolic phase has been described as being nearly incompressible (Liu et al., 1994). To simulate the effect of a nearly incompressible material it is necessary for the strain energy function to be divided into a dilation component and a deviatoric component (Weiss et al., 1996). The strain energy function that was used in this study has been mentioned previously in the literature; section 2.6.1.3.:

$$W = \frac{1}{2}C(e^Q - 1) + C_{comp}(I_3 ln I_3 - I_3 + 1)$$

(3-1)

where

$$Q = b_{ff}E_{ff}^2 + b_{cc}(E_{cc}^2 + E_{ss}^2 + E_{cs}^2 + E_{sc}^2) + b_{fc}(E_{fs}^2 + E_{sf}^2 + E_{fc}^2 + E_{cf}^2).$$

(3-2)
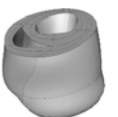
An extensive description of this strain energy function can be found in section 2.6.1.3. From equation ( 3-1 ) it is seen that the second term represents the nearly incompressible nature of the material, it represents the penalty function (Doll and Schweizerhof, 2000). $C$ in equation ( 3-1 ) denotes the stress scaling factor, which gives a measure of the stiffness of the myocardial tissue. $I_3$ represents the determinant of the deformation gradient. The exponent $Q$ in equation ( 3-2 ). The coefficients denoted as $b_{ff}$, $b_{cc}$ and $b_{fc}$ represent the strain characteristic properties of the material of interest, and is the fibre strain coefficient, the cross-fibre strain coefficient and the shear strain coefficient respectively. Furthermore $E_{ff}$ is the in-fibre strain; $E_{cc}$ is the in-plane, cross-fibre strain; $E_{ss}$ represents the ventricular radial strain, taken to be transverse to the fibre; $E_{cs}$ is the shear strain in the transverse plane; the in-fibre – cross-fibre shear strain is given by $E_{fc}$ and similarly the in-fibre – radial shear strain is given by $E_{fs}$.

The geometry of the healthy rat heart was the control used for the purpose of comparison and is used as the benchmark for the optimal cardiac function. The tissue in this heart has full contractility, and the myocardium throughout is defined using the parameters that represent the healthy myocardial tissue. These parameters that are used were based on a study by Omens et al. (1993):

| | |
|---|---|
| $C$ (kPa) | 1.1 |
| $b_{ff}$ | 9.2 |
| $b_{cc}$ | 2.0 |
| $b_{fc}$ | 3.7 |
| RMS error | 0.0071 |

The RMS error indicates the root-mean-square difference between the experimental strain values and the computational prediction of the strain (Omens et al., 1993). These material parameters were adjusted based on the stress and strain outputs when compared to literature. The final passive material property values for both the healthy and the infarcted tissue were equivalent since the early ischemic phase was modelled and no effect is observed on the passive properties of the myocardium. These values are:

| | |
|---|---|
| C(kPa) | 2.0 |
| $b_{ff}$ | 9.2 |
| $b_{cc}$ | 3.0 |
| $b_{fc}$ | 3.7 |

These values yielded stress and strain results closest to those found by Omens et al. (1993).

The systolic phase in the cardiac cycle requires an additional component added to the strain energy function described for the passive material properties. This component is known as the active component. The active component used in this study has also been described earlier in section 2.6.1.4. For the case of the active component, an algorithm is needed to describe the stresses and strains experienced during the systolic phase of the cardiac function. For the purpose of this study an algorithm governed by the calcium concentrations within the myocardium was used. This active component is defined by an active fibre directional component ($T_0$), maximum calcium concentration within the tissue ($Ca_0$), the sarcomere length where there is no active tension observed ($l_0$), the peak isometric tension taken at the longest sarcomere length ($T_{max}$) and sarcomere length with no stress present ($l_R$). The active component is as follows:

$$T_0 = T_{max} \frac{Ca_0{}^2}{Ca_0{}^2 + ECa_{50}{}^2} C_t \qquad (\textit{3-3})$$

where:

$$ECa_{50} = \frac{(Ca_0)_{max}}{\sqrt{exp[B(l - l_0)] - 1}}, \qquad (\textit{3-4})$$

$$C_t = \frac{1}{2}\left[1 - cos\left(\pi \frac{0.25 + m \cdot l + b}{m \cdot l + b}\right)\right].$$

Here $m$ represents the gradient and $b$ the time-intercept of the linear relaxation duration-sarcomere length relation. These are constants and were taken to be $m$ = 1.0489 s/μm and $b$ = -1.429 s (Guccione and McCulloch, 1993). Additionally, equation ( 3-4 ) $ECa_{50}$, which is dependent on the sarcomere length, has constants, B, a constant giving the shape of the peak isometric tension to sarcomere length relation. The value of B is taken to be 4.75 μm$^{-1}$. The material constant $(Ca_0)_{max}$ shows the maximum peak to the concentration of intracellular calcium (Guccione and McCulloch, 1993) and is taken to be 4.35 μmol/l (Ter Keurs, 1983), $l$ is dependent on $l_R$ the sarcomere length at its stress-free state. The sarcomere length at zero tension is denoted by $l_0$ with a constant value of 1.58 μm (Ter Keurs et al., 1980).

Additionally, the other values used for the material constants for the systolic phase are 1.85 μm for $l_R$ with $T_{max}$ = 135.7 kPa (Guccione and McCulloch, 1993); $Ca_0$ equal to $(Ca_0)_{max}$ with a value of 4.35 μmol/l (Ter Keurs, 1983).

The values for the active contraction discussed are the values used for the healthy heart. In the case describing the non-contractile tissue, that is the infarcted tissue and the hydrogel, the parameter for the calcium concentration $Ca_0$ was set to zero. This consequently showed zero contractile ability since contraction is directly dependent on calcium concentration within the tissue. For tissue with partial contractile ability, that is in the case of the BZ, the value for this calcium concentration was set to half that of the healthy case (2.175 µmol/l). This ensured that the BZ retained partial contractility, with some loss in contractile ability.

### 3.1.3.2    Constitutive Model for Hydrogel Injectate

Gel material does not have the same material properties as that of the myocardium. The lack of contractile ability and fibre structure as well as the gel having uniform mechanical properties throughout emphasise this point. It was therefore important to find a way to best describe this material such that accuracy in material definition was achieved. The material properties used to describe the gel used in this study were taken from an experimental study (unpublished data); the gel used is vinyl sulfone derivatized polyethylene glycol (PEG). The mechanical testing on the gel was performed using a method based on the procedures and set-up used by Cox et al. (2008). Figure 3-5 shows the set-up used for the mechanical testing of the hydrogel.
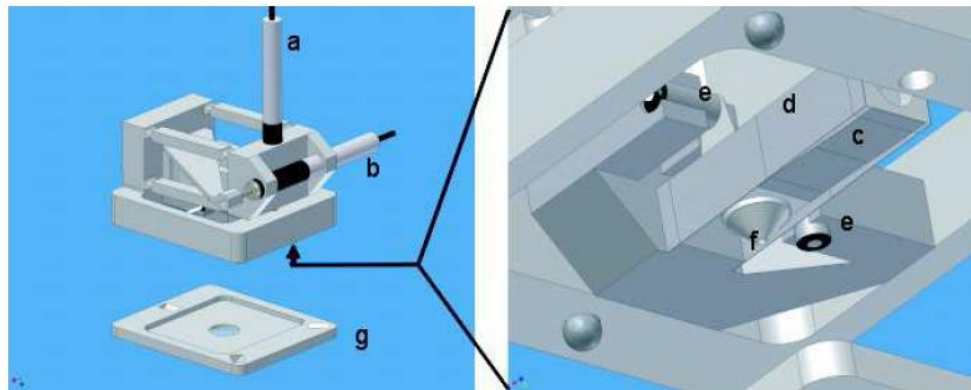


*Figure 3-5: Illustration of the force displacement apparatus (a and b are the vertical and horizontal actuators; c and d are leaf springs; e represents the capacitive sensors; f is the spherical indenter and; g is the counter plate) (Cox et al., 2010)*

Six gel disc samples were each subjected to three quasi-static indentation tests at different locations. The indenter used was spherical with a diameter of 2mm and a displacement rate of 0.01 mm/s was used. Furthermore three indentations were performed at each location where the force displacement and indentation depth was recorded (unpublished data, C.K. Chai, F.P.T. Baajiens, Department of Biomedical Engineering, Eindhoven University of Technology). In these tests, the first indentation was considered as preconditioning (Cox et

al., 2010) and therefore the force displacement data was only taken for the second and third indentation.

The material data obtained from the mechanical quasi-static indentation tests were used with inverse methods using computational software Abaqus® to determine the material properties of the hydrogel (unpublished data, L. Dubuis, Cardiovascular Research Unit, University of Cape Town). It was found that the material properties of the gel could be described using a neo-Hookean incompressible term. This neo-Hookean term was added to the current strain energy function to accurately represent the gel material properties. The term used to calculate the right Cauchy-Green stress representing the gel material properties is show below:

$$W_{gel} = 2 \cdot C_{10} \cdot (\overline{I_1} - 3),$$  *( 3-5 )*

where $C_{10}$ is a material determined neo-Hookean parameter, it represents the elastic modulus of the material. From the inverse methods a value of 0.0123 MPa was found for $C_{10}$. The complete strain energy function was made up using three terms:

$$W = \alpha \cdot W_{healthy} + \beta \cdot W_{infarct} + \gamma \cdot W_{gel}.$$  *( 3-6 )*

In this function $\alpha$, $\beta$ and $\gamma$ represent the ratio of healthy, infarcted and gel material respectively in the tissue.

### 3.1.4 Boundary Conditions

For both the diastolic and systolic situations, the boundary conditions were set to be the same. Boundary conditions were applied to the coordinates of the basal nodes as well as the derivatives in the circumferential and transmural directions of these nodes, limiting the extension of the epicardial base, and thus simulating the effects of stiff valve annuli. The heart was therefore anchored at the base to prevent rigid body movement. Futhermore, the basal nodes were constrained fully in the longitudinal plane. These boundary conditions allowed the basal nodes to expand and contract to allow for the filling phase and the contraction phase. For the case of the apical nodes, they were fixed relative to each other; derivatives in the longitudinal and circumferential directions were fixed to prevent unrealistic deformations and to remove the effect of a "hole" (Guccione et al., 1995, Vetter and McCulloch, 2000). The apex though was allowed to move in space including rotation as well as linear movement, this allowed for effective filling and contraction.

#### 3.1.4.1 *Mathematical Implementation of the Boundary Conditions*

The mathematical implementation of the boundary conditions that were applied are described below

The initial condition for boundary coordinate 1 was set such that the first derivative as well as the derivatives which have the first derivative as a constituent of the most apical nodes were set to zero. In the case of the deformed coordinate 1 all the base nodes were set to be constrained in the location (value), s(1) derivative, s(3) derivative and the s(1,3) derivative. The apical nodes were all set to be constrained by setting the displacement of the derivatives for s(1), s(2), s(1,2), s(1,3), s(2,3) and s(1,2,3) to be constrained. The apical boundary conditions were set to ensure that the apical nodes did not move relative to each other such that the "hole" described earlier would not affect the results. The external pressures were set to circulatory model and defined according to:

- The right ventricle free wall elements (RVFW) were set to have pressure on the inner surface of the free wall endocardium.
- The epicardium (Epi) elements were set to experience external pressure on the outer surface of the epicardium.
- The right ventricle septum (RVSEPTUM) elements were set to experience external pressure on the outer surface of the RV septum.
- For the left ventricle (LV) elements, the external pressure was set on the inner surface of the LV endocardium.

These boundary conditions were the same conditions used for the canine model in the study by Kortsmit et al. (2012).

### 3.1.5   Loading

#### 3.1.5.1   EDPVR Loading

For the loading in the model of the healthy heart, all conditions were set such that the strain deformations matched the MRIs. The loading in this case involved a linear increase in the pressure in both the LV and RV of 0.01 and 0.0053 respectively. The loading conditions were taken to start at zero load where the heart would be in the complete relaxed state and was stopped at a pressure of 3.36 kPa at which the corresponding volume compared to the MRIs which represented the ED point. This pressure for EDP was taken to be the same for all simulations.

#### 3.1.5.2   ESPVR Loading

In the case of the RV loading conditions, a linear increase in volume circulation model was used, where the volume was kept constant in both the LV and RV. The external pressures included in this stage were the same as in the EDPVR simulations. The start of the ESPVR is marked by the x-intercept on the pressure volume curve. This point is known as the dead volume and is found by extrapolating the curve to the x-axis. Three points are needed to

determine the ESPVR and therefore three simulations are run for each case. Each point is found by running a simulation from a given pressure state and deformation condition obtained from the simulation of the EDPVR. In all simulations, the corresponding pressure points used were 0.03, 0.5 and 1.0 kPa. The ESP point of interest was taken to be 14 kPa, and corresponding stresses and strains were extracted from this point. In Figure 3-6, the method of finding the ESPVR is seen graphically.
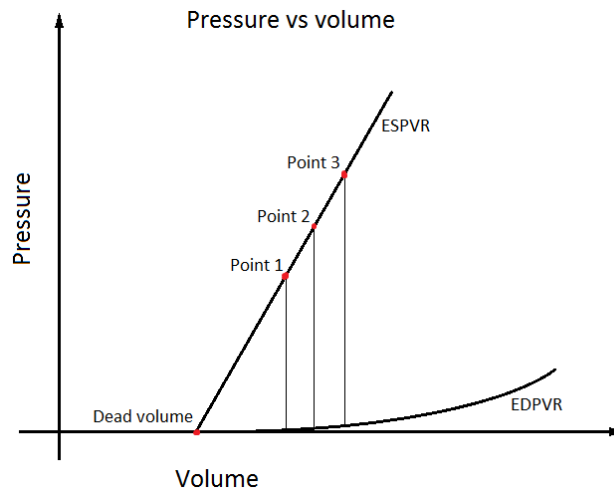


*Figure 3-6: Creating the ESPVR using the three points method*

## 3.2   Model Verification

This section covers the verification of the geometry using the volumes measured in the LV and RV from the MRI's. The units of measurement used in the study of rats are in the order of microliters. In literature the volumes vary widely. A study by Pacher et al. (2004) showed that the volume of the LV at end systole was approximately 75 microliters for fischer male rats. Dai et al. (2005) show an end-systole LV volume of about 180 microliters for fischer rats. The volumes for the geometry used after the mesh was fitted were determined and compared with the volumes obtained from the MRI's.

The Figure 3-7 shows the image of the segmented geometry. Here the green surface represents the epicardium, the red represents the LV cavity and the purple represents the RV cavity.
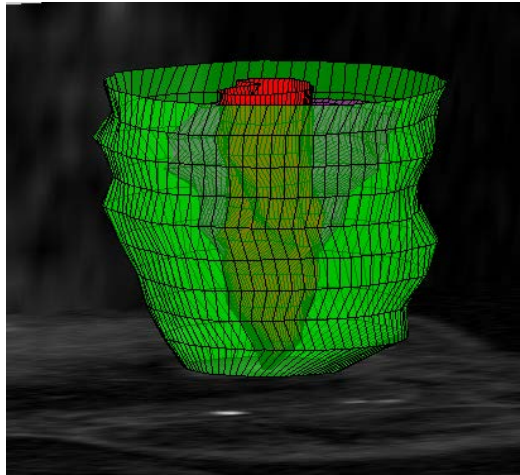
*Figure 3-7: Segmentation geometry*

For the circulatory model, a linear increase in the pressure for both the left and the right ventricle was used.

## 3.3 Infarcted Models

Since myocardial tissue is supplied with oxygenated blood by the coronary arteries which run from the base to the apex of the heart, it is expected that an occlusion of a coronary artery would prevent blood supply any point supplied by that artery closer to the apex. In confirmation with this, Heger et al. (1979) indicated in their study that most infarcts cause asynergy in the apical regions of the LV. Furthermore a study by Thanavaro et al. (1982) indicated that 55.3 % of 1105 patients with myocardial infarction had an anterior infarct.

Two methods can be used to define a region of material that is different to that of the other material present. The first of these methods uses elements to define the material of the respective region. In this case, the relevant elements are selected and their material properties are set to be different from the rest. The other method uses a predefined set of field variables as the new material. This method requires more time to define the region, but the region can be more accurately described as these field variables can cross elemental boundaries and therefore do not have rigid boundaries and borders. Another benefit of using the field variable method is that once the respective field variables have been defined as the new material, a transition boundary can be easily implemented and thus a BZ can be easily defined. The BZ of an infarct possesses partial contractile ability, therefore retaining some of the characteristics of the healthy tissue, but with some functional loss. The Figure 3-8 shows a view of the geometry of the rat heart used in the study from the anterior apical point. The infarcted region in blue and the healthy tissue is represented by the red; the BZ is shown by the multi-coloured region marking the transition

between the infarcted area and the healthy tissue. This was obtained using the field variable method.
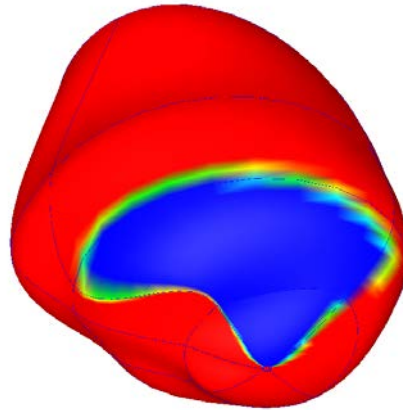


*Figure 3-8: Infarcted region in blue; Healthy region in red; BZ as the multi-coloured region*

The process whereby the field variables were implemented is described in the following section.

### 3.3.1 Field Variables

To implement field variables into a model, the field variables need to be defined and set. Field variables are the number of points within an element used to define the material properties at that point. The number of field variables per element is set by the user within *Continuity* for each of the coordinate directions. Thereafter the field variable points are evenly spaced throughout each element, allowing for the material properties within the element to change. Furthermore, each field variable could represent different material properties from those field variables within the local vicinity. The benefit of using field variables in a model is that a realistic region of differing material properties can be clearly defined. Additionally, a gradient exists and can be weighted between field variables, causing the transition from one region to the next to either be rapid or slow. By using this correctly, a BZ can be accurately modelled. Figure 3-9 represents the distribution of 5x5x5 field variables for one element.
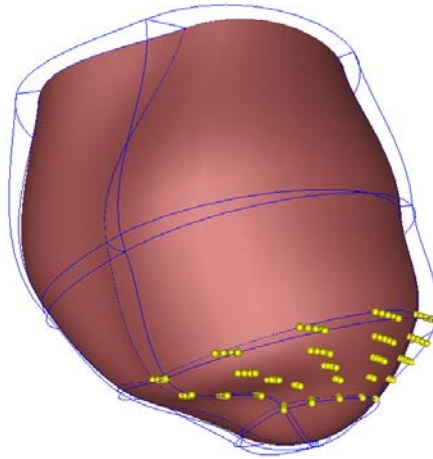
*Figure 3-9: Field variables of one element*

The number of field variables is defined in a matrix set per element. The set of field variables used for this study were 5x5x5 yielding 125 field variables per element, and therefore 10,000 field variables for the entire geometry. More or less field variables can be set, but it was found that using this configuration was the most effective. More field variables increase the calculation time, whereas less, decrease the accuracy of the geometry definition.

Since the model does not automatically create field variables, these points need to be assigned to the geometry. Furthermore, a value is assigned to each field variable to represent various regions of the geometry. Each field variable by default has a value of 2; therefore a value of -2 was assigned for all the field variables within the infarcted region. The field variables with their assigned values are then imported into *Continuity* as a data set and are added to the model using the fitting function. The fitting of the field variable data set follows the same process as the fitting of the mesh onto the data from the segmentation.

After the fitting of the field variables, a range of values are obtained displaying a transition zone from the infarcted region to the healthy region. This transition zone is dependent on the weighting method used as well as the difference in field variable value. For the case of this study a weighting of 1 to 1 was used, therefore representing a linear transition from one region to the next. Additionally, the transition zone was used to define the border zone of the infarcted tissue, where partial contractility is observed. For the case of this study, the all field variables in this region were set to have 50 % contractile ability. The width under these conditions described included about one field variable. Therefore, the border zone included one field variable thickness around the infarct region. The importance here is that

this forms an estimation of the border zone and further studies should be performed to define this region more accurately.

## 3.4 Hydrogel Implementation

From section 2.6, for hydrogel injection into an early infarct, the hydrogel would be best represented by very thin layers within the infarcted tissue. Multiple attempts at defining very thin layers was done, but proved to be very difficult and presented with errors of divergence. It was then decided to represent the gel layer as a bulk homogenisation layer, containing a mixture of both the infarcted tissue and the hydrogel. A computational study performed by Kortsmit et al. (2012) described the injectate as four thin layers within the infarcted myocardium to approximate the very fine layers observed (Ifkovits et al., 2010, Dobner et al., 2009). Another study by Wall et al. (2006) used a volume mixing method where the various materials were represented. Image processing was performed to determine the ratio of gel to infarcted tissue. Three segments from histological samples were used to determine the ratio of hydrogel to the infarcted tissue and an average was calculated the following steps were taken to determine the ratios:

- Defined a specific region of interest (ROI) in a histology picture. This ROI contained a good quality and clear distribution of the gel
- 2D masks of gel and surrounding tissue were defined respectively
- A measure of the area of gel and tissue masks were taken
- Percentages of gel and tissue were calculated relative to the area of the overall ROI
- The method was repeated in two additional histological images

The calculated percentages of gel and tissue in three different histology images/sections were found to be:

*Table 3-3: Ratios of gel and tissue in the injectate region*

|  | Gel (%) | Tissue (%) |
|---|---|---|
| Image 1 | 49.3 | 50.7 |
| Image 2 | 44.4 | 55.6 |
| Image 3 | 39.0 | 61.0 |
| Average | 44.2 % ± 4.2 % | 55.8 % |

To implement the hydrogel within the geometry, the wall volume needs to be increased by the amount of volume of hydrogel that is infused into the myocardium. The wall thickening

was performed by applying a negative pressure to both the endocardial side and the epicardial side of the wall. All nodal points except those in the area of injection were constrained to ensure the thickening was applied locally to the region where injection occurred. The volumes of hydrogel used in each therapy were based on a percentage of the infarct size. This was defined as follows: 25 % hydrogel, 50 % hydrogel and 75 % hydrogel of the infarcted volume.

*Table 3-4: Gel volumes for respective infarct sizes*

| % of LV | Infarct Volume (µl) | Gel Volume (µl) (% of infarct size) | | |
|---|---|---|---|---|
| | | 25 % | 50 % | 75 % |
| 10 % | 60.669 | 15.2 | 30.3 | 45.5 |
| 20 % | 119.031 | 29.8 | 59.5 | 89.3 |
| 38 % | 226.909 | 56.7 | 113.5 | 170.2 |

## 3.5  Simulations

As a start to running simulations and to initialise the investigation of the effect of hydrogel on an infarcted rat heart based on a computational geometry a healthy control heart is needed so that the effect of an infarct as well as the hydrogel treatment can be determined. The simulations in this study are of geometries representing infarcted rat hearts as well as geometries representing infarcted rat hearts with the hydrogel treatment implemented.

Further simulations are of variations of the hydrogel treatment on the infarcted geometry. The aim of these simulations is to determine the most effective volume of the hydrogel in the treatment method.

### 3.5.1   End-Diastolic Pressure Volume Relationship (EDPVR)

A linear increase in pressure for the LV and RV is used with the pressure gradients described earlier (0.01 for the systemic circulation and 0.0053 for the pulmonic circulation.).

The end-diastolic volume was verified at a pressure of 3.36 kPa, which is considered a relatively high diastolic pressure (Omens et al., 1993).

### 3.5.2   End-Systolic Pressure Volume Relationship (ESPVR)

The ESPVR, in Continuity, is determined by simulating the reverse cardiac cycle starting from the geometry at the end of relaxation to the end-systolic pressure and volume point. A minimum of three simulations are needed to find three points on the curve of the ESPVR. The curve is then extrapolated, and the dead volume is found as the volume or x-intercept.

In the case of finding the ESPVR, in contrast to using a linear increase in the pressure, a linear increase in volume is used. For this, the pressure gradient is set to zero in both cases.

## 3.6 Data Analysis

The EDPVR and ESPVR for each case was determined and compared. From the characteristic curves of the cardiac cycle, the cardiac parameters were found and possible trends were analysed to determine what the most effective volume of hydrogel injectate would be per infarct size. The cardiac functional parameters that were analysed were the EF, the dead volume, the elastance, the contractility as well as both the EDV and the ESV at the predefined EDP (3.36 kPa) and ESP (14 kPa) respectively. These functional parameters give an indication on the performance of the heart under each of the various conditions. Furthermore all parameters of the geometries of the infarcted hearts with and without the hydrogel injectate were compared to the healthy control parameters obtained.

Additionally, the stress and strain data for each case was analysed. This included the Cauchy stress and the Green-Lagrangian strain. The stress matrix was composed of three components, representing the material types represented in each case. These material types included the healthy myocardium, the infarcted myocardium, and the hydrogel material. Another material region was also defined within the geometries; the BZ. The BZ included a mixture between the healthy myocardium and the infarcted myocardium. The infarcted myocardium in the early stages after an infarct retains all of its healthy material properties, but loses the ability to contract. Therefore the infarcted region could simply be defined as healthy myocardium with zero contractile ability. The main reason for defining the healthy and infarcted material as two separate materials was to allow for ease of defining of the various regions. The stress was analysed in the direction of the myofibres as well as the cross-fibre direction.

Unrealistically high stress concentrations were observed at and near to the apical and basal nodes. These high stress concentrations were due to restriction of movement of nodes relative to neighbouring nodes caused by lateral and circumferential boundary conditions in the apex and base. Since the boundary conditions applied caused unrealistically high stress concentrations along these boundaries, these stress and strain values were excluded. Furthermore all outlier stress values were also excluded. The outliers were taken to be all those values not within three standard deviations of the norm. Additionally, since each element has different dimensions, as well as different stress and strain values, the average for each element was weighted in the calculation of the total average for the specific region of interest. The following equation was used for the weighting process:

$$\bar{\sigma} = \frac{1}{n} \sum_{i=1}^{n} \left[ \left( \frac{1}{k} \sum_{j=1}^{k} \sigma_j \right) \cdot \frac{V_i}{\bar{V}} \right].$$

(3-7)

Maximum stress values were taken from the total sample set. In equation (3-7), $n$ is the number of elements within the region of interest, $k$ is the number of Gauss points within the element, $\sigma_j$ represents the stress per Gauss point $j$, $V_i$ is the volume per element, and $\bar{V}$ is the average volume of all the elements within the region of interest. For this study, the region of interest was the infarcted region for each case.

# 4 Results

## 4.1 Cardiac FE Models

Before simulations could be run and tests undertaken to determine the effects of infarct size and hydrogel volume on the cardiac parameters as well as stress and strain characteristics, the finite element models representing each case of the rat heart needed to be validated.

### 4.1.1 Healthy Rat Heart

In the case of the healthy rat heart, MRI data were used to develop a realistic structural geometry. Since simplifications needed to be made, to keep computational costs to a minimum without affecting the outcome of the results, the volumes of the specific regions on the MRI's were measured and compared to those volumes of the geometry after the mesh was fitted and ready for simulations.

Figure 4-1 shows the reconstruction of the healthy rat heart. Both images are side views where the apex can be seen in Figure 4-1 (a). Figure 4-1 (b) shows the LV and RV cavities from a more basal view. The LV cavity is the circular cavity seen in this image.



|  (a)  |  (b)  |
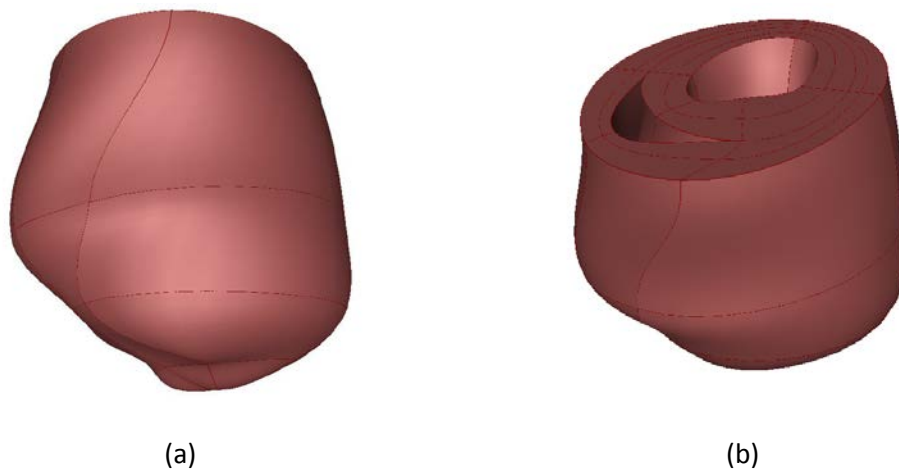
*Figure 4-1: Computational reconstruction of the healthy rat heart; (a) side view where the apex can also be seen; (b) base of the heart with the LV and RV cavity seen*

The volume differences found between those derived from the *Continuity* version of the computational model and those from the MRI's were considered to be acceptable and were recorded to be within 2 %. Table 4-1 shows the volumes obtained from the MRI's compared to the volumes of the computational model used.

*Table 4-1: Comparison of reconstructed geometry volumes to MRI volumes at the end-systolic time point*

|  | Reconstructed geometry | Segmented geometry (MRI) | Difference (%) |
|---|---|---|---|
| LV cavity (µl) | 115.06 | 115.52 | -0.39 |
| RV cavity (µl) | 28.03 | 28.51 | -1.70 |
| Wall (µl) | 640.04 | 639.47 | 0.09 |

The volume of the LV cavity used in *Continuity* is smaller than the volume measured from the segmented volume. This is also the case with the RV and the total cardiac volume. The difference seen in these cavity volumes is within 5 % and is therefore taken to be within an acceptable range.

The stress versus strain results from the Omens et al. (1993) paper showed that a strain representing a 20 % increase reflected a stress value in the fibre direction to be near 7.5 kPa and the cross-fibre stress at the same strain was observed to be about 2 kPa. For this study, at the ED time point, the in-fibre stress at 20 % strain was higher than that seen in the Omens et al. (1993) study, and showed a value of approximately 9 kPa, whereas the cross-fibre stress at 20 % strain gave an approximate value of 2 kPa, agreeing very closely with the result seen in the (Omens et al., 1993) study. These stress versus strain characteristics are graphically presented in Figure 4-2. In the figure, the data points represented by this study show the average stress and strain values in the elements.
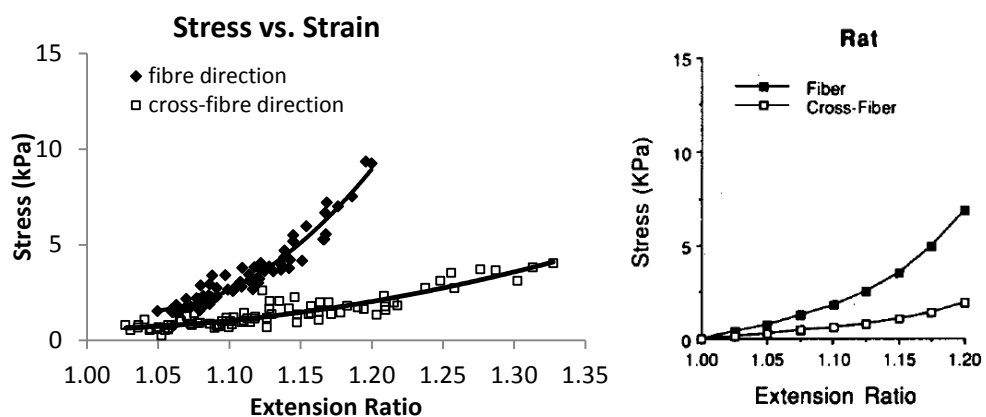


*Figure 4-2: Stress vs. strain (right: results from this study; left: results from the Omens et al. (1993) study)*

Figure 4-3 shows the characteristic curves of the end-diastolic pressure volume relationship as well as the end-systolic pressure volume relationship.
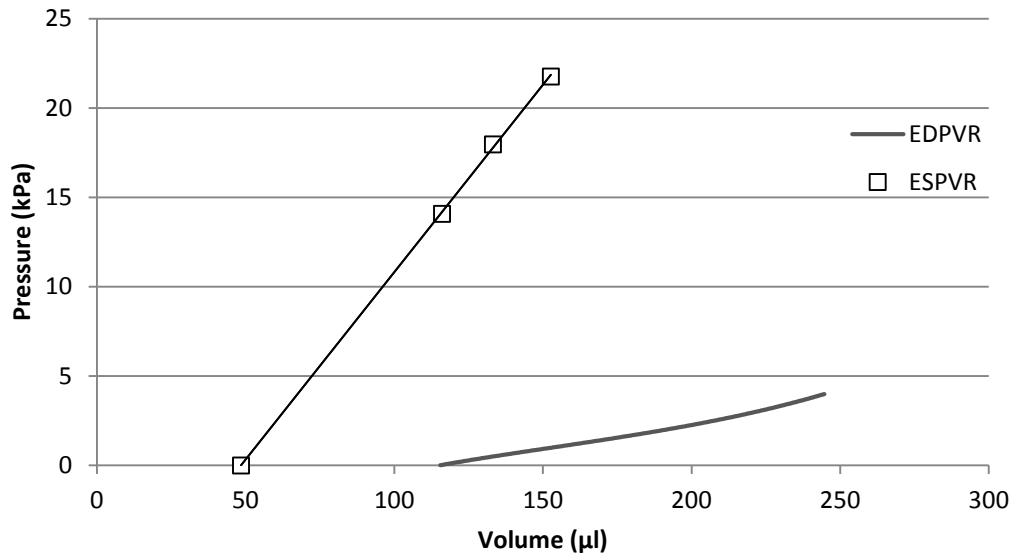


*Figure 4-3: Graph showing the EDPVR and ESPVR for the case of the healthy heart*

The EDP was taken to be 3.36 kPa. The ESP was found to be approximately 14 kPa. Table 4-2 shows the accuracy achieved when comparing the volume of the computational model and the MRI's at the ED time point. From Table 4-2 the maximum difference was 0.56 % and was therefore taken to be acceptable.

*Table 4-2: Comparison of reconstructed geometry volumes to MRI volumes at the end-diastolic time point*

|  | Continuity simulation geometry | Segmented geometry | Difference (%) |
|---|---|---|---|
| LV cavity (μl) | 357.19 | 355.37 | 0.51 |
| RV cavity (μl) | 90.22 | 90.73 | -0.56 |
| Wall (μl) | 814.87 | 816.04 | -0.14 |

Finally, the cardiac functional parameters were calculated from the cardiac characteristic curves. The functional parameters are tabulated in Table 4-3.

*Table 4-3: Cardiac function of the model of the healthy rat heart*

| Parameter | Model for this study |
|---|---|
| $E_{max}$ (kPa/µl) | 0.21 |
| $V_0$ (µl) | 48.44 |
| SV (µl) | 114.57 |
| EF (%) | 49.7 |

## 4.1.2   Infarcted Rat Hearts

The models of the three infarct sizes were created from the model of the healthy sham rat heart. Since an early ischemic infarct was modelled, there was no wall thinning that took place; hence the geometries remained the same. Therefore only the material properties were changed in the anterior apical region. The three infarct sizes were created based on a percentage of the LV wall volume. The infarcts that were created were 10 %, 20 % and 38 % of the LV wall volume. Figure 4-4 shows the infarct sizes. The dark (blue) area represents the infarcted tissue; the lighter (red) region represents the healthy tissue and the transition region between represents the BZ. In each case an apical view is shown since the infarcts are anterior apical.

(a)

(b)

(c)
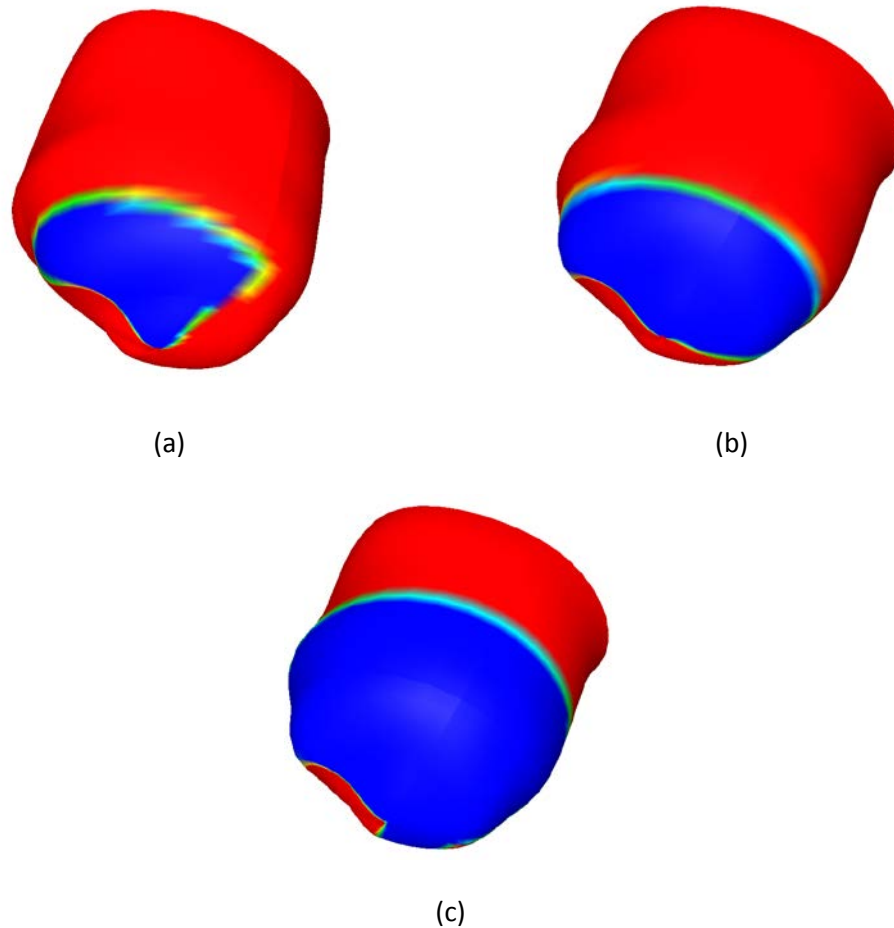
*Figure 4-4: Apical view of the infarct sizes 10 % (a), 20 % (b) and 38 % (c); The dark (blue) region shows the infarct area and the lighter (red) region represents the healthy tissue in each case, the lightest area between is the BZ*

### 4.1.3    Infarcted Rat Hearts with Hydrogel Injectates

The hydrogel injectates in each of the infarcted heart cases involved the injection of additional material into the myocardium and therefore wall thickening would necessarily take place. The volume of hydrogel that was injected in each case was given as a percentage of the infarct size, and thus the wall volume increase was calculated from the infarct sizes for each infarct. The hydrogel volumes injected were set to be a standard ratio for the infarct size. These injectate volumes were typically taken to be 25 %, 50 % and 75 %. Since the wall volume increased due to the injected material in each case, it was necessary to validate the volume of the computational model with the calculated wall volume after the myocardial wall thickening had taken place. The Table 4-4 presents both the calculated wall volume increase as well as the wall volume increase obtained from the computational wall thickening. Further volume data is also indicated in Table 4-4 to show how the increase in wall volume affected the cavity volumes as well as the total epicardial volume. The RV cavity volume remains unchanged in every instance where the wall thickening had been

applied due to the hydrogel injectate. The maximum difference between the calculated volume increase compared with the actual computational geometry obtained is given in Table 4-4 for the 25 % hydrogel representation. This difference is 6.3 % and is considered low and acceptable. Furthermore, the epicardial volume in each case increases as more injectate volume is modelled for each infarct size. Additionally, the LV cavity volume decreases with greater wall thickening.

*Table 4-4: Wall thickening volumes for the 10 %, 20 % and 38 % infarcts due to hydrogel injectates*

|  | Volume increase (calculated) (µl) | Volume increase (model) (µl) | Difference (%) | Wall volume (µl) | LV cavity (µl) | RV cavity (µl) | Epicardial volume (µl) |
|---|---|---|---|---|---|---|---|
| No gel | N/A | N/A | N/A | 640.04 | 115.06 | 28.03 | 783.13 |
| 10 % infarct | | | | | | | |
| Gel 25 % | 15.17 | 16.19 | 6.3 | 656.23 | 109.88 | 28.03 | 794.13 |
| Gel 50 % | 30.33 | 29.98 | -1.2 | 670.02 | 106.17 | 28.03 | 804.22 |
| Gel 75 % | 45.50 | 45.68 | 0.4 | 685.72 | 103.79 | 28.03 | 817.54 |
| 20 % infarct | | | | | | | |
| Gel 50 % | 59.52 | 59.69 | 0.3 | 699.73 | 106.90 | 28.03 | 834.65 |
| 38 % infarct | | | | | | | |
| Gel 25 % | 56.73 | 56.49 | -0.4 | 696.53 | 113.34 | 28.03 | 837.90 |

## 4.2 Effect of Infarct Size on Cardiac Function and Myocardial Stress and Strain

### 4.2.1 Cardiac Function

In Figure 4-5 the comparison of all infarct sizes are analysed and compared to the healthy control heart. The EDPVR remains unaffected. From the ESPVR, a steady decrease in cardiac function is observed by the changes in dead volume and the ESV. The horizontal line represents the end-systolic pressure (ESP). From the ESP there is a steady increase in the ESV with an increase in the infarct size. An increase in the ESV shows a decrease in the stroke volumes provided EDV remains constant and therefore indicates a decrease in the EF.
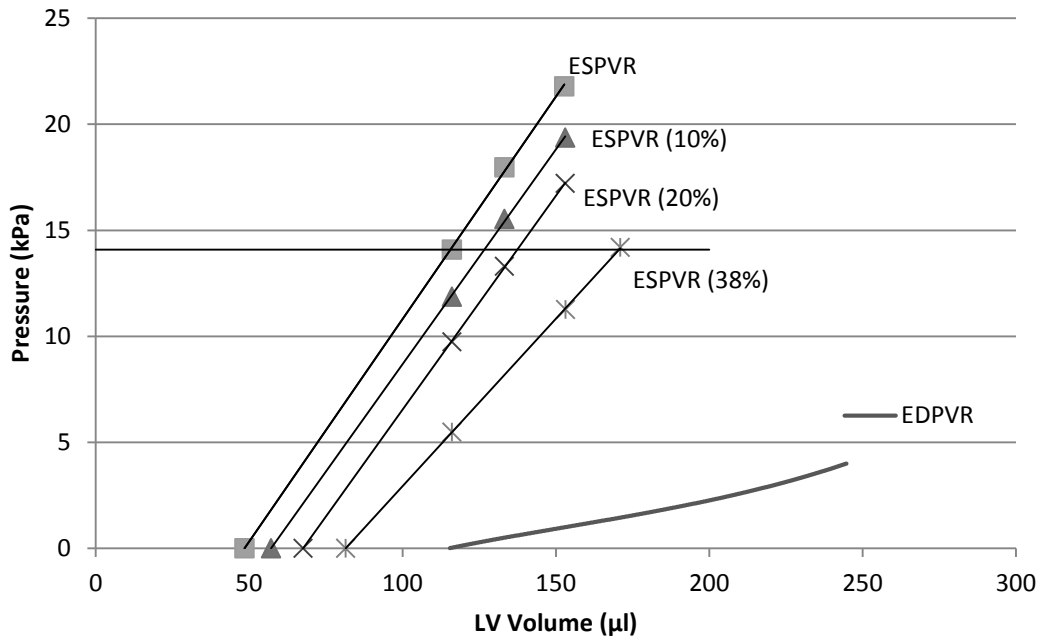
*Figure 4-5: Pressure volume relationship curves for EDPVR and ESPVR of the healthy heart and hearts with infarct sizes of 10 %, 20 % and 38 %. All models display the same EDPVR, but differing ESPVRs are observed for the early infarct*

Figure 4-6 shows the results of EF, stroke volume, dead volume and ES elastance plotted against the infarct size. The decrease in EF and SV is near to linear. Figure 4-6 (a) shows that with increasing infarct size, there is a continual decrease in the EF. The decrease in EF for an infarct size of 10 % is about 10 %, dropping from the healthy EF value of 50 % to about 45 % in the 10 % infarct. The 20 % infarct shows a further decrease in the EF of about 8 %. The greatest decrease in EF was observed for the 38 % infarct. For this case, a decrease to about 50 % of the healthy EF was observed. The EF decreased from 50 % to about 25 % for an infarct size of 38 %.

The dead volume, which represents the theoretical amount of blood that cannot be ejected, is represented in Figure 4-6 (b). A steady increase is observed in the dead volume with increasing infarct size. The infarct size of 10 % gives rise to an increase in the dead volume of about 18 % when compared to the dead volume of the healthy case. The 20 % infarct, (20 % of the LV wall volume) showed an increase in the dead volume of 40 % from the healthy case and finally, the 38 % infarct size showed the greatest increase in the dead volume parameter of 68 % from the healthy case.

An infarct size of 10 % gave a reduction of about 10 % in the SV from the SV of the healthy case. A reduction of about 17 % was recorded for the infarct size of 20 % and a further 31 %

decrease for the 38 % infarct size. The total decrease in SV from the infarct size was therefore 48 % from the SV of the healthy case.

The trend of $E_{max}$ that was observed between the infarct size and the end-systolic elastanceis presented in Figure 4-6 (d). It is noted that for the 10 % and 20 % infarcts, only a small decrease in the elastance was present. A decrease of about 3 % was recorded from the healthy case to the 10 % infarct case and a further 1 % in the 20 % infarct case. There was a greater decrease from the 38 % infarct, where the decrease in the elastance was about 25 % from the healthy case.



(a)

(c)

(b)

(d)
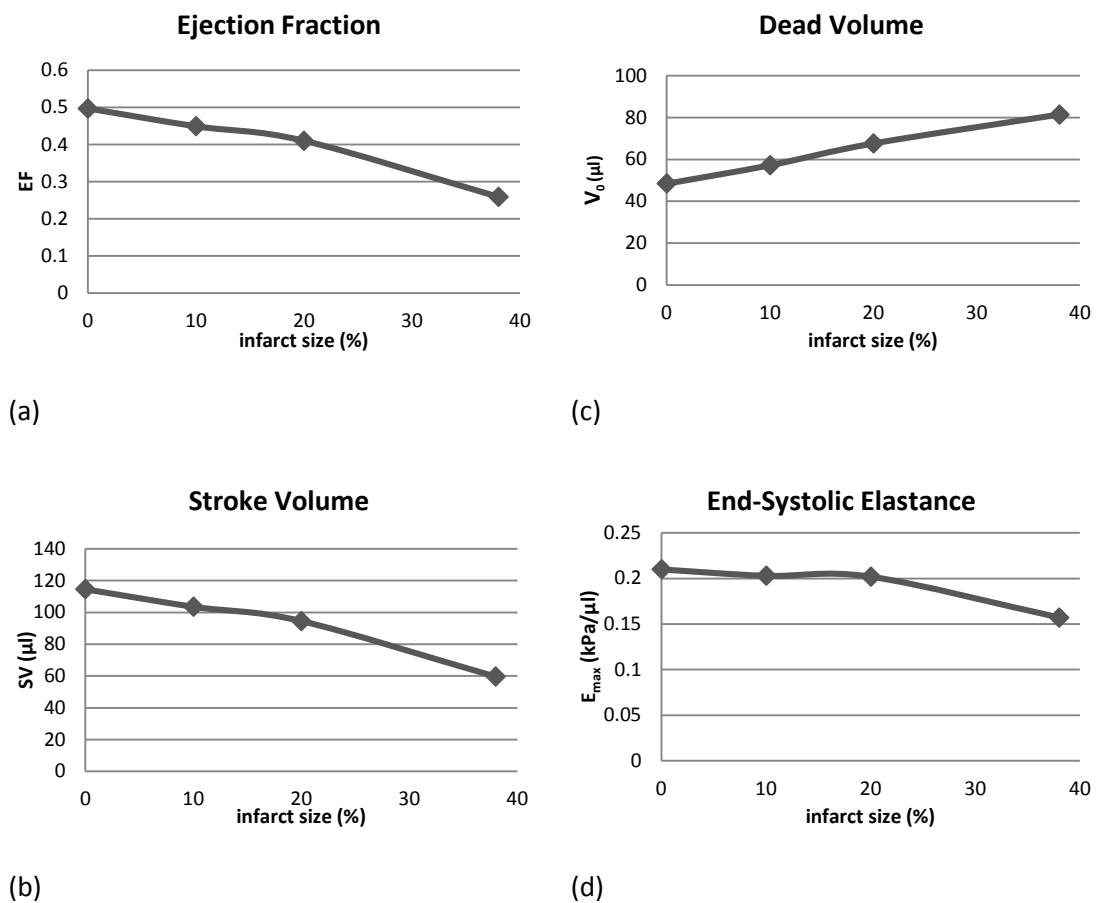
*Figure 4-6: The effect of infarct size on the EF, stroke volume, dead volume (V₀) and end-systolic elastance (E_max)*

### 4.2.2 Myocardial Stress and Strain

The graphs in Figure 4-7 plot the ED stress and strain for the healthy case compared to the infarct cases. The stress and strain data in each case is extracted from the region of interest i.e. the infarcted area. Here the data showing the healthy case represents the same region as the infarcted region in each instance.

Figure 4-7 (a) shows no change between the maximum in-fibre stress at ED representing the healthy heart tissue and the infarcted cases. The maximum stress for the ED in-fibre case for each infarct was 17.6 kPa.

In Figure 4-7 (b) the average stress, like the maximum stress at the end-diastolic time point also showed no change between the stress representing the healthy heart to the stress representing the infarcted heart in each case. Although, the average stress when compared across infarct sizes showed differences. These differences observed are due to the different areas being compared in each case. For each case, the area focussed on is the region where the infarct is present. Therefore for the case of the 10 % infarct size, it is compared to the case of the healthy heart for the same region, and similarly with the 20 % and 38 % infarct sizes. The average in-fibre stress for the infarcts were: 4.2 kPa for the infarct of 10 %, 4.6 kPa for the 20 % infarct and 3.9 kPa for the infarct of 38 %.

The maximum in-fibre strain, in Figure 4-7 (c) for the ED time point similarly showed no difference from the results representing the healthy case to the results representing the infarcted case for each infarct size. A large increase in the maximum in-fibre strain was recorded from the 10 % infarct to the 20 % infarct, but there was no change between the 20 % and 38 % infarcts. The maximum in-fibre strain for the 10 % infarct was 0.293, and for both the 20 % infarct and the 38 % infarct the strain was 0.342.

Average in-fibre strain at the ED time point in Figure 4-7 (d); display the same characteristic of no change between the strain representing the healthy case and the infarcted models in each case. The average in-fibre strain for the 10 % infarct was 0.115, for the 20 % infarct it was 0.121 and for the 38 % infarct it was 0.109.

**In-fibre ED max stress** ■Healthy □G0%

**In-fibre ED max strain**

**In-fibre ED average stress**

**In-fibre ED average strain**

(a)

(b)

(c)

(d)
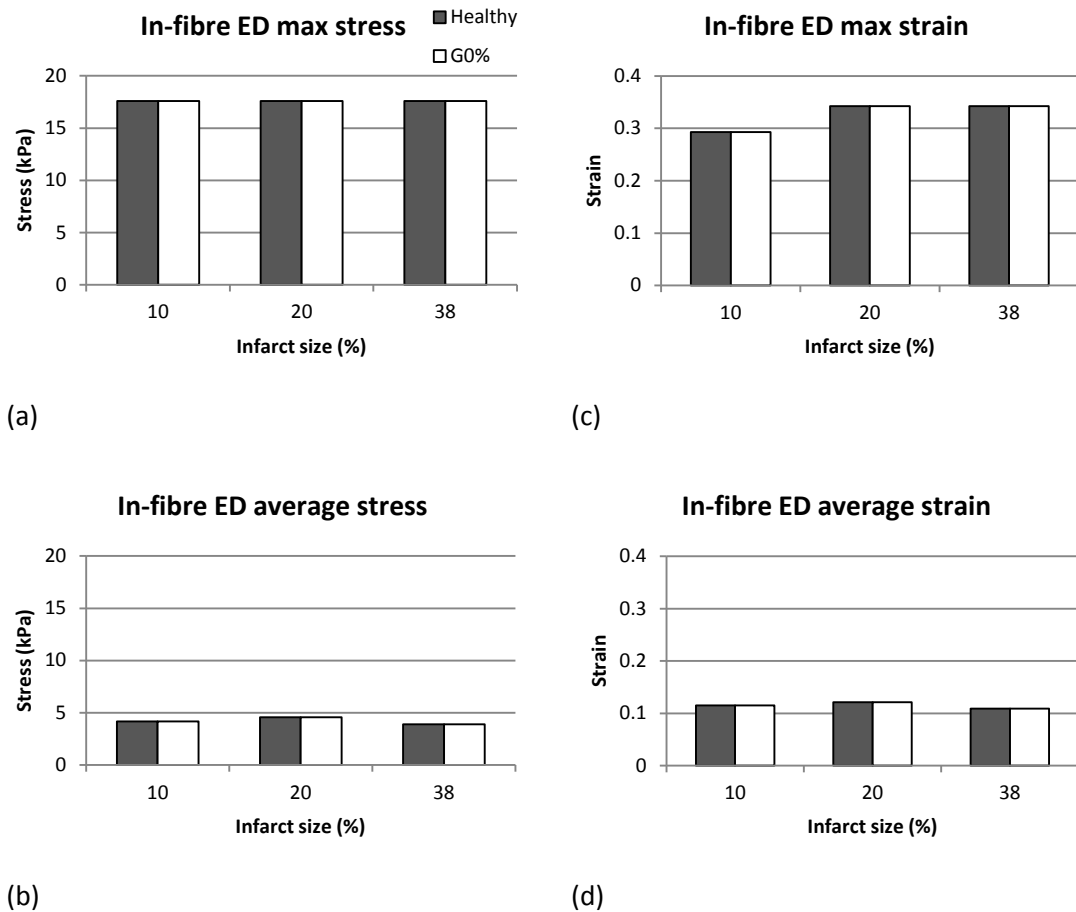
*Figure 4-7: The effect of infarct size on the ED stress and strain within the infarcted region*
*(Black represents the healthy case; white represents the infarcted case)*

Figure 4-8 of the ES time point, the region representing the infarct in each model contains no contractile ability, and therefore will differ from the control case in that region. The maximum in-fibre stresses recorded from the respective regions representing the infarcts in the model of the healthy heart is constant in all three cases. This stress was recorded as 41.6 kPa. For the simulations where the infarcted effect had been implemented, there is an increase in the maximum in-fibre stress within the region with the increase in infarct size. The geometry representing the 10 % infarct size showed a maximum in-fibre end-systolic stress of 53.4 kPa. The maximum in-fibre, end-systolic stress for the 20 % infarct model showed 90.6 kPa and the 38 % infarct showed a maximum stress of 101.5 kPa.

## In-fibre ES max stress

**Figure 4-8 (a)**

## In-fibre ES max strain

**Figure 4-8 (c)**

(a)

(c)

## In-fibre ES average stress

**Figure 4-8 (b)**

## In-fibre ES average strain

**Figure 4-8 (d)**

(b)

(d)
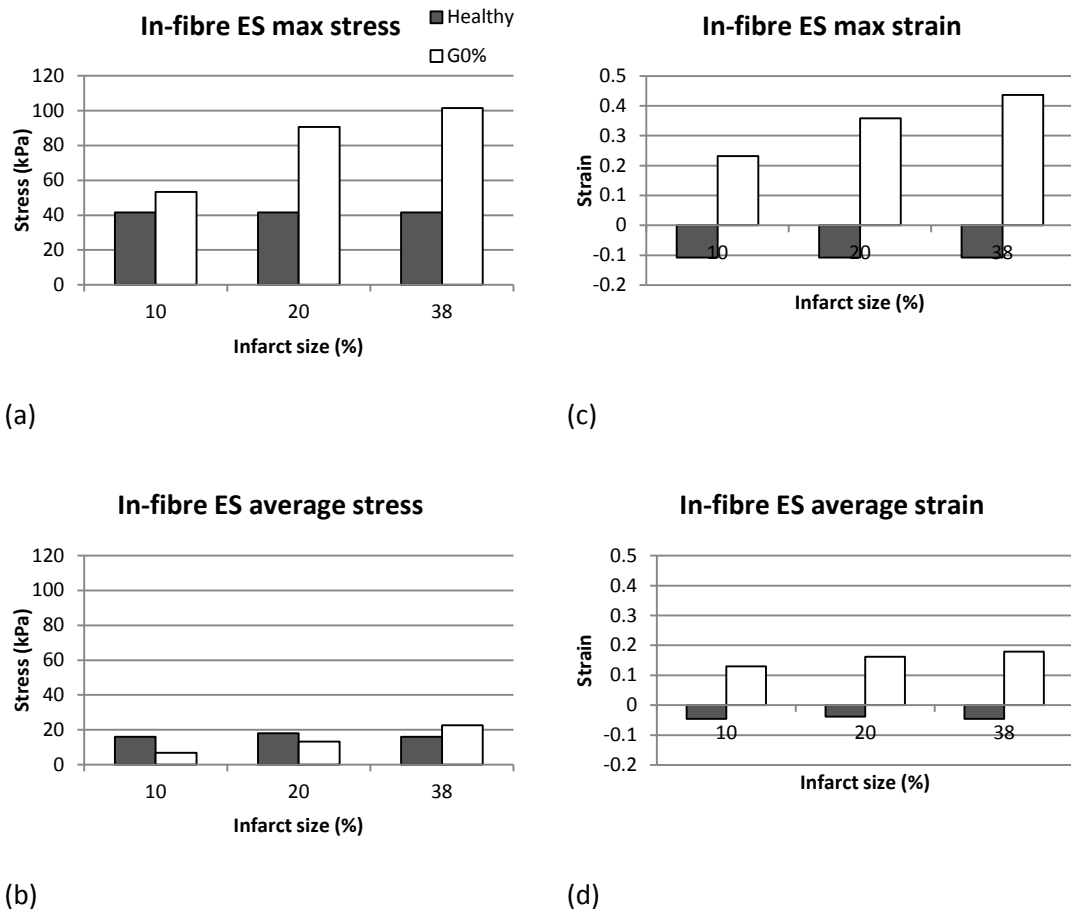
*Figure 4-8: The effect of infarct size on the ES stress and strain within the infarcted region*

*(Black represents the healthy case; white represents the infarcted case)*

The average end-systolic, in-fibre stress is plotted in Figure 4-8 (b). Unlike the maximum stresses observed at the same time point, the average stresses for both the 10 % and the 20 % infarct sizes show a decrease when compared to the average stress in the healthy heart case representing the same region. The average in-fibre stress at the ES time point recorded for the infarct sizes are respectively, 6.8 kPa, 13.3 kPa and 22.6 kPa. The average stresses for the case of the healthy heart for the infarct regions were recorded as 15.9 kPa, 18.1 kPa and 16.0 kPa respectively.

The maximum in-fibre strain in Figure 4-8 (c), at the ES time point, indicates that the strain in the healthy myocardium in the healthy heart is negative. The maximum contractile strain observed in the healthy heart for each of the infarct regions is -0.108 for all cases. The maximum in-fibre strain for the end-systolic time point showed strains of 0.428 for the 10 % infarct size, 0.481 for the 20 % infarct size and 0.509 for the 38 % infarct size indicating that bulging occurs in the infarct region.

Figure 4-8 (d) shows the average in-fibre strain observed within the respective regions of the infarct zones. Similarly to the maximum in-fibre strain, the average end-systolic strain in

the healthy tissue shows negative strains. The region of the geometries that represent the infarcted tissue also shows a positive strain like the maximum end-systolic strains. The negative strains representing the tissue in the healthy situation were recorded as -0.046, -0.038 and -0.045 for the regions of the 10 %, 20 % and 38 % infarct sizes respectively. The models with the infarct regions gave average in-fibre, end-systolic strain as 0.129 for the 10 % infarct, 0.162 for the 20 % and 0.179 for the 38 % infarct.

## 4.3   Effect of Injectates

The hydrogel injectate that was simulated was based on the percentage of the infarct size. Therefore the hydrogel of 25 % (G25) is 25 % of the infarct size. Three hydrogel volumes were simulated namely 25 %, 50 % (G50) and 75 % (G75) volumes.

### 4.3.1   Effect of Volume of Hydrogel Injectate on the 10 % Infarct

For the infarct size of 10 % all three hydrogel injectate volumes were simulated to determine the effect of different hydrogel injectate volumes.

#### 4.3.1.1   Cardiac Function

The hydrogel therapy had an effect on the strain characteristics of the myocardial wall and therefore affected the EDPVR. The EDPVR's for the 10 % infarct, compared to the EDPVR's of the hydrogel injectates in this geometry of 10 % infarct size were compared. Figure 4-9 shows the plotted comparison of these models. It is noted from the graph that the slope increases, indicating that the ED compliance decreases with increasing volume of hydrogel injectate. As a result of the added hydrogel injectate, there is an increase in the overall stiffness to the wall tissue causing the deformation to be less with more hydrogel volume. It is also noted that with a constant EDP, the EDV decreases with increasing biomaterial injectate volume.
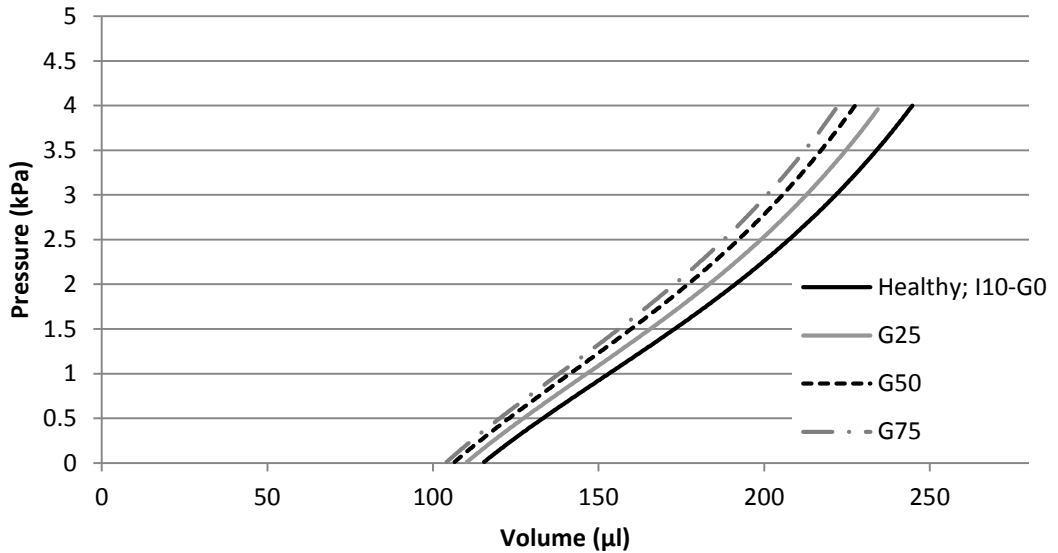
*Figure 4-9: Graph of the end-diastolic pressure volume relationships of the 10 % infarct size with the three gel injectate volumes; curves from left to right represent the 75 %, 50 %, 25 % and 0 % gel volumes*

The end-systolic pressure volume relationships for the 10 % infarct size with the three injectate volumes of 25 %, 50 % and 75 % are shown in Figure 4-10. The dead volume decreases with the addition of 25 % hydrogel and decreases further with the addition of the 50 % hydrogel volume. The dead volume of the G50 and G75 decrease beyond the dead volume of the health case of 48.4 μl. The ESV decreases from the infarcted situation to the G25 model with a further decrease in the G50 model.
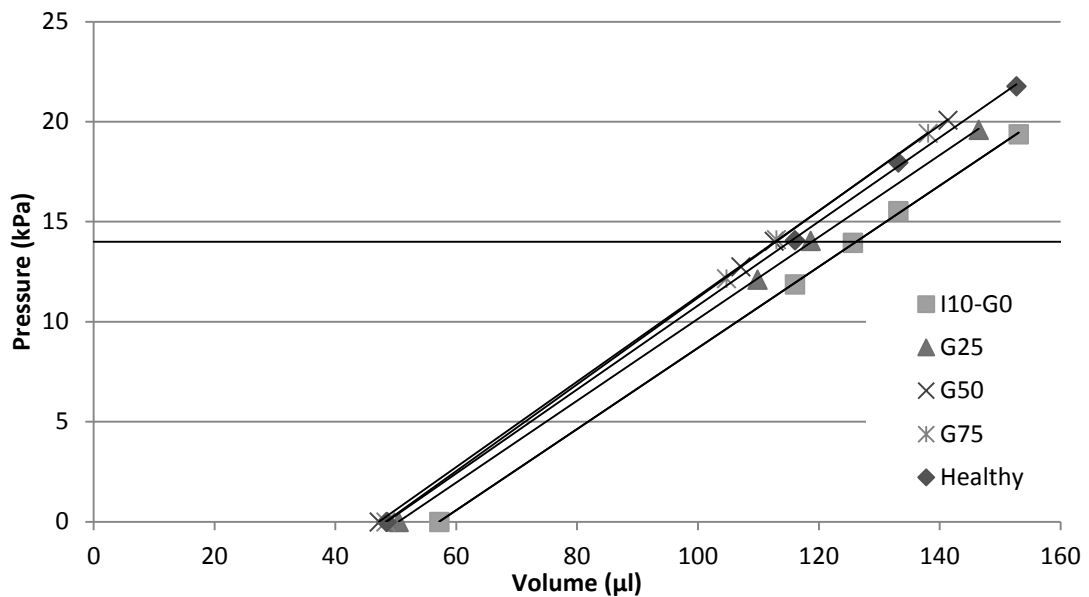


*Figure 4-10: Graph of the end-systolic pressure volume relationships of the 10 % infarct size with the three gel injectate volumes*

The functional parameters are tabulated in Table 4-5. The ES elastance firstly decreases after ischemia, but increases with increasing hydrogel volume. Although there are changes in the ES elastance, these changes are very small. An initial increase is observed with the dead volume, from the healthy case to the ischemic case. With the injectate added to the myocardial wall though, there is a decrease in the dead volume. A maximum decrease in the dead volume is observed with the injectate therapy volume of 50 %. The SV results show a continual decrease from the healthy case to the ischemic case and continue to decrease with increasing hydrogel injectate volume. Furthermore, the results of the EF indicate a decrease after ischemia, but a rise with the hydrogel injectate therapy. The greatest increase in the EF was with the G50 injectate volume of 47.4 % this is 4.6 % less than the healthy case, but is a 5.3 % increase from the ischemic EF.

*Table 4-5: Functional parameter comparison of the geometries of the healthy heart, 10 % infarcted heart and the three injectate models for the 10 % infarct*

|  | Healthy | 10 % infarct | G25 | G50 | G75 |
|---|---|---|---|---|---|
| $E_{max}$ (kPa/μl) | 0.210 | 0.203 | 0.205 | 0.214 | 0.217 |
| $V_0$ (μl) | 48.44 | 57.18 | 50.45 | 47.25 | 48.35 |
| SV (μl) | 114.57 | 103.63 | 102.83 | 101.49 | 101.41 |
| EF (%) | 49.7 | 44.9 | 46.4 | 47.4 | 47.3 |

### 4.3.1.2   *Myocardial Stress and Strain*

Mechanical properties are also affected by the addition of hydrogel into the myocardial wall. The average stress and strain data were weighted by the elemental volumes. Additionally, all data were recorded from the region of interest; that is the 10 % infarction region.

Figure 4-11 shows the fibre end-diastolic stresses within the infarct region. For the fibre stress, the maximum stress is approximately 4 times greater than the average stress within the region. In all stress cases, maximums and averages, the stress decreases with increasing hydrogel injectate volume. Focusing on the average fibre stress, a maximum decrease in stress of 56.7 % is obtained in the G75 model compared to the healthy case.

**In-fibre ED max stress**

(a)

**In-fibre ED max strain**

(c)

**In-fibre ED average stress**

(b)

**In-fibre ED average strain**

(d)
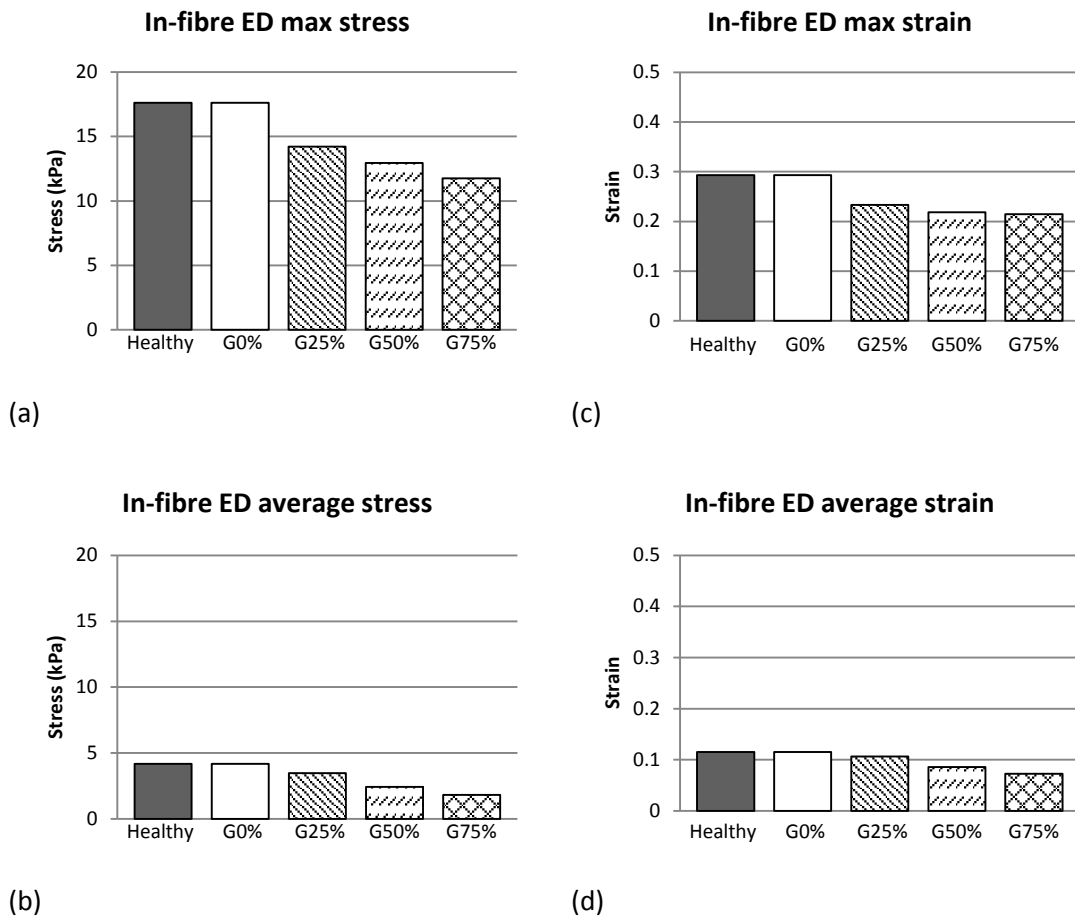
*Figure 4-11: Maximum and average stresses and strains for the geometry at end-diastole of the 10 % infarct with 25 %, 50 % and 75 % hydrogel injectates modelled: (a) maximum fibre stress in each model, (b) fibre average stress, (c) and (d), fibre maximum and average strains respectively*

Strain results for the biomaterial injectate volumes are shown in Figure 4-11 (c) and (d).The maximum strain shows a value of 14.2 with the G25 model, and with additional volume of injectate, the maximum strain decreases further. The maximum strain values are 9.57 for both the healthy case and the G0 case, and 9.00 and 8.08, 6.63 for the G25, G50 and G75 cases respectively. The average strains in the fibre direction show a decrease with increasing hydrogel volume.

Figure 4-12 shows the stresses and strains at the ES time point. Figure 4-12 (a) shows the maximum ES stress observed within the infarcted region. The maximum stress after the implementation of hydrogel injectate shows a decrease from the infarcted case. The maximum decrease is obtained by the G50 hydrogel volume with a stress of 44.0 kPa, indicating a decrease of about 21 %. Similarly, the hydrogel gives rise to a decrease in the average in-fibre stress from the infarcted case. The maximum decrease is seen with the G75 hydrogel volume. The average stress for the G75 case is 3.9 kPa, showing a decrease of

approximately 54.8 % from the average stress of the infarcted case without hydrogel injectate.



**In-fibre ES max stress**

(a)

**In-fibre ES max strain**

(c)

**In-fibre ES average stress**

(b)

**In-fibre ES average strain**

(d)
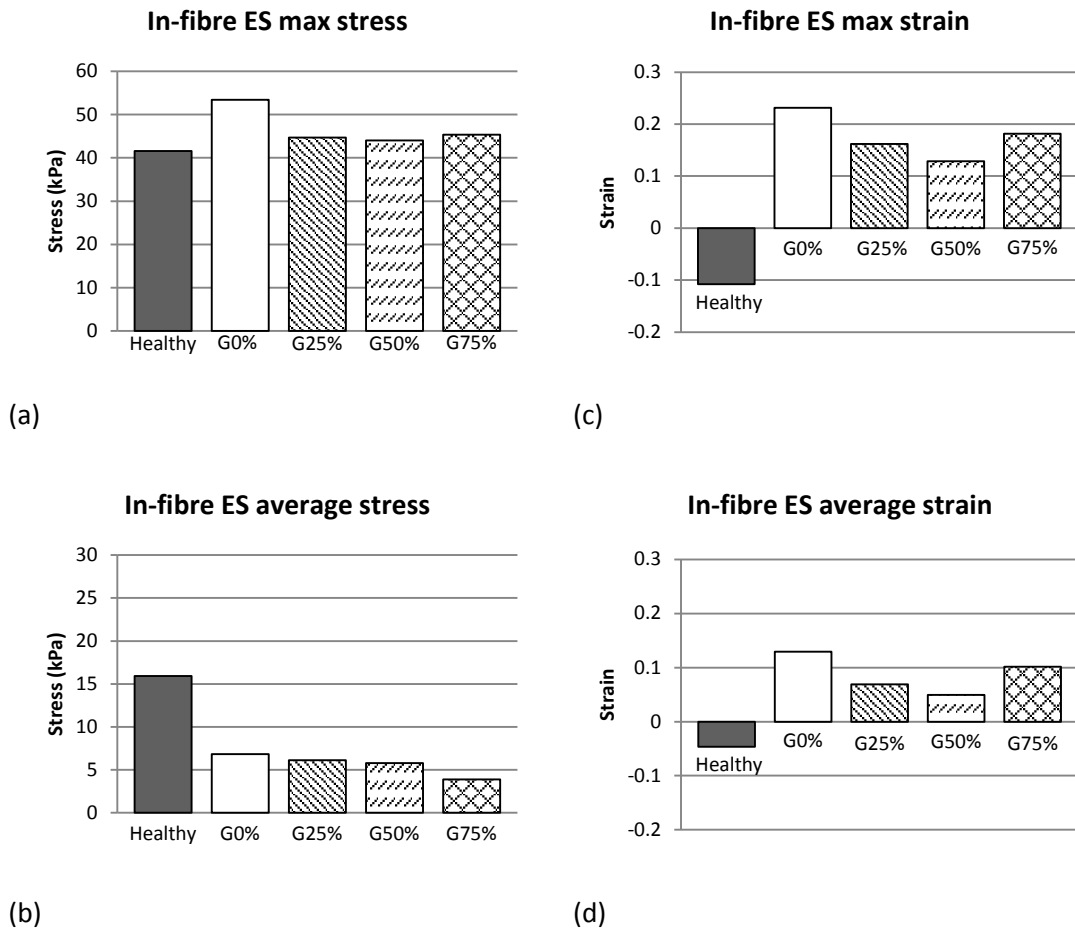
*Figure 4-12: Maximum and average stresses and strains for the model at ES of the 10 % infarct with 25 %, 50 % and 75 % hydrogel injectates modelled: (a) maximum fibre stress in each model, (b) fibre average stress, (c) fibre maximum stress and (d), fibre average stress*

Strain in Figure 4-12 show a decrease in the maximum and average in-fibre values with the addition of the hydrogel injectate when compared to the infarcted case. From Figure 4-12 (d) the average in-fibre strain of the G50 gives the greatest decrease in the in-fibre ES strain. Furthermore, the strains presented do not indicate the same difference between the G50 and the G75 case with respect to maximum and average values observed for stress. The graph indicates that for strain, the G50 model is the most effective for both maximum and average strain.

### 4.3.2   Effect of 50 % Injectate in 10 % and 20 % Infarcts

The effect of the hydrogel injectate achieved with the 10 % infarct size was compared with the G50 case in the 20 % infarct size. Firstly the functional parameter results are given, then the stress and strain data at both the end-diastolic and end-systolic time points.

### 4.3.2.1 Functional Parameters

Figure 4-13 shows the pressure-volume relationships of both the 10 % and 20 % infarct sizes with the injectate of 50 % volume. EDPVRs of the healthy and infarcted cases without gel are all equal as indicated previously in section 4.3.1. The EDPVR is very similar for both injectate models. For ESPVR, comparing the injectate in the 10 % infarct size to the healthy case, the gel has caused a slight increase in the elastance, and a very small decrease in the dead volume. Conversely, comparing the 20 % infarct size with the G50 volume to the healthy case, a clear increase is observed in the dead volume with a small decrease in the elastance. In both infarcts, there is a decrease in the dead volume from the infarct without gel to the hydrogel treated models. For more insight on the results, the functional parameters of the infarct sizes with no gel are also compared along with the function of the healthy case.

**Graph of EDPVR and ESPVR of healthy case and infarct sizes 10 % and 20 % without gel and with 50 % hydrogel injectate**
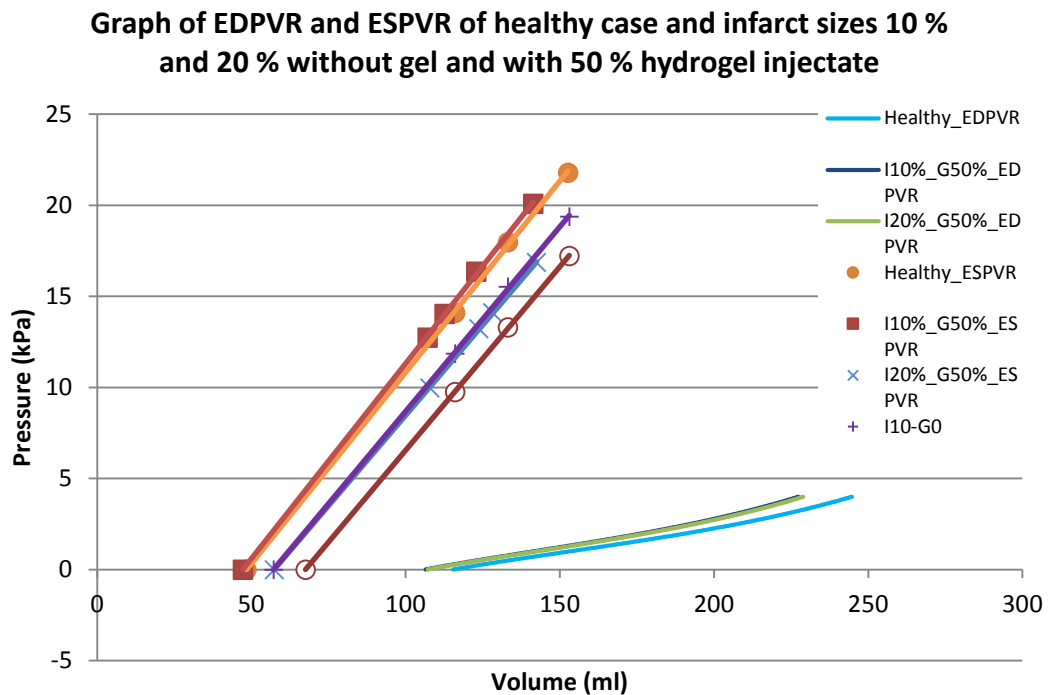


*Figure 4-13: Graph of the EDPVR and the ESPVR of the healthy case and infarct sizes 10 % and 20 % without gel and with hydrogel injectate of 50 %*

The Table 4-6 shows the comparison between the cardiac functional parameters of the 10 % and 20 % infarct sizes with the G50 including the percentage change for each case. For the elastance ($E_{max}$), the effect of the 50 % biomaterial volume shows an increase for the 10% infarct, whereas the 50 % biomaterial in the 20 % infarct shows a decrease in this value. The dead volume is caused to decrease in both cases from the infarcted state. The decrease in both infarct sizes shows a substantial decrease. Looking at the SV, the results show that a small decrease was observed in the case of the 10 % infarct, but there was a

substantial increase in the 20 % infarct size. This increased value is still less than the healthy SV of 114.57 µl. Furthermore, the G50 hydrogel case caused an increase in the SV, in both models, from the infarcted cases without gel. The effect on the 20 % infarct size was an increase of 28.0 %, but there was a decrease in EF from the healthy EF.

*Table 4-6: Comparison of the cardiac functional parameters of the healthy case compared with the infarct sizes 10 % (I10) and 20 % (I20) with 50 % hydrogel injectate*

|  | *Healthy* | I10 | I10-G50 | *Change (%)* | I20 | I20-G50 | *Change (%)* |
|---|---|---|---|---|---|---|---|
| $E_{max}$ (kPa/µl) | *0.210* | 0.203 | 0.214 | *5.1* | 0.202 | 0.199 | *-1.5* |
| $V_0$ (µl) | *48.44* | 57.18 | 47.25 | *-21.0* | 67.60 | 57.42 | *-17.7* |
| SV (µl) | *114.57* | 103.63 | 101.49 | *-2.1* | 67.34 | 87.46 | *23.0* |
| EF (%) | *49.7* | 44.9 | 47.4 | *5.3* | 29.2 | 40.6 | *28.1* |

### 4.3.2.2   Myocardial Stress and Strain

Stress and strain results are shown at the ED and ES time points during the cardiac cycle. In all cases only the maximum and average in-fibre stresses and strains are given. For the end-diastolic time point, Figure 4-14 shows in both infarct cases there is a decrease in the stresses and strains due to the 50 % hydrogel injectate. Average values show a greater decrease in the stresses and strains than the maximum values. It is also noted that a greater relative decrease is recorded with the 20 % infarct size than the 10% infarct. The relative decrease in the average stress is 42.2 % and 50.6 % for the 10 % and 20 % infarct sizes respectively. For the strain, the relative decrease is 25.5 % and 32.5 % for the maximum strains; and 25.3 % and 35.5 % for the average strains.

**In-fibre ED max stress**



(a)

**In-fibre ED average stress**



(b)

**In-fibre ED max strain**



(c)

**In-fibre ED average strain**



(d)

*Figure 4-14: Maximum and average stresses and strains for the model at end-diastole of the 10 % and 20 % infarct with the healthy case, the infarcted case (no gel), and 50 % hydrogel injectates modelled: (a) maximum in-fibre stress in each model, (b) in-fibre average stress, (c) in-fibre maximum strain and (d) in-fibre average strain*

End-systolic stresses indicate that the hydrogel volume of 50 % causes decrease for both infarcts for both the stress and the strain. The effect of the biomaterial brings the maximum stresses near to the maximum stress in the healthy case. The relative increase for the maximum stress from the healthy case to the infarct cases is 28.4 % and 117.86 % for the 10 % and 20 % infarcts respectively. Furthermore, the relative decrease in the maximum stress from the infarct state to the G50 hydrogel treated state is 17.6 % and 40.3 % for the infarcts 10 % and 20 % respectively. Average stresses within the infarcted region show that from the healthy case, the average stress drops with the infarct, and decreases further with the addition of the hydrogel. This occurs in both infarct models, although the decrease from the gel in the 10 % infarct is less than the decrease in the 20 % infarct. Conversely, the average strain recorded at end-systole shows a greater decrease in the strain in the 10 % infarct as compared with the 20 % infarct.

## In-fibre ES max stress



(a)

## In-fibre ES max strain



(c)

## In-fibre ES average stress



(b)

## In-fibre ES average strain



(d)

*Figure 4-15: Maximum and average stresses and strains for the model at end-systole of the 10 % and 20 % infarct with the healthy case, the infarcted case (no gel), and 50 % hydrogel injectates modelled: (a) maximum in-fibre stress in each model, (b) in-fibre average stress, (c) in-fibre maximum strain and (d) average in-fibre strain*

### 4.3.3    Effect of 25 % Injectate in 10 % and 38 % Infarcts

The following section presents the results of the effect of a G25 in the 10 % infarct and the 38 % infarct. The results of the cardiac functional parameters and the stress and strain data are shown and relevant data are presented.

#### 4.3.3.1    *Functional Parameters*

Table 4-7 shows the results of the cardiac functional parameters for the injectate volume of 25 %. The results show a small increase in the ES elastance for the 10 %infarct, whereas a decrease in the 38 % infarct case. In both cases, the model of the infarcted case with no gel shows an elevated dead volume. The biomaterial caused a large decrease in the dead volume of the infarcted case. Furthermore, SV data show a decrease with the 25 % injectate in the 10 % infarct case, but an increase in the 38 % infarct case. Finally, in both infarcted cases, an increase is observed in the EF. The increase in both cases is about 3 %.

*Table 4-7: Comparison of the cardiac functional parameters of the healthy case compared*

*with the infarct sizes 10 % (I10) and 38 % (I38) with 25 % hydrogel injectate*

|  | *Healthy* | I10 | I10-G25 | *Change (%)* | I38 | I38-G25 | *Change (%)* |
|---|---|---|---|---|---|---|---|
| $E_{max}$ (kPa/µl) | *0.210* | 0.203 | 0.205 | *1.0* | 0.157 | 0.145 | *-8.3* |
| $V_0$ (µl) | *48.44* | 57.18 | 50.45 | *-13.3* | 81.43 | 72.40 | *-12.5* |
| SV (µl) | *114.57* | 103.63 | 102.83 | *-0.8* | 59.60 | 61.71 | *3.4* |
| EF (%) | *49.7* | 44.9 | 46.4 | *3.2* | 25.8 | 26.7 | *3.4* |

### 4.3.3.2   Myocardial Stress and Strain

Maximum and average in-fibre stress and strain results after passive inflation are shown in Figure 4-16. From Figure 4-16 (a), the maximum stress within the infarcted region decreases in the 10 % infarct size with the addition of G25 biomaterial volume, conversely, for the 38 % infarct, a rise in the maximum stress is observed. On the other hand, in both cases the average in-fibre stress decreases for both the 10 % and 38 % infarct for this volume of gel. In the case of the maximum strain, there is a decrease in both models after the injectate therapy is undertaken. Additionally, the average strain decreases in both cases, but in the case of the 38 % infarct, the decrease is very small.

**In-fibre ED max stress**



(a)

**In-fibre ED average stress**



(b)

**In-fibre ED max strain**



(c)

**In-fibre ED average strain**



(d)

*Figure 4-16: Maximum and average stresses and strains for the rat heart model at end-diastole of the 10 % and 38 % infarct with the healthy case, the infarcted case (no gel), and 25 % hydrogel injectates modelled: (a) maximum in-fibre stress in each model, (b) in-fibre average stress, (c) in-fibre maximum strain and (d) average in-fibre strain*

Figure 4-17 shows the stress and strain at the end-systolic time point. The maximum stress is shown to decrease in both the 10 % and the 38 % infarcts with the inclusion of the G25 from the infarct case without gel. In the case of the 10 % infarct; there is a smaller decrease than in the 38 % infarct. From the average stress in both infarcted models there is a decrease in the stresses within the infarcted region as a result from the G25 volume. Additionally, it is noted that there is a substantial decrease to below the average stress of the healthy case. It should be noted that the geometry of the 38 % infarct with no gel shows an increase in the average stress whereas that of the 10 % infarct shows a decrease in the average stress from the healthy state. Figure 4-17 (c) and (d) show the maximum and average strain observed in the two geometries. In all cases, the G25 shows a decrease in the strains. Furthermore, the decrease in the strains in both the maximum and the average is shown to be greater in the 10 % infarct model than in the 38 % infarct model. The

decrease in the average in-fibre strain for the 10 % infarct model is 46.4 % whereas for the 38 % infarct model it is 23.7 %.
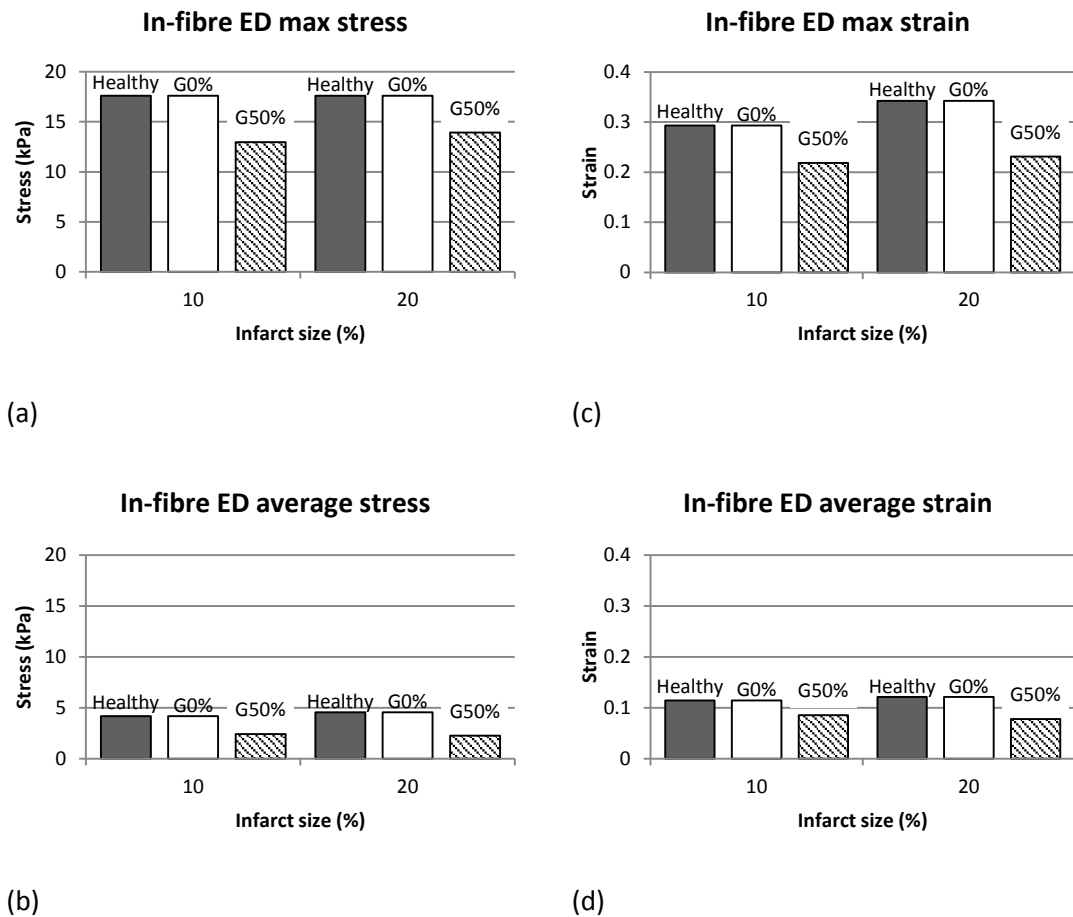


(a)

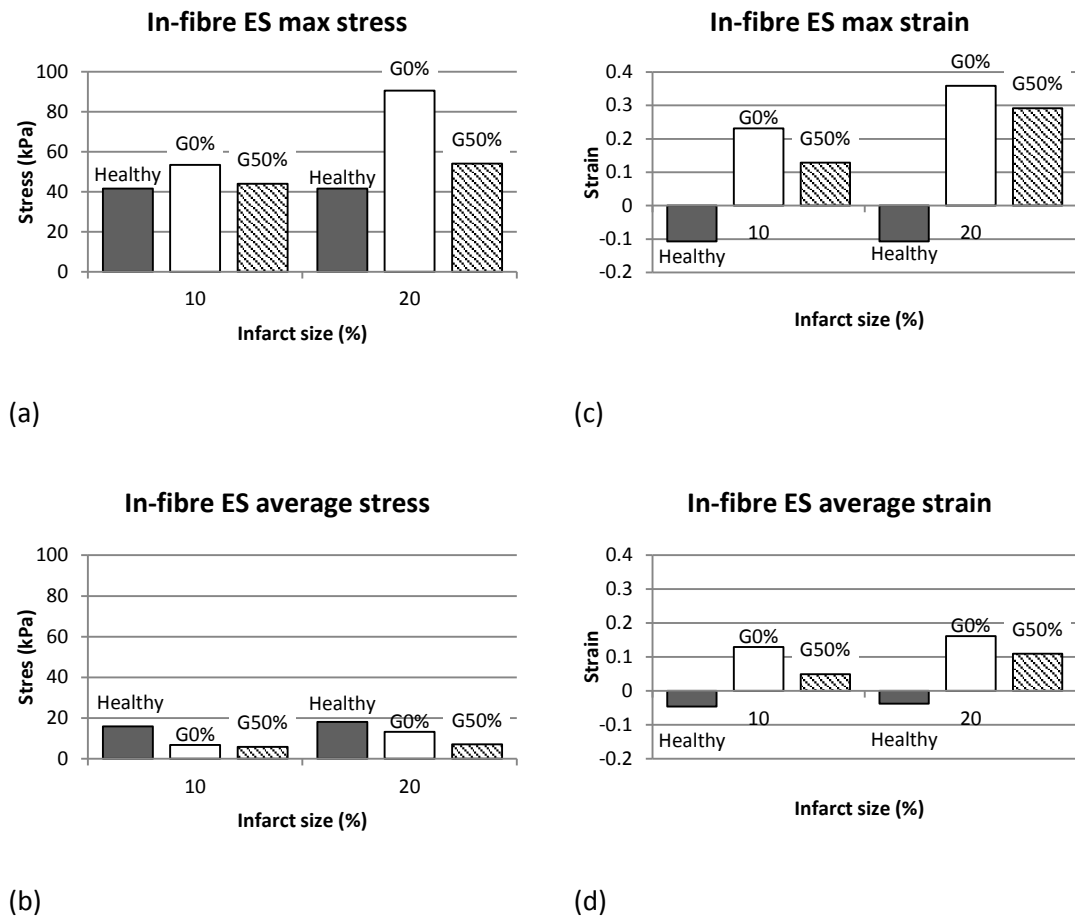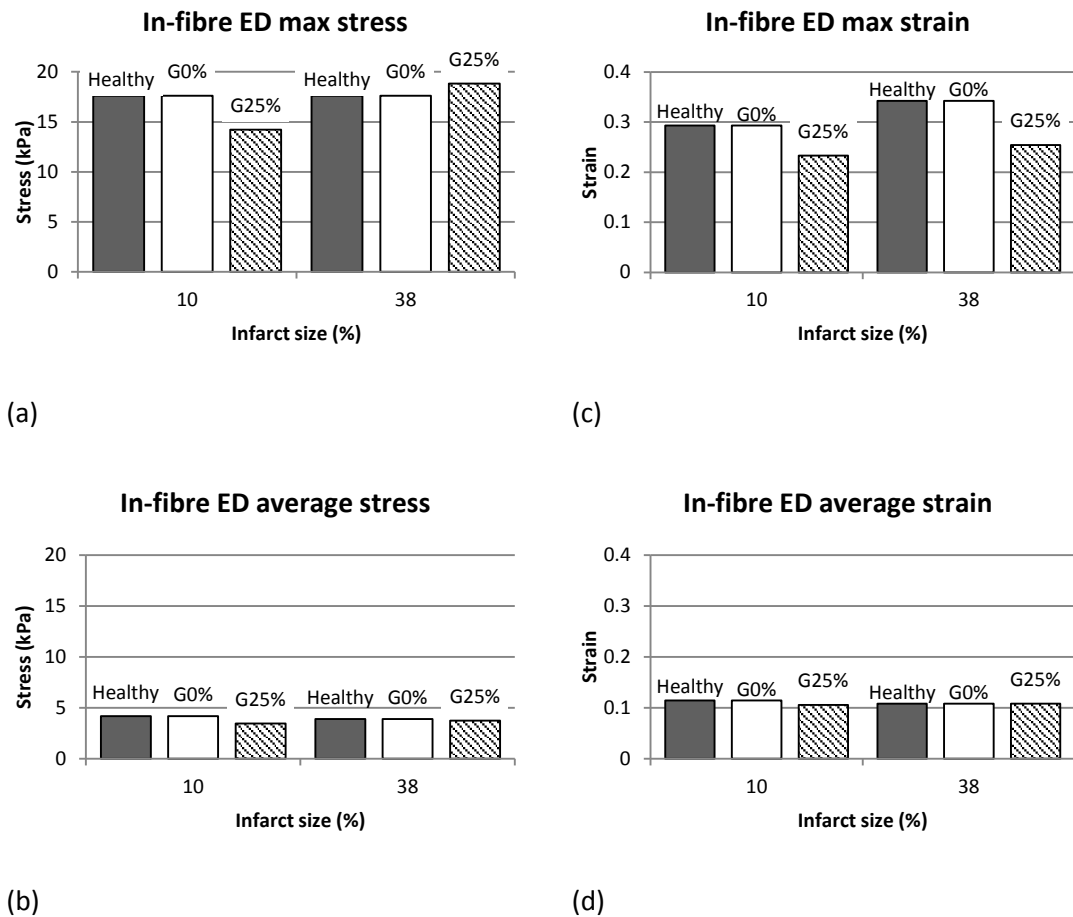

(c)



(b)



(d)
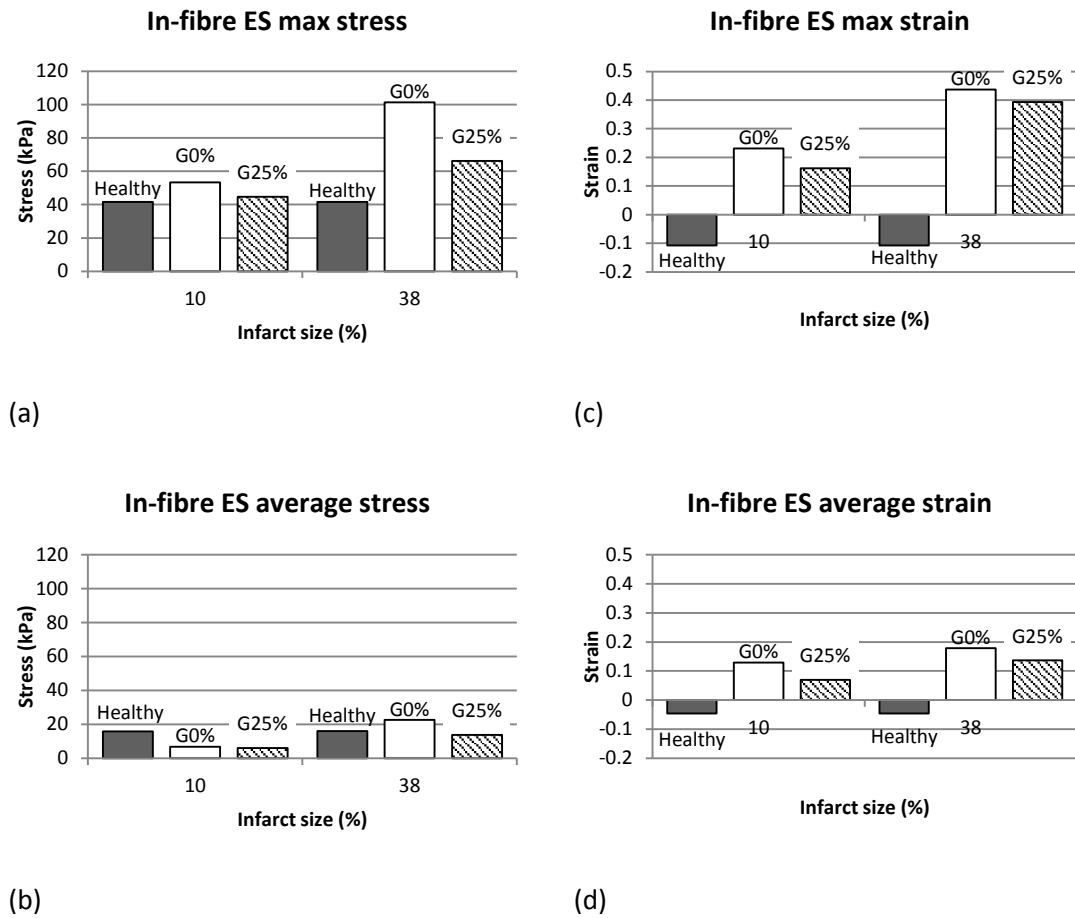
*Figure 4-17: Maximum and average stresses and strains for the rat heart model at end-systole of the 10 % and 38 % infarct with the healthy case, the infarcted case (no gel), and 25 % hydrogel injectates modelled: (a) maximum in-fibre stress for each case, (b) in-fibre average stress, (c) in-fibre maximum strain and (d) average in-fibre strain*

# 5   Discussion

In this study, a realistic geometry of a rat heart was created based on MRIs. This geometry was validated by the calculated volumes as well as literature. The geometry of the healthy case was used as a control to which further models were compared. Initially various anterior apical ischemic infarct sizes were included into the geometry and the effect was recorded. With these results possible trends were observed and analysed. It aimed at determining the relationship of increasing infarct size to both the functional parameters and the stress and strain characteristics. Additional studies involved hydrogel injection into the myocardial wall. A series of injectate models were simulated and similarly compared to the healthy and infarct cases without the treatment. Furthermore, various volumes of hydrogel were also modelled with the goal of determining a relationship between the functional and mechanical improvement to infarct size. This relationship would be important in the development of a clinical tool to determine the optimal volume of hydrogel injectate for each specific infarct case.

The hydrogel modelled was a polymeric biomaterial, known as polyethylene glycol (PEG). Modelling involved the injection of the gel into an ischemic anterior apical infarct. A biventricular model was created based on the Magnetic Resonance Images of a healthy rat heart. Hydrogel and infarcted tissue was modelled by assigning relevant material parameters to the region of interest. Since the infarct described for this study was an early infarct, there was no change in the passive material properties of the tissue for the case of the infarct, but only active contraction was removed. Additionally, no wall thinning was needed during this phase of the infarct since wall thinning occurs predominantly in the later stages of healing after myocardial infarction. Moreover, the implementation of the hydrogel into the infarcted tissue involved the addition of volume and therefore wall thickening. The gel material properties were assigned according to a homogenized model that was created involving a mixture of both the gel and the infarcted tissue.

The passive filling phase was simulated by increasing the internal pressure in the LV from 0 kPa to 3.36 kPa, and in the RV from 0 kPa to 1.78 kPa. This showed the diastolic phase of the cardiac cycle. For the case of the active contraction phase, the myocardial tissue was contracted with constant cavity volume. This marked the end-systolic point in the cardiac cycle. The active modelling was achieved by combining both the passive material properties described by the constitutive equation and the active material properties described by the Guccione et al. (2001) active stress model on the cellular level. Output cardiac performance data as well as the predicted stress and strain data for each instance were presented in

section 4. This chapter will cover the discussion of the generation of the model, including boundary and loading conditions as well as the results.

## 5.1 Development of the Finite Element Models

### 5.1.1 Generation of the Geometry of the Healthy Heart

The model creation involved the implementation of the myofibre orientation within the myocardial wall. These were set by assigning the end point orientations using MS *excel*, after which *Continuity* was then used to average the orientations throughout the myocardium. The fibre angles used were of a rat heart taken from the data in the study by Omens et al. (1993). These angles presented were -52° on the epicardial surface and 53° on the LV surface. It was found that although several species exhibit similar fibre angles, it is most accurate to determine the fibre orientation of each individual within a species since the orientation differs between individuals within a species. It was therefore taken to be important to use data specific for rats for the sake of this study, although other studies have modelled one species of heart using another species fibre orientation (Wenk et al., 2011).

### 5.1.2 Boundary and Loading Conditions

Boundary conditions are required to restrain the model simulating the physical/real situation. In this study, due to the element type that is used in *Continuity*, it is necessary to apply boundary conditions to the apex of the geometry to ensure that the geometry does not display non-realistic behaviour. The boundary conditions applied at the apex constrain the geometry from acting like a cylinder due to the apical hole. Furthermore, boundary conditions were needed to anchor the base to the global coordinates as well as describe effects that would be present due to valve openings and annuli (Guccione et al., 1995, Vetter and McCulloch, 2000).

Loading conditions are different for the EDPVR as compared to the ESPVR. In the case of the EDPVR the internal cavity pressures of both the LV and RV were set to increase linearly to model the passive filling process. For this study, the end-diastolic LVP was chosen to be 3.36 kPa. Values of pressures range substantially in literature for rat cardiac hemodynamics. Additionally, some studies give a measurement of the LV end-diastolic diameter, and the LV end-systolic diameter (Landa et al., 2008, Dobner et al., 2009). The reason for this substantial difference seems to be due to the complexity of accurately measuring the pressure within such a small volume. According to the study by Dai et al. (2005) the EDP is approximately 106 mmHg (14.13 kPa), but another study by Shioura et al. (2007) shows an EDP of approximately 5.0 mmHg (0.67 kPa). Therefore the end-diastolic pressure for this

study was determined by the pressure at which the EDV was achieved that retains stability for the geometry.

Running the ESPVR simulations involved choosing initial conditions for the simulation from the EDPVR results. The active contraction function was applied while the cavity volumes were held constant.

In the case of the ESP for the infarcted cases and hydrogel injectate models, the ESP was taken to be constant for all situations. In the literature there was no conclusive results found representing the effect that an infarct has on ESP. The theory whereby this method was based is that the aortic valve will only open once the aortic pressure is reached. It is unclear if this is the case in experimental data.

### 5.1.3 Constitutive Law and Active Stress Model

Biaxial testing showed that passive myocardial tissue displayed anisotropic material behaviour, with greater stiffness in the fibre direction (Demer and Yin, 1983); therefore, the tissue was approximated to be transversely isotropic for this study. This approximation shows isotropic behaviour in the plane normal to the fibre orientation. Furthermore, myocardial tissue also displayed nonlinear, viscoelastic properties, which can be approximated to be pseudo-elastic (Bogen et al., 1980). The transversely isotropic nature has often been used in previous studies, and is well established in the cardiac mechanic field (Guccione et al., 2001, Kortsmit et al., 2012, Wenk et al., 2011). The material parameters required by the strain energy function were based on the studies by Omens et al. (1993) with minor changes made in the verification process.

For compressibility, myocardial tissue has been defined as slightly compressible under physiological loads (Yin et al., 1996). Therefore the myocardial tissue for this study was defined as quasi-incompressible with the aid of a penalty function (Doll and Schweizerhof, 2000).

Active myocardium has been described computationally as the summation of both the passive strain energy function and a fibre directional active component. The active component used in this study has often been used in literature (Wenk et al., 2011, Walker et al., 2005, Kortsmit et al., 2012, Guccione et al., 2001), and is based on the calcium concentration within the tissue as well as sarcomere length relationships. For the case of the infarcted tissue, the calcium concentration in the localized area of the infarct was set to zero thus turning active contraction off in that area.

Furthermore, an additional term was used in this study in order to describe the hydrogel tissue. This neo-Hookean term and was added to the pre-existing constitutive functions

which then allowed representing the healthy tissue, the infarcted tissue and the hydrogel. The different material regions were defined as: the healthy tissue where no gel was present; the BZ where partial contractility was preserved, but no gel was present; the infarcted tissue with no gel as well as the active contraction turned off; and a homogenized layer of gel and infarcted tissue.

### 5.1.4  Developing the Infarct and Gel Injectate Models

An acute anterior apical infarct was modelled in the biventricular model of the rat heart. Three sizes were modelled, namely 10 %, 20 % and 38 % of the LV wall volume. The acute phase marks the very early stage directly after the infarct takes place, and therefore represents seconds to minutes after the infarct takes place. It has been shown by Holmes et al. (2005) that in the early stage after an infarct, there are no passive mechanical changes that take place on the properties of the myocardium. On the other hand though, the infarcted myocardium loses all active contractile ability and therefore is significantly impaired during the systolic phase of the cardiac cycle. This can be seen in Figure 2-8. Therefore in the case of modelling, the material properties for the infarcted region was set to retain all passive mechanical properties, but the active contraction was turned off by setting the calcium concentration to zero. The transition region around the infarcted area composed of partially infarcted material known as the BZ. This area was set to have 50 % contractile ability based on the results of the study by Guccione et al. (2001).

Regarding the location of the injectate inclusions, it is unclear whether greater benefit is obtained from multiple inclusions around the infarct as opposed to the inclusion within the infarct region itself. It is understood however, that since wall thinning occurs as part of the remodelling phase of the infarct that elevated stresses would be present and therefore injectate to merely increase the wall thickness would be of more benefit than no gel within the infarct. On the other hand though, causing the inclusion of the injectate to cross the boundaries of the infarct could cause an anchoring effect; whereby the infarcted portion of the myocardial wall will have greater structural strength and resistance to dilation. The question still remains though as to what the effect of different gel injectate locations have on the functionality of the heart. To clearly determine this, a comprehensive study would be required comparing purely the injectate sites and their individual effect. For the purpose of this study, only inter-infarct injectates are considered and therefore the effect of different injectate locations are beyond the scope of this study.

Three main hydrogel injectate volumes were analysed, namely 25 %, 50 % and 75 % of the infarct volume. Although a realistic model of gel injected into an early infarct forms thin layers within the myocardial tissue (Kadner et al., 2012), it is very difficult to accurately

simulate this. Recent studies have been performed involving the reconstruction of the hydrogel seen in histological by Sirry et al. (2013). In this study, the aim was to accurately reconstruct the thin layers observed *in situ*, and to therefore increase the geometrical accuracy of the model. Although this model accurately represents the hydrogel layers the model is highly complex and cannot be represented using *Continuity*. Therefore the gel was modelled as a homogenized mixture of the gel and the infarcted tissue, similar to that seen in previous studies (Wall et al., 2006, Wenk et al., 2011). Furthermore, the gel was modelled as an inter-infarct injectate where all the added gel volume was within the infarcted region. Although the bulk homogenized mixture is a simplification of the real thin layers, it was understood that this simplification would give a good estimation of the real case.

## 5.2   Validation of the Finite Element Models

The models describing the constitutive and active stress used in this study have been verified by experimental data. Material parameters specific for the rat heart were taken from the parameters used in the study by Omens et al. (1993). Using these parameters and the constitutive and active stress models, the entire model was validated. It was found that for the specific rat model in this study, small adjustments were needed for the specific material parameters to ensure accurate end-diastolic and end-systolic volumes were obtained when compared to the MRI's. Moreover, stress and strain data at the end-diastolic time point was compared to the experimental data presented by Omens et al. (1993). Consequently, the difference in the volumes was less than 2 % for the geometry of the healthy heart and was considered to be acceptable and therefore the geometry would give a realistic representation of the rat heart. Moreover, the cavity volumes as well as the total volume of the recreated model were smaller than the volume measured from the MRI's. The difference is due to the mesh fitting process losing some accuracy in the creation of the mesh. Another cause for the difference is the limited amount of contour points and the undefined region between the points.

Very little literature was found on experimental data of the stress and strain characteristics for the rat heart. The study performed by Omens et al. (1993) showed some stress versus strain characteristics which were used to validate the stress and strain characteristics observed in the computational model used in this study. With the adjustment of the stress scaling coefficient as well as the strain coefficient in the cross fibre direction, a comparable stress versus strain relationships was obtained to those in the Omens paper (1993).

The healthy case showed end-diastolic in-fibre stress to be about 9 kPa at a 20 % strain. This was compared to the data from the Omens (1993) study, which showed in-fibre stress to be approximately 7 kPa at 20 % strain. In the cross-fibre direction, both this study and the experimental data from the Omens (1993) study showed a stress of 2 kPa at 20 % strain. Areas that would give rise to differences in the stress results here are due to the geometrical differences, where the geometry is species as well as individual specific. Further differences could be cause by the simplifications of the computational model when compared to experimental data.

Further validation procedures were to determine the EF of the computational model of the rat heart and compare this with experimental data. EF for the healthy case of this study was 49.7 %, whereas literature indicated higher values for the healthy case (Saleh et al., 2012, Wang et al., 2009). Although the literature does indicate higher values for healthy EF, some studies have indicated values ranging from about 48.5 % to about 56.0 % (Ruetten et al., 2005, Yoon et al., 2009). Furthermore, since the ED and ES volumes were validated with the MRI data, the EF was considered to be accurate for this study. Table 5-1 shows a comparison between the experimental values for EFs of several studies with the EF of the healthy rat heart case used in this study.

*Table 5-1: Comparison of EF from the model of this study to experimental data*

|  | EF (%) |
|---|---|
| Rat model (this study) | 49.7 |
| Rat data (Ruetten et al., 2005) | 56 ± 2 |
| Rat data (Yoon et al., 2009) | 48.5 ± 8.0 |
| Rat data (Saleh et al., 2012) | 75.7 ± 1.2 |
| Rabbit data (Wang et al., 2009) | 75.3 ± 6.0 |

For the validation of the geometries representing the gel injectate, the wall thickening needed to be confirmed to include the respective added volume. The calculated volumes were compared to the actual volumes in the geometry after wall thickening. The difference between these volumes was less than 6.5 %.

From the volume data presented in Table 4-4 it is shown how the increase in wall volume affected the cavity volumes as well as the total epicardial volume. The RV cavity volume remains unchanged in every instance where the wall thickening had been applied due to

the hydrogel injectate. This is because the wall thickening was applied to the region of the geometry representing the LV wall; this is within the modelled infarct region. The wall thickening was not applied into either the septal region or the right ventricular free wall region, and therefore no noticeable effect on the RV cavity volume was observed. Studies have showed that there is wall thickening that occurs as a result of hydrogel injectate (Ifkovits et al., 2010, Kadner et al., 2012), suggesting a reduction in the LV cavity volume. Additionally, an experimental study on sheep hearts indicated a reduction in the LV cavity volume after the injectate of a biomaterial into an infarct (Morita et al., 2011).

## 5.3 Comparison and Effect of Infarct Sizes

In cardiac mechanics there are two main methods for determining the performance of the heart. These two methods involve analysing the pressure volume relationships as well as the functional parameters, and analysing the stress and strain characteristics. This section will compare and discuss the effect of infarct sizes on both the cardiac functional parameters and the stress and strain characteristics.

According to Abraham and Nishimura (2001) the most common method of determining the performance of a heart is to calculate the EF. Although this is the case, the EF does have limitations and is subject to error. Additionally, the EF is a functional parameter of the overall LV performance, and seems to overlook localised dysfunction within minor regions of the heart structure. Therefore multiple parameters were analysed in this study as well as the stress and strain characteristics.

### 5.3.1 Cardiac Function

Cardiac functional parameters represent measurable aspects that give an indication of the effectiveness of the heart as a pump. In this section, the cardiac functional parameters of various infarct sizes are compared with a control heart model to determine the effect of infarct size on the heart. The functional parameters that will be discussed include the dead volume, the ES elastance, the SV, and the EF. Furthermore, other important characteristics observed in the results will also be discussed such as the ES volume.

From the comparison of the EDPVR's and the ESPVR's of the healthy case and the three infarct sizes (Figure 4-5), it is shown that the EDPVR remains unchanged. This is expected since the infarcts in each case represent very early infarcts, therefore no passive mechanical changes had yet taken place in the myocardium. On the other hand, the ESPVR shows change. There is a clear indication that the intercept on the horizontal axis increases with increasing infarct size, and the ES elastance decreases to a small extent. These two observations will be discussed in greater detail with the use of Figure 4-6. From the graph

of Figure 4-5 there is a considerable increase in the ESV with increasing infarct size. The ESV of the healthy case is about 116 µl, showing that the maximum increase in the ESV is an increase of 55 µl for the 38 % infarct size. Furthermore the ESV increase is non-linear. The reason for the substantial increase in the volume is due to the bulging out of the infarcted tissue. Since this tissue does not contract it acts as passive material and therefore dilates while the pressure increases due to the contracting healthy myocardium. In the case of the smaller infarct sizes (10 % and 20 % infarcts), it is understood that a small amount of compression takes place, compressing the infarcted tissue in the plane of the wall. The smaller infarct area results in a smaller resultant force due to this pressure. This may lead to less bulging compared to the larger infarct area.

From Figure 4-6, the effect of infarct size on the functional parameters is observed. Figure 4-6 (a) shows the EF for each case. There is a clear reduction in the EF with an increase in the infarct size. This shows that the heart pumps less blood in ratio to the EDV with increasing infarct size for an early infarct. It is understood that since there is an increase in the ESV, and for no change in the EDV for an early infarct, the SV is expected to decrease. The SV represents the amount of blood that is ejected by the LV, and thus a decrease in this indicates a drop in the functionality of the heart. The dilation caused by the infarcted region therefore causes the SV to decrease and less blood is pumped by the LV. In the case of the 38 % infarct, there is only about 50 % of the healthy EF retained and also a drop of almost 50 % in the SV. The observation here of 38 % infarct gave a reduction in the EF of about 50 % for the experimental study performed by Wang et al. (2009). In this study, infarct sizes of around 40 % were analysed showing the EF dropping from 75 % to 38 % showing a decrease of about 50 %.

The dead volume represents the volume of blood in the LV when the transmural pressure is zero. An increase in the dead volume appears to be a result of a decrease in the ES performance. From the results of this study, it is evident that there is an increase in the dead volume with an increase in the infarct size. This indicates that there is a decrease in the performance of the heart with an increase in the dead volume as a result of the increase in the size of an infarct. This is substantiated by the decrease in function due to EF and increase in ESV.

Furthermore, $E_{max}$ which represents the elasticity as well as the contractility of the myocardium decreases with an increase in infarct size. From this it is noted that the tissue is impaired in its ability to return to its original structure as before. To determine a clearer relationship of infarct size to the respective cardiac dysfunction more infarct sizes need to

be analysed. For the purpose of this study, the observations that there is a steady decrease in the performance are sufficient.

## 5.3.2  Myocardial Stress and Strain

Although very little reliable experimental stress and strain data for a rat heart were available in the literature, the stress and strain characteristics display integral characteristics of the change in the material's mechanical properties. The stress and strain data is especially beneficial when comparing to a control for the purpose of determining the effect on the mechanical properties that changes have on the myocardial tissue. Therefore the stress and strain data representing the healthy rat heart has been obtained, and is used as the control for the models of the infarcted hearts.

Figure 4-7 displays the end-diastolic stresses and strains of the infarcted cases compared to the healthy case for the same region. In each case, the stress and strain data was taken from the respective infarct region. It is observed that there is no difference between the infarct cases and the healthy comparison for each instance. This once again indicates that the infarct is an early infarct and still retains all passive material properties. Therefore, there are no stress or strain changes. On the other hand, there are differences from infarct to infarct. These differences are region dependent, since the larger infarct includes more volume, there is more tissue included in the region analysed in each case.

Figure 4-8 shows the behaviour of the infarcted models compared with the healthy case for the same region at the ES time point. It is noted that both the maximum and the average stress increases with increasing infarct size, aligned with this the strain also increases with increasing infarct size. These results are expected since in the greater infarct, there is a greater region, more myocardial tissue is unable to contract and thus acts purely passively. This passive behaviour causes the tissue to dilate while the healthy tissue contracts increasing the cavity pressure. There is understandably a different degree of bulging in different infarct sizes and also different stresses experienced within the infarcted regions.

Figure 4-8 (b) shows average end-systolic stress. It is observed that the myocardial average stresses for both the 10 % and the 20 % infarct sizes indicate a decrease in the stress. A closer analysis of the stress results displayed negative stresses within the infarcted region, which implied that compression occurred in these regions. This was seen in the BZ of the infarct. Therefore, the compression that was taking place was not due to the infarction region contracting as healthy tissue, but rather being compressed by the contracting healthy tissue on the edge of the infarct region. For the case of the 38 % infarct, the compression effect was still present, but the infarct was so large that it did not have a

substantial effect on the average stress within the infarct. Therefore with an increase in the ratio of BZ to infarct volume, there is an increase in negative pressures, thus decreasing the average stress for the infarcted region.

In the Figure 4-8 (c) and (d) the ES myocardial strain is shown. The negative strain observed in the case of the healthy heart is due to the active contraction present in the tissue. Since the area representing the infarcted regions contains no contractile ability, the active compression is not possible and therefore the tissue in this region dilates, showing a positive strain.

## 5.4 Comparison and Effect of Hydrogel Injectate

In an attempt to determine the true value and effect of hydrogel as an injectate for the treatment of myocardial infarction, an analysis to determine the effect of hydrogel volume on an infarct was performed. The infarct size of 10 % was modelled with three injectate volumes, namely 25 %, 50 % and 75 % of the infarct size. Furthermore, the following comparisons are also made: 10 % and 20 % infarct with an injectate volume of 50 %; and 10 % and 38 % infarct with an injectate volume of 25 %. The objective was to obtain a better understanding of the hydrogel as a therapy as well as to determine the relationships of hydrogel volume on functional parameters.

### 5.4.1　10 % Infarct Size with Three Volumes of Hydrogel Injectate

The hydrogel does affect both the diastolic and systolic phase of the cardiac cycle. Within the region of the infarct, the added volume of the gel into the myocardial wall causes a thickening of the wall. Moreover, the wall with the gel becomes a mixture material of both the passive infarcted myocardium and the injectate causing an increase in the wall thickness. An increase in the thickness of the wall increases the stiffness of the material. Therefore, indicating that the addition of a greater volume of gel within the localized region causes the wall to have a greater thickness and thus a greater stiffness. From the Figure 4-9 more gel volume causes an increase in the slope of the EDPVR. This consequently causes the EDV to decrease for the constant EDP of 3.36 kPa. The volume decrease from the healthy and infarcted case without gel of approximately 230 µl is about 220 µl, 215 µl, and 208 µl for the hydrogel injectate volumes 25 %, 50 % and 75 % respectively. This decrease in the EDV does indicate a negative impact due to the hydrogel injectate. According to literature an increase is often seen in the EDV, although the degree to how much is unclear. Therefore in this study a constant EDP was used to analyse the results, similar cardiac modelling studies also used this method (Miller, 2012, Kortsmit et al., 2012).

The comparison of the ESPVR's in Figure 4-10 display beneficial effects of the hydrogel injectate. The dead volume decreases as well as the ESV. The reason for the ESV decreasing is caused by the increase in the stiffness within the infarcted area. Since there is an increase in the gel volume within the infarcted area, there is a decrease in the average ES strain in Figure 4-12 for the G25 and G50 models. The increase in the strains in the fibre direction observed in the G75 model is understood to be due to a greater surface area of infarct region, created by the injecting of the large volume of gel. Since there is a greater surface area, there is a greater resultant force that acts on the infarct causing larger strain. There is though, a reduction in the strain from the healthy case to the G75 model for this region, showing that there is the expected stiffening effect of the addition of gel into the myocardial wall. From the results of Table 4-5, although small, there is an increase in the ES elastance, restoring this function closer to the healthy case. Furthermore, from these results there is an increase in the dead volume from the G50 model to the G75, this shows a detrimental effect, since an increase in the dead volume indicates a decrease in cavity volume. Additionally, the EF in the G75 model also displays a detrimental effect when compared to the G50 model. Although the EF of the G75 is an improvement on the infarcted case, there is a slight decrease from the G50 case. Therefore the results display non-linear relationships for the gel and the effect on the cardiac functional parameters. It is understood that the reason for the decrease in EF and increase in the dead volume from the G50 to the G75 cases is due to the large amount of gel in the case of the G75 model causing a large decrease in the LV cavity volume. Figure 4-10 indicates that the benefit observed in ES for the G25 and G50 models is not present in the G75 model. Furthermore, Figure 4-9 of the ED indicates consistent change with the increasing volume of hydrogel injectate. This suggests that the increased volume of injectate to 75 % caused impairment on the contractility of the heart. The increased volume is understood to have caused an overall increase in the ventricular stiffness preventing the healthy tissue from contracting. This is not seen in the G25 and G50 models since the gel volume is less than the G75 case.

Looking at Figure 4-11, at the ED time point with respect to the stresses and strains, it is clear that there is a continual decrease in the stress. Average strains also decrease with increasing gel volumes. This reduction is expected, especially in the results of the averages, since the added gel causes stiffening in the region of interest, giving rise to less deformation and less stress experienced. Although, a decrease in the stress is beneficial in most applications, it is noted that in the case of the ED time point, the stress experienced by the infarct tissue with no gel is the same as the stress for the case of the healthy model. This decrease in stress corresponds to an increase in the wall stiffness for the localized area. An

increase in the stiffness impairs the passive function of the heart and therefore although there is a decrease in the stress, this is seen to be a detrimental change due to the hydrogel. It should be noted that, for the average and maximum strains in the fibre direction, there is a decrease from the healthy case to the G25 model. Moreover, with the addition of more gel, the strains are decreased further.

The maximum stress in Figure 4-12 at the ES time point shows an increase from the healthy case, whereas the average stress shows a substantial decrease. Negative stresses were found near the borders of the infarct and were understood to be the result of passive compression due to the active tissue contracting around these regions. The maximum positive stresses were experienced near the centres of the infarct region. Therefore the average stresses for the active compression for the 10 % infarct showed a significant decrease from the healthy case. It should be noted that as indicated in section 4.3.1, the healthy tissue under active contraction experiences positive stress whereas the infarcted tissue under passive compression experiences negative stress.

### 5.4.2    Effect of 50 % Injectate on 10 % and 20 % Infarcts

It is necessary to determine whether the results from the 10% infarct cases can be extrapolated from one infarct size to another, and to determine universal trends. The next two sections (5.4.2 and 5.4.3) compare: the 10 % infarct to the 20 % infarct size with 50 % gel volume; and the 10 % infarct size with the 38 % infarct with G25 injectate.

The EDPVR results (Figure 4-13) of the G50 models show that in both infarcts, the gel has similar effects. From the EDPVR's, a stiffening is noted by the increase in the gradient. From the ESPVR, the G50 in the 10 % infarct causes the ESPVR to be very close to that of the healthy ESPVR. On the other hand, the 20 % infarct still shows an elevated dead volume as well as an increased ESV. From the $E_{max}$, unlike the case for the 10 % infarct case, there is a decrease from the 20 % infarct case to the gel model. This decrease though is less than a 2 % decrease and is therefore taken to be minor. In both infarct models with G50 there is a substantial decrease in the dead volume, the difference is within 4 % of each other, both showing a decrease of about 20 %. There is also a beneficial increase in the EF in both models, although the increase in the 20 % infarct model is considerably more than in the 10 % infarct model. Contrary to this, the SV increases for the 20 % infarct, but decreases in the case of the 10 % infarct. The SV of the healthy case is 114.6 µl; therefore although there is a substantial increase in the case of the 20 % infarct, the SV remains to be impaired, but has improved.

The stress and strain results show similar trends in both cases. For the ED time point there is a reduction in both the models for the stress as well as the strain. The stress and strain results at the ES time point show that there is also a decrease in both the infarct cases for the 50 % gel volume. This shows beneficial results since an increase was observed from the healthy case to the infarcted cases without gel with respect to the maximum stress and strain as well as the average strain. It is understood that the beneficial decrease in the stress as well as the strain is due to the increased stiffness within the myocardial wall. The decrease in the stress and strain data, although in both models, is not the same or a similar ratio of change in both infarct models.

### 5.4.3    Effect of 25 % Injectate on 10 % and 38 % Infarcts

From the cardiac functionality of the G25 in the infarcts of 10 % and 38 % there is a similar decrease in the dead volume, as well as a similar increase in the EF. The results of the 10 % and 20 % infarcts with the G50 indicate a very similar difference as in the decrease in the dead volume. For the case of the 38 % infarct with G25, there is a decrease in the value of $E_{max}$. Furthermore an increase is observed in the SV due to G25 injectate. The 20 % infarct with G50 gel case had a similar result

From the ED time point, the maximum stress for the 10 % infarct there is a decrease, whereas there is an increase for the 38 % infarct (Figure 4-16). The increase indicated in the maximum stress of the 38 % infarct is very small. On closer analysis, it was observed that the maximum stress was found along the border of the gel, and was therefore considered to be due to a stress concentration caused by the difference in material properties of the gel and the infarcted tissue. In the case of the average stress though, there is a decrease in the 10 % infarct model as well as the 38 % infarct model. The relative decrease in the 38 % infarct though, is much less. The decrease observed in the stress is due to the added hydrogel increasing the wall thickness. Looking at the strain, both models show a decrease in the maximum strain. The average strain shows a decrease for both models. The decrease in the average ED strain of the 38 % infarct is very small; less than 1 % difference.

The end-systolic stresses and strains show that the addition of the hydrogel injectate causes a decrease in both the maximum and the average values as compared to the infarcts with no gel. The decrease in each case of both the 10 % and the 38 % infarct is substantial showing that G25 injectate improves the impaired stress and strain for the end-systolic time point. It is noted that the decrease in the stress and strain for the end-systolic time point is due to the added gel increasing the mechanical stiffness, preventing the myocardial wall in the infarcted region from dilating. This is a beneficial effect since critical stresses

which could cause rupture in the cardiac wall could be reduced and evident heart failure would be averted.

## 5.5 Limitations and Recommendations

In an attempt to clearly determine the relationship of the gel volume on the infarct sizes, each of the gel volumes should be modelled for each infarct size. Unfortunately due to time constraints, this was not possible. Therefore this study performed the starting stages in determining the relationship of hydrogel volume to infarct size.

For this thesis, some results did not exhibit similar trends, and therefore more models are needed to clearly understand the behaviour and reaction of each individual infarct to the hydrogel injectate. The differences in these simulation results could be influenced by the geometrical differences between the models, and even the difference in the geometrical layout of the different infarct sizes. For instance, it is unclear whether an infarct of 10 % located in a different region would behave and respond to the hydrogel treatment as the anterior apical infarct represented in this study.

This study only explored the effects of the hydrogel on the acute infarct, whereas the mechanical properties of the myocardial tissue change considerably after an infarct depending on the time post-infarction (Holmes et al., 2005). Therefore it is also necessary to perform the same studies of the hydrogel injectate for different healing phases post-infarction.

This study involved an MRI constructed geometry representing both the LV and the RV. Previously many studies have only modelled the LV, although this is a step in modelling the heart, it is a simplification. It has been indicated by Fogel et al. (1995) that both the septum between the RV and LV as well as the thin pericardium surrounding the heart add to the accuracy of the modelling of the heart. Although the biventricular model was used in this study, simplifications were still made, and improvement in these areas can be made. Firstly the fibre orientation used in this study was simplified such that the computational model would be robust, avoiding areas of discontinuous stress. An accurate fibre model would therefore improve the model.

Another simplification that was made was the layout of the hydrogel injectate. Although an attempt was made to accurately define the hydrogel as a homogenized mixture of both the infarcted tissue and the gel material, the method of defining the homogenized mixture needs to be refined. The difficulty with refining the layout is that, in practice, the gel does not cover the exact same region every time. Furthermore, the an improvement on the modelling of the gel would be either to define more field variables and use higher

computational power to be able to run the simulations or to use another FE software package where the elements can be accurately defined as the gel layout. It is recommended that the accurate hydrogel reconstructed geometry from the study by Sirry et al. (2013) be used and simulations modelled using another FE modelling software package that can incorporate this geometry.

There are many different strains and breeds of rat, for various weights and age, under very different environmental conditions that have been experimented on with regards to hydrogel therapy. Furthermore, many different species of hearts are used in hydrogel therapy studies, both experimental and computational. It is important to use the correct tissue mechanical properties for the cardiac geometry being modelled. Unfortunately due to the complex nature of testing the mechanical characteristics as well as accurately determining hemodynamics it was not possible to use the rat heart specific to the mechanical and hemodynamic data. It is advised that in future studies, patient specific data is obtained and used in the modelling process for the specific geometry used. Furthermore, obtaining the hemodynamic data for a rat heart is very complex since the structural dimensions of a probe used to determine the pressures occupies a significant volume of the cavity, and therefore the results obtained are affected by the probe. A method suggested for small heart models is MRI tagging.

Further recommendations include determining the effect of the hydrogel injectate incorporated into the BZ causing an anchoring effect as well as within the healthy tissue and not only the infarct region. For this study, the hydrogel was modelled purely within the infarct region to ensure that additional effects would not interfere with the aim of the study.

# 6 Conclusions

From this study, apart from the ES maximum and average strain, and the maximum stress for the 10 % infarct with G75 case, the stress and strain in all other models was reduced as a result of inclusion of the biomaterial injectate. A decrease in the stress reduces the possibility of rupture, and similarly the reduction in the strain shows a decrease in impairment due to energy loss from the ventricular wall dilating. An increase in the infarct stiffness due to the increased wall thickness causes the BZ healthy tissue to be affected less by the dilating infarcted tissue. A decrease in the total heart stresses and strains displays a reduction in total ventricular hypertrophy. Furthermore it is also noted that the cardiac functional parameters are also improved by the addition of the hydrogel injectate.

Apart from the improvement of the adverse effects caused by the hydrogel treatment on myocardial infarction as well as the improvement in the cardiac functional parameters, very little research has been performed to determine the most effective parameters to be used for the injectate in the treatment. No studies as far as this study could find have been performed to determine the optimal volume of hydrogel to be used for patient specific infarct size. This study has begun to address this issue of the relationship of hydrogel injectate to infarct size. It is apparent from the results in this study that although injecting hydrogel into the infarcted myocardial tissue shows functional improvement, too much injectate could cause a detrimental effect on the performance. Additional adverse effects started to arise with the G75 injectate model indicated by increased average and maximum strain and increased maximum ES stress. Additionally, an increase in the dead volume was recorded with the G75 injectate volume from the G50 case, indicating a greater difference from the healthy case. All models indicated an improvement in EF, reducing the impairment due to infarction. The point at which the most benefit from the hydrogel injectate is obtained is considered to be the optimal volume of hydrogel injectate. This optimal volume is based on the reduction of stress and strain as well as the cardiac functional improvement. Although, due to time constraints, it was not possible to determine the exact relationship of the optimal hydrogel volume to infarct sizes; this study shows that the greatest benefit was obtained using the G50 injectate volume in the case of the 10 % infarct. With a comprehensive model showing the relationship of the optimal hydrogel to infarct size, clinicians would be able to easily determine the correct amount of hydrogel to treat a patient specific infarct size. A tool in critical clinical situations could prove invaluable such to ensure the conservation of cardiac function. The other two infarct sizes, 20 % and 38 % infarcts, indicated improvements similar to those recorded with the 10 % infarcts.

Although this study did not conclusively determine the relationship for the optimal hydrogel volume to infarct size, it marks the start for proceeding studies to continue the development of this crucial, clinical data. It is encouraged that following studies build on the results of this study to determine this critical relationship for all healing phases as well as infarcts for different regions of the heart.

# 7 Bibliography

ABRAHAM, T. & NISHIMURA, R. 2001. Myocardial strain: can we finally measure contractility? *Journal of the American College of Cardiology,* 37**,** 731.

AGUADO-SIERRA, J., KRISHNAMURTHY, A., VILLONGCO, C., CHUANG, J., HOWARD, E., GONZALES, M. J., OMENS, J., KRUMMEN, D. E., NARAYAN, S. & KERCKHOFFS, R. C. P. 2011. Patient-specific modeling of dyssynchronous heart failure: a case study. *Progress in Biophysics and Molecular Biology,* 107**,** 147.

AHA 2008. Heart Disease and Stroke statistics: Our guide to current statistics and the supplement to our Heart and Stroke Facts. Dallas: American Heart Association.

ALONSO, D. R., SCHEIDT, S., POST, M. & KILLIP, T. 1973. Pathophysiology of cardiogenic shock: quantification of myocardial necrosis, clinical, pathologic and electrocardiographic correlations. *Circulation,* 48**,** 588.

ANTMAN, E., BASSAND, J., KLEIN, W., OHMAN, M., LOPEZ SENDON, J., RYDEN, L., SIMOONS, M. & TENDERA, M. 2000. Myocardial infarction redefined--a consensus document of The Joint European Society of Cardiology/American College of Cardiology committee for the redefinition of myocardial infarction: The Joint European Society of Cardiology/American College of Cardiology Committee. *Journal of the American College of Cardiology,* 36**,** 959.

BEYAR, R. & SIDEMAN, S. 1984. A computer study of the left ventricular performance based on fiber structure, sarcomere dynamics, and transmural electrical propagation velocity. *Circulation Research,* 55**,** 358-375.

BIRNBAUM, Y., CHAMOUN, A. J., ANZUINI, A., LICK, S. D., AHMAD, M. & URETSKY, B. F. 2003. Ventricular free wall rupture following acute myocardial infarction. *Coronary artery disease,* 14**,** 463.

BOGAERT, J., BOSMANS, H., MAES, A., SUETENS, P., MARCHAL, G. & RADEMAKERS, F. E. 2000. Remote myocardial dysfunction after acute anterior myocardial infarction: impact of left ventricular shape on regional function:: A magnetic resonance myocardial tagging study. *Journal of the American College of Cardiology,* 35**,** 1525-1534.

BOGEN, D. K., RABINOWITZ, S. A., NEEDLEMAN, A., MCMAHON, T. A. & ABELMANN, W. H. 1980. An analysis of the mechanical disadvantage of myocardial infarction in the canine left ventricle. *Circulation Research,* 47**,** 728-741.

BOVENDEERD, P. H., ARTS, T., DELHAAS, T., HUYGHE, J. M., VAN CAMPEN, D. H. & RENEMAN, R. S. 1996. Regional wall mechanics in the ischemic left ventricle:

numerical modeling and dog experiments. *American Journal of Physiology - Heart and Circulatory Physiology,* 270**,** H398-H410.

BURKHOFF, D., MIRSKY, I. & SUGA, H. 2005. Assessment of systolic and diastolic ventricular properties via pressure- volume analysis: a guide for clinical, translational, and basic researchers. *American Journal of Physiology: Heart & Circulatory Physiology,* 58**,** H501-H512.

BURTON, R. A., PLANK, G., SCHNEIDER, J. E., GRAU, V., AHAMMER, H., KEELING, S. L., LEE, J., SMITH, N. P., GAVAGHAN, D. & TRAYANOVA, N. 2006. Three-Dimensional Models of Individual Cardiac Histoanatomy: Tools and Challenges. *Annals of the New York Academy of Sciences,* 1080**,** 301-319.

CHEN, J., SONG, S.-K., LIU, W., MCLEAN, M., ALLEN, J. S., TAN, J., WICKLINE, S. A. & YU, X. 2003. Remodeling of cardiac fiber structure after infarction in rats quantified with diffusion tensor MRI. *American Journal of Physiology-Heart and Circulatory Physiology,* 285**,** H946-H954.

CHRISTMAN, K. L. & LEE, R. J. 2006. Biomaterials for the treatment of myocardial infarction. *Journal of the American College of Cardiology,* 48**,** 907-913.

CHRISTMAN, K. L., VARDANIAN, A. J., FANG, Q., SIEVERS, R. E., FOK, H. H. & LEE, R. J. 2004. Injectable fibrin scaffold improves cell transplant survival, reduces infarct expansion, and induces neovasculature formation in ischemic myocardium. *Journal of the American College of Cardiology,* 44**,** 654-660.

CINGOLANI, O. H., YANG, X. P., CAVASIN, M. A. & CARRETERO, O. A. 2003. Increased systolic performance with diastolic dysfunction in adult spontaneously hypertensive rats. *Hypertension,* 41**,** 249-254.

COX, M. A., KORTSMIT, J., DRIESSEN, N., BOUTEN, C. V. & BAAIJENS, F. P. 2010. Tissue-engineered heart valves develop native-like collagen fiber architecture. *Tissue Engineering Part A,* 16**,** 1527-1537.

COX, M. A. J., DRIESSEN, N. J. B., BOERBOOM, R. A., BOUTEN, C. V. C. & BAAIJENS, F. P. T. 2008. Mechanical characterization of anisotropic planar biological soft tissues using finite indentation: Experimental feasibility. *Journal of Biomechanics,* 41**,** 422-429.

DAI, W., WOLD, L. E., DOW, J. S. & KLONER, R. A. 2005. Thickening of the infarcted wall by collagen injection improves left ventricular function in rats: a novel approach to preserve cardiac function after myocardial infarction. *Journal of the American College of Cardiology,* 46**,** 714-719.

DEMER, L. L. & YIN, F. 1983. Passive biaxial mechanical properties of isolated canine myocardium. *The Journal of physiology,* 339**,** 615-630.

DOBNER, S., BEZUIDENHOUT, D., GOVENDER, P., ZILLA, P. & DAVIES, N. 2009. A Synthetic Non-degradable Polyethylene Glycol Hydrogel Retards Adverse Post-infarct Left Ventricular Remodeling. *Journal of Cardiac Failure,* 15**,** 629-636.

DOLL, S. & SCHWEIZERHOF, K. 2000. On the development of volumetric strain energy functions. *Journal of applied mechanics,* 67**,** 17-21.

FISHBEIN, M., MACLEAN, D. & MAROKO, P. 1978. Experimental myocardial infarction in the rat: qualitative and quantitative changes during pathologic evolution. *The American journal of pathology,* 90**,** 57.

FLATHER, M. D., YUSUF, S., KØBER, L., PFEFFER, M., HALL, A., MURRAY, G., TORP-PEDERSEN, C., BALL, S., POGUE, J., MOYÉ, L. & BRAUNWALD, E. 2000. Long-term ACE-inhibitor therapy in patients with heart failure or left-ventricular dysfunction: a systematic overview of data from individual patients. *The Lancet,* 355**,** 1575-1581.

FOGEL, M. A., WEINBERG, P. M., FELLOWS, K. E. & HOFFMAN, E. A. 1995. A study in ventricular–ventricular interaction single right ventricles compared with systemic right ventricles in a dual-chamber circulation. *Circulation,* 92**,** 219-230.

FRANGI 2001. Three-Dimensional Modeling for Functional Analysis of Cardiac Images: A Review. *IEEE Transactions on Medical Imaging,* 20**,** 24.

FUKAMACHI, K. & MCCARTHY, P. M. 2005. Initial safety and feasibility clinical trial of the myosplint device. *Journal of Cardiac Surgery,* 20**,** S43-S47.

GEERTS, L., BOVENDEERD, P., NICOLAY, K. & ARTS, T. 2002. Characterization of the normal cardiac myofiber field in goat measured with MR-diffusion tensor imaging. *American Journal of Physiology-Heart and Circulatory Physiology,* 283**,** H139-H145.

GIBBONS, R. J., VALETI, U. S., ARAOZ, P. A. & JAFFE, A. S. 2004. The quantification of infarct size. *Journal of the American College of Cardiology,* 44**,** 1533-1542.

GÖKTEPE, S., ABILEZ, O. J., PARKER, K. K. & KUHL, E. 2010. A multiscale model for eccentric and concentric cardiac growth through sarcomerogenesis. *Journal of theoretical biology,* 265**,** 433-442.

GONZÁLEZ BALLESTER, M. Á., ZISSERMAN, A. P. & BRADY, M. 2002. Estimation of the partial volume effect in MRI. *Medical Image Analysis,* 6**,** 389-405.

GUCCIONE, J., MOONLY, S., MOUSTAKIDIS, P., COSTA, K., MOULTON, M., RATCLIFFE, M. & PASQUE, M. 2001. Mechanism underlying mechanical dysfunction in the border zone of left ventricular aneurysm: a finite element model study. *The Annals of thoracic surgery,* 71**,** 654-662.

GUCCIONE, J. M., COSTA, K. D. & MCCULLOCH, A. D. 1995. Finite element stress analysis of left ventricular mechanics in the beating dog heart. *Journal of biomechanics,* 28**,** 1167-1177.

GUCCIONE, J. M. & MCCULLOCH, A. D. 1993. Mechanics of active contraction in cardiac muscle: Part I--Constitutive relations for fiber stress that describe deactivation. *J Biomech Eng,* 115**,** 72-81.

GUYTON, A. C. & HALL, J. E. 2006. *Textbook of Medical Physiology,* Philadelphia, Elsevier Saunders.

HANNAN, E. L., RACZ, M. J., MCCALLISTER, B. D., RYAN, T. J., ARANI, D. T., ISOM, O. W. & JONES, R. H. 1999. A comparison of three-year survival after coronary artery bypass graft surgery and percutaneous transluminal coronary angioplasty. *Journal of the American College of Cardiology,* 33**,** 63-72.

HANNAN, E. L., RACZ, M. J., WALFORD, G., JONES, R. H., RYAN, T. J., BENNETT, E., CULLIFORD, A. T., ISOM, O. W., GOLD, J. P. & ROSE, E. A. 2005. Long-term outcomes of coronary-artery bypass grafting versus stent implantation. *New England Journal of Medicine,* 352**,** 2174-2183.

HAO, X., SILVA, E. A., MÅNSSON-BROBERG, A., GRINNEMO, K. H., SIDDIQUI, A. J., DELLGREN, G., WÄRDELL, E., BRODIN, L. Å., MOONEY, D. J. & SYLVÉN, C. 2007. Angiogenic effects of sequential release of VEGF-A165 and PDGF-BB with alginate hydrogels after myocardial infarction. *Cardiovascular research,* 75**,** 178.

HAUTEMANN, D. J. 2007. *Fiber architecture of the post-mortem rat heart obtained with Diffusion Tensor Imaging.* Masters, Eindhoven University of Technology.

HEGER, J. J., WEYMAN, A. E., WANN, L., DILLON, J. C. & FEIGENBAUM, H. 1979. Cross-sectional echocardiography in acute myocardial infarction: detection and localization of regional left ventricular asynergy. *Circulation,* 60**,** 531-538.

HEIBERG, E., SJÖGREN, J., UGANDER, M., CARLSSON, M., ENGBLOM, H. & ARHEDEN, H. 2010. Design and validation of Segment--freely available software for cardiovascular image analysis. *BMC Medical Imaging,* 10**,** 1-1.

HEIBERG, E., WIGSTRÖM, L., CARLSSON, M., BOLGER, A. & KARLSSON, M. 2005. Time resolved three-dimensional automated segmentation of the left ventricle.

HERRMANN, K. L., MCCULLOCH, A. D. & OMENS, J. H. 2003. Glycated collagen cross-linking alters cardiac mechanics in volume-overload hypertrophy. *American Journal of Physiology-Heart and Circulatory Physiology,* 284**,** H1277-H1284.

HOCHMAN, J. & BULKLEY, B. H. 1982. Expansion of acute myocardial infarction: an experimental study. *Circulation,* 65**,** 1446-1450.

HOLMES, J. W., BORG, T. K. & COVELL, J. W. 2005. Structure and mechanics of healing myocardial infarcts. *Annu. Rev. Biomed. Eng.,* 7**,** 223-253.

HOLZAPFEL, G. A. & OGDEN, R. W. 2009. Constitutive modelling of passive myocardium: a structurally based framework for material characterization. *Philosophical*

*Transactions of the Royal Society A: Mathematical, Physical and Engineering Sciences,* 367**,** 3445.

HONG, C., BECKER, C. R., HUBER, A., SCHOEPF, U. J., OHNESORGE, B., KNEZ, A., BRÜNING, R. & REISER, M. F. 2001. ECG-gated reconstructed multi-detector row CT coronary angiography: effect of varying trigger delay on image quality. *Radiology,* 220**,** 712-717.

HUNTER, P., NASH, M. & SANDS, G. 1997. *Computational electromechanics of the heart*, John Wiley, New York.

IFKOVITS, J. L., TOUS, E., MINAKAWA, M., MORITA, M., ROBB, J. D., KOOMALSINGH, K. J., GORMAN, J. H., GORMAN, R. C. & BURDICK, J. A. 2010. Injectable hydrogel properties influence infarct expansion and extent of postinfarction left ventricular remodeling in an ovine model. *Proceedings of the National Academy of Sciences,* 107**,** 11507-11512.

JANZ, R. F. & GRIMM, A. F. 1972. Finite-element model for the mechanical behavior of the left ventricle: Prediction of deformation in the potassium-arrested rat heart. *Circulation Research,* 30**,** 244-252.

JIANG, X. J., WANG, T., LI, X. Y., WU, D. Q., ZHENG, Z. B., ZHANG, J. F., CHEN, J. L., PENG, B., JIANG, H. & HUANG, C. 2009. Injection of a novel synthetic hydrogel preserves left ventricle function after myocardial infarction. *Journal of biomedical materials research Part A,* 90**,** 472-477.

JOHN, R., RAJASINGHE, H. A., CHEN, J. M., WEINBERG, A. D., SINHA, P., MANCINI, D. M., NAKA, Y., OZ, M. C., SMITH, C. R. & ROSE, E. A. 2001. Long-term outcomes after cardiac transplantation: an experience based on different eras of immunosuppressive therapy. *The Annals of thoracic surgery,* 72**,** 440.

KADNER, K., DOBNER, S., FRANZ, T., BEZUIDENHOUT, D., SIRRY, M. S., ZILLA, P. & DAVIES, N. H. 2012. The beneficial effects of deferred delivery on the efficiency of hydrogel therapy post myocardial infarction. *Biomaterials*.

KAUS, M. R., BERG, J. V., WEESE, J., NIESSEN, W. & PEKAR, V. 2004. Automated segmentation of the left ventricle in cardiac MRI. *Medical Image Analysis,* 8**,** 245-254.

KLEIN, S. A. 1970. *Morphologic Patterns in the Growing Rat Heart.* M.S. Thesis, University of Illinois.

KOFIDIS, T., LEBL, D. R., MARTINEZ, E. C., HOYT, G., TANAKA, M. & ROBBINS, R. C. 2005. Novel injectable bioartificial tissue facilitates targeted, less invasive, large-scale tissue restoration on the beating heart after myocardial injury. *Circulation,* 112**,** I-173-I-177.

KONSTAM, M. A. 2005. Reliability of ventricular remodeling as a surrogate for use in conjunction with clinical outcomes in heart failure. *Am J Cardiol,* 96**,** 867-71.

KORTSMIT, J., DAVIES, N. H., MILLER, R., MACADANGDANG, J. R., ZILLA, P. & FRANZ, T. 2012. The effect of hydrogel injection on cardiac function and myocardial mechanics in a computational post-infarction model. *Computer Methods in Biomechanics and Biomedical Engineering,* 15**,** 1-99.

LAFLAMME, M. A. & MURRY, C. E. 2005. Regenerating the heart. *Nature biotechnology,* 23**,** 845-856.

LAFORTUNE, P., ARIS, R., VAZQUEZ, M. & HOUZEAUX, G. 2011. Coupled Parallel Electromechanical Model of the Heart. *International Journal for Numerical Methods in Biomedical Engineering.*

LANDA, N., MILLER, L., FEINBERG, M. S., HOLBOVA, R., SHACHAR, M., FREEMAN, I., COHEN, S. & LEOR, J. 2008. Effect of injectable alginate implant on cardiac remodeling and function after recent and old infarcts in rat. *Circulation,* 117**,** 1388-96.

LEGRICE, I., HUNTER, P., YOUNG, A. & SMAILL, B. 2001. The architecture of the heart: a data–based model. *Philosophical transactions of the Royal Society of London. Series A: Mathematical, physical and engineering sciences,* 359**,** 1217-1232.

LITTLE, R. C. & LITTLE, W. C. 1981. *Physiology of the Heart and Circulation*, Year Book Medical Publishers.

LIU, C., HOFSTETTER, G. & MANG, H. 1994. 3D finite element analysis of rubber-like materials at finite strains. *Engineering computations,* 11**,** 111-128.

LLOYD-JONES, D., ADAMS, R. J., BROWN, T. M., CARNETHON, M., DAI, S., DE SIMONE, G., FERGUSON, T. B., FORD, E., FURIE, K. & GILLESPIE, C. 2010. Heart disease and stroke statistics—2010 update. *Circulation,* 121**,** e46-e215.

MACADANGDANG, J. R. 2010. Computation Study of Functional Impact of Hydrogel Injection into Post-Infarction Scar Tissue. *In:* A.G. MALAN, P. N., AND B.D. REDDY (ed.) *Second African Conference on Computation Mechanics.* Cape Town, South Africa.

MAIER, K. 2011. *What Is the Most Common Myocardial Infarction Pathophysiology?* [Online]. Available: http://www.wisegeek.com/what-is-the-most-common-myocardial-infarction-pathophysiology.htm [Accessed 29/08 2011].

MARKS, J. W. 2012. *Heart Attack* [Online]. Available: http://www.medicinenet.com/heart_attack/page2.htm#what_causes_a_heart_attack [Accessed 21/01 2013].

MENASCHÉ, P. 2007. Skeletal myoblasts as a therapeutic agent. *Progress in cardiovascular diseases,* 50**,** 7-17.

MILLER, R. 2012. *A Computational Study of Post-Infarct Mechanical Effects of Injected Biomaterial into Ischaemic Myocardium.* Masters Dissertation, University of Cape Town.

MIURA, T. & MIKI, T. 2008. Limitation of myocardial infarct size in the clinical setting: current status and challenges in translating animal experiments into clinical therapy. *Basic Research in Cardiology,* 103**,** 501-513.

MORITA, M., ECKERT, C. E., MATSUZAKI, K., NOMA, M., RYAN, L. P., BURDICK, J. A., JACKSON, B. M., GORMAN, J. H., SACKS, M. S. & GORMAN, R. C. 2011. Modification of infarct material properties limits adverse ventricular remodeling. *The Annals of thoracic surgery,* 92**,** 617-624.

NAGY, V. 2001. [Left ventricular hypertrophy: pathogenesis, diagnosis and therapy]. *Orvosi Hetilap,* 142**,** 1375-1383.

NASH, M. & HUNTER, P. 2000. Computational mechanics of the heart. *Journal of Elasticity,* 61**,** 113-141.

NELSON, D. M., MA, Z., FUJIMOTO, K. L., HASHIZUME, R. & WAGNER, W. R. 2011. Intra-myocardial biomaterial injection therapy in the treatment of heart failure: Materials, outcomes and challenges. *Acta Biomaterialia,* 7**,** 1-15.

NIELSEN, P., LE GRICE, I., SMAILL, B. & HUNTER, P. 1991. Mathematical model of geometry and fibrous structure of the heart. *American Journal of Physiology-Heart and Circulatory Physiology,* 260**,** H1365-H1378.

OHNESORGE, B., FLOHR, T., BECKER, C., KOPP, A. F., SCHOEPF, U. J., BAUM, U., KNEZ, A., KLINGENBECK-REGN, K. & REISER, M. F. 2000. Cardiac imaging by means of electrocardiographically gated multisection spiral CT: initial experience. *Radiology,* 217**,** 564-571.

OKADA, M., PAYNE, T. R., OSHIMA, H., MOMOI, N., TOBITA, K. & HUARD, J. 2010. Differential efficacy of gels derived from small intestinal submucosa as an injectable biomaterial for myocardial infarct repair. *Biomaterials,* 31**,** 7678-7683.

OMENS, J. H., MACKENNA, D. A. & MCCULLOCH, A. D. 1993. Measurement of strain and analysis of stress in resting rat left ventricular myocardium. *Journal of Biomechanics,* 26**,** 665-676.

OPIE, L. H., COMMERFORD, P. J., GERSH, B. J. & PFEFFER, M. A. 2006. Controversies in ventricular remodelling. *Lancet,* 367**,** 356-67.

PACHER, P., MABLEY, J. G., LIAUDET, L., EVGENOV, O. V., MARTON, A., HASKÓ, G., KOLLAI, M. & SZABÓ, C. 2004. Left ventricular pressure-volume relationship in a rat model of advanced aging-associated heart failure. *American Journal of Physiology-Heart and Circulatory Physiology,* 287**,** H2132-H2137.

PAGE, D. L., CAULFIELD, J. B., KASTOR, J. A., DESANCTIS, R. W. & SANDERS, C. A. 1971. Myocardial changes associated with cardiogenic shock. *New England Journal of Medicine,* 285**,** 133-137.

PARAGIOS, N. 2003. A level set approach for shape-driven segmentation and tracking of the left ventricle. *IEEE Transactions on Medical Imaging,* 22**,** 773-776.

PFEFFER, M. A. & BRAUNWALD, E. 1990. Ventricular remodeling after myocardial infarction. Experimental observations and clinical implications. *Circulation,* 81**,** 1161.

POTHINENI, K. R., INAMDAR, V., MILLER, A. P., NANDA, N. C., BANDARUPALLI, N., CHAURASIA, P., KIRKLIN, J. K., MCGIFFIN, D. C. & PAJARO, O. E. 2007. Initial Experience with Live/Real Time Three-Dimensional Transesophageal Echocardiography. *Echocardiography,* 24**,** 1099-1104.

ROGER, V. L., GO, A. S., LLOYD-JONES, D. M., ADAMS, R. J., BERRY, J. D., BROWN, T. M., CARNETHON, M. R., DAI, S., DE SIMONE, G. & FORD, E. S. 2011. Heart Disease and Stroke Statistics. *Circulation,* 123**,** e18-e209.

ROHMER, D., SITEK, A. & GULLBERG, G. T. 2007. Reconstruction and visualization of fiber and laminar structure in the normal human heart from ex vivo diffusion tensor magnetic resonance imaging (DTMRI) data. *Investigative radiology,* 42**,** 777-789.

RUETTEN, H., GEHRING, D., HISS, K., SCHINDLER, U., GERL, M., BUSCH, A. E. & SCHAEFER, S. 2005. Effects of combined inhibition of the Na+–H+ exchanger and angiotensin-converting enzyme in rats with congestive heart failure after myocardial infarction. *British journal of pharmacology,* 146**,** 723-731.

SABBAH, H., WANG, M., ILSAR, I., JIANG, A. & TUVIA, S. 2008. Intracoronary administration of BL-1040 prevents progressive left ventricular enlargement in dogs with acute myocardial infarction. *Cardiovascular Revascularization Medicine,* 9**,** 121-121.

SALEH, M. G., SHARP, S.-K., ALHAMUD, A., SPOTTISWOODE, B. S., VAN DER KOUWE, A. J. W., DAVIES, N. H., FRANZ, T. & MEINTJES, E. M. 2012. Long-Term Left Ventricular Remodelling in Rat Model of Nonreperfused Myocardial Infarction: Sequential MR Imaging Using a 3T Clinical Scanner. *Journal of Biomedicine and Biotechnology,* 2012**,** 10.

SARTIPY, U., ALBAGE, A. & LINDBLOM, D. 2005. The Dor procedure for left ventricular reconstruction. Ten-year clinical experience. *European journal of cardio-thoracic surgery,* 27**,** 1005-1010.

SEGERS, V. F. & LEE, R. T. 2008. Stem-cell therapy for cardiac disease. *Nature,* 451**,** 937-942.

SHIOURA, K. M., GEENEN, D. L. & GOLDSPINK, P. H. 2007. Assessment of cardiac function with the pressure-volume conductance system following myocardial infarction in

mice. *American Journal of Physiology-Heart and Circulatory Physiology,* 293**,** H2870-H2877.

SIRRY, M. S., DAVIES, N. H., KADNER, K., DUBUIS, L., SALEH, M. G., MEINTJES, E. M., SPOTTISWOODE, B. S., ZILLA, P. & FRANZ, T. 2013. Micro-structurally detailed model of a therapeutic hydrogel injectate in a rat biventricular cardiac geometry for computational simulations. *Computer Methods in Biomechanics and Biomedical Engineering***,** 1-7.

SMITH, M. K., RUSSELL, R. O., FEILD, B. J. & RACKLEY, C. E. 1974. Left ventricular compliance and abnormally contracting segments in postmyocardial infarction patients. *Chest,* 65**,** 368.

STARLING, R. C., JESSUP, M., OH, J. K., SABBAH, H. N., ACKER, M. A., MANN, D. L. & KUBO, S. H. 2007. Sustained benefits of the CorCap Cardiac Support Device on left ventricular remodeling: three year follow-up results from the Acorn clinical trial. *The Annals of thoracic surgery,* 84**,** 1236.

SUGA, H. & SAGAWA, K. 1974. Instantaneous pressure-volume relationships and their ratio in the excised, supported canine left ventricle. *Circulation Research,* 35**,** 117-126.

SUN, K., STANDER, N., JHUN, C., ZHANG, Z., SUZUKI, T., WANG, G., SAEED, M., WALLACE, A., TSENG, E. & BAKER, A. 2009. A computationally efficient formal optimization of regional myocardial contractility in a sheep with left ventricular aneurysm. *Journal of biomechanical engineering,* 131**,** 111001.

TER KEURS, H. 1983. Calcium and contractility. *Cardiac Metabolism, New York: Wiley***,** 73-99.

TER KEURS, H. E., RIJNSBURGER, W. H., VAN HEUNINGEN, R. & NAGELSMIT, M. J. 1980. Tension development and sarcomere length in rat cardiac trabeculae: evidence of length-dependent activation. *Cardiac Dynamics.* Springer.

THANAVARO, S., KLEIGER, R., PROVINCE, M., HUBERT, J., MILLER, J., KRONE, R. & OLIVER, G. 1982. Effect of infarct location on the in-hospital prognosis of patients with first transmural myocardial infarction. *Circulation,* 66**,** 742-747.

TSUR-GANG, O., RUVINOV, E., LANDA, N., HOLBOVA, R., FEINBERG, M. S., LEOR, J. & COHEN, S. 2009. The effects of peptide-based modification of alginate on left ventricular remodeling and function after myocardial infarction. *Biomaterials,* 30**,** 189-195.

UNKNOWN. 2012. *What is computational mechanics* [Online]. Available: http://www.usacm.org/what-is-computational-mechanics [Accessed 16/04/2013 2013].

USYK 2002. Computational Methods for Soft Tissue Biomechanics. 84.

VETTER, F. J. & MCCULLOCH, A. D. 2000. Three-dimensional stress and strain in passive rabbit left ventricle: a model study. *Annals of Biomedical Engineering,* 28**,** 781-792.

WALKER, J. C., RATCLIFFE, M. B., ZHANG, P., WALLACE, A. W., FATA, B., HSU, E. W., SALONER, D. & GUCCIONE, J. M. 2005. MRI-based finite-element analysis of left ventricular aneurysm. *Am J Physiol Heart Circ Physiol,* 289**,** H692-700.

WALL, S. T., WALKER, J. C., HEALY, K. E., RATCLIFFE, M. B. & GUCCIONE, J. M. 2006. Theoretical impact of the injection of material into the myocardium - A finite element model simulation. *Circulation,* 114**,** 2627-2635.

WANG, T., WU, D. Q., JIANG, X. J., ZHANG, X. Z., LI, X. Y., ZHANG, J. F., ZHENG, Z. B., ZHUO, R., JIANG, H. & HUANG, C. 2009. Novel thermosensitive hydrogel injection inhibits post-infarct ventricle remodelling. *European journal of heart failure,* 11**,** 14-19.

WEHRENS, X. H. T. & DOEVENDANS, P. A. 2004. Cardiac rupture complicating myocardial infarction. *International journal of cardiology,* 95**,** 285-292.

WEISMAN, H. F. & HEALY, B. 1987. Myocardial infarct expansion, infarct extension, and reinfarction: pathophysiologic concepts. *Progress in cardiovascular diseases,* 30**,** 73-110.

WEISS, J. A., MAKER, B. N. & GOVINDJEE, S. 1996. Finite element implementation of incompressible, transversely isotropic hyperelasticity. *Computer methods in applied mechanics and engineering,* 135**,** 107-128.

WENK, J., SUN, K., ZHANG, Z., SOLEIMANI, M., GE, L., SALONER, D., WALLACE, A., RATCLIFFE, M. & GUCCIONE, J. 2011. Regional left ventricular myocardial contractility and stress in a finite element model of posterobasal myocardial infarction. *Journal of biomechanical engineering,* 133**,** 044501.

WENK, J., WALL, S., PETERSON, R., HELGERSON, S., SABBAH, H., BURGER, M., STANDER, N., RATCLIFFE, M. & GUCCIONE, J. 2009. A method for automatically optimizing medical devices for treating heart failure: designing polymeric injection patterns. *Journal of biomechanical engineering,* 131**,** 121011.

WHELAN, R. S., MANI, K. & KITSIS, R. N. 2007. Nipping at cardiac remodeling. *J Clin Invest,* 117**,** 2751-3.

WHO 2008. WHO: The Atlas of Heart Disease and Stroke. Geneva: World Health Organization.

WOLLERT, K. C. & DREXLER, H. 2005. Clinical applications of stem cells for the heart. *Circulation Research,* 96**,** 151-163.

WU, E., ORTIZ, J. T., TEJEDOR, P., LEE, D. C., BUCCIARELLI-DUCCI, C., KANSAL, P., CARR, J. C., HOLLY, T. A., LLOYD-JONES, D. & KLOCKE, F. J. 2008. Infarct size by contrast enhanced cardiac magnetic resonance is a stronger predictor of outcomes than left

ventricular ejection fraction or end-systolic volume index: prospective cohort study. *Heart,* 94**,** 730-736.

YIN, F., CHAN, C. & JUDD, R. M. 1996. Compressibility of perfused passive myocardium. *American Journal of Physiology-Heart and Circulatory Physiology,* 271**,** H1864-H1870.

YOO, T. S., ACKERMAN, M. J., LORENSEN, W. E., SCHROEDER, W., CHALANA, V., AYLWARD, S., METAXAS, D. & WHITAKER, R. 2002. Engineering and algorithm design for an image processing api: a technical report on itk-the insight toolkit. *Studies in health technology and informatics***,** 586-592.

YOON, S. J., FANG, Y. H., LIM, C. H., KIM, B. S., SON, H. S., PARK, Y. & SUN, K. 2009. Regeneration of ischemic heart using hyaluronic acid-based injectable hydrogel. *Journal of Biomedical Materials Research Part B: Applied Biomaterials,* 91**,** 163-171.

YUSHKEVICH, P. A., PIVEN, J., CODY, H., HO, S., GEE, J. C. & GERIG, G. 2005. User-guided level set segmentation of anatomical structures with ITK-SNAP. *Insight Jounral,* 1.

ZIENKIEWICZ, D. C. (ed.) 1967. *Finite Element Method in Structural and Continuum Mechanics,* New York: McGraw-Hill Publishing Co.